Study on Development of $BiFeO_3$ - based Multiferroic Thin Films with Excellent Magnetic Properties and Investigation on their Magnetic Device Applicability

By

Soumyaranjan Ratha

Department of Material Science
Graduate School of Engineering Science

Submitted

In fulfillment of the requirement for the degree of

Doctor of Engineering

Akita University

1-1 Tegatagakuen-machi, Akita City, 010-8502

Japan

January-2024

Dedicated

to

my beloved late father,

Dr. Nanda Kishore Ratha,

whose cherished dream was to witness my attainment of this academic milestone.

CERTIFICATE

This certification attests that the thesis entitled “Study on Development of $BiFeO_3$-based Multiferroic Thin Films with Excellent Magnetic Properties and Investigation on their Magnetic Device Applicability,” submitted to Akita University, Japan, for the partial fulfillment of the Doctor of Engineering degree in material science, reflects the original research endeavors of Mr. Soumyaranjan Ratha under my diligent supervision from 2021 to 2024. To my knowledge and belief, the thesis encapsulates the candidate's independent scholarly contributions, adhering to the requisite standards of the Institute's Ph.D. program. Importantly, neither the complete nor partial contents of the thesis have been presented for consideration to any other academic institution for the conferral of a degree.

Supervisor

Prof. Satoru Yoshimura

Professor

Department of Material Science

Graduate School of Engineering Science

Akita University

Japan

Place: Akita, Japan
Date:

DECLARATION

I solemnly affirm that the thesis titled "Study on Development of $BiFeO_3$-based Multiferroic Thin Films with Excellent Magnetic Properties and Investigation on their Magnetic Device Applicability," submitted to Akita University, Japan, for the partial fulfillment of the requirements for the award of the Doctor of Engineering degree in Physics, is an authentic record of my original research work under the expert guidance and supervision of Prof. Satoru Yoshimura, Akita University, Japan 010-8502. I further confirm that neither the entire nor any part of the contents of this thesis has been previously submitted to any other Institute or University for the purpose of obtaining any degree.

Signature of Candidate

Soumyaranjan Ratha

Place: Akita, Japan
Date:

ACKNOWLEDGEMENT

This doctoral thesis has been made possible through the invaluable help and support of the kind individuals in my life, and while it is challenging to acknowledge everyone, I would like to express my gratitude to those whom I can mention here.

Foremost, I wish to express my deep gratitude to my thesis supervisor, Prof. Satoru Yoshimura, whose unwavering patience, continuous support, and encouragement have been instrumental in shaping this work. When I embarked on my Ph.D. journey with limited knowledge in experimental research, Prof. Yoshimura demonstrated remarkable patience, dedicating ample time to instruct me on instruments, data analysis, and more. His extensive knowledge, logical problem-solving approach, and effective presentation skills have not only been a source of motivation but have also significantly influenced the development of this work.

I extend my heartfelt gratitude to Professor Azusa N. Hattori of Osaka University for invaluable help in microfabrication and etching experiments. My sincere appreciation also goes to Dr. Yuya Sakuraba from the National Institute of Materials Science for expert assistance with XPS measurements. Additionally, I am deeply thankful to Professor Tsukasa Katayama for his instrumental support in PFM measurements.

I am equally grateful to all my lab mates, whose unwavering support proved instrumental throughout various experiments. Their full cooperation and constant presence have been invaluable, creating an environment of camaraderie and shared dedication. I extend my heartfelt thanks to each of them for their collaborative efforts, which significantly contributed to the success and progress of our collective endeavors.

Special acknowledgment is to Mr. Genta Egawa, our esteemed technical specialist, whose continuous assistance played a pivotal role in the seamless execution of numerous experiments and measurements. His expertise and unwavering support have been invaluable to my research journey. Additionally, I extend my sincere gratitude to Mrs. Masaki Watanabe for her consistent aid in all official matters and meticulous documentation from the inception of my tenure at Akita University to its conclusion. Her dedication and assistance have greatly facilitated my academic and administrative responsibilities.

I extend heartfelt appreciation and gratitude to the friends, elders, and younger colleagues who have provided unwavering encouragement throughout my PhD journey. Their support has been a source of strength and motivation, shaping my path towards success. Additionally, I am deeply indebted to all my teachers in India, whose guidance and encouragement have played a pivotal role in helping me reach my academic goals. Their mentorship has been invaluable, and I am sincerely thankful for the positive impact they have had on my educational journey.

I wish to express my profound gratitude to my mother Mrs. Santilata Ratha for her unwavering patience and steadfast support throughout my pursuit of higher education. My heartfelt thanks extend to my entire family and relatives for their boundless love and affection, providing the strength needed to thrive in a foreign land. A special acknowledgment is reserved for my sister, Mrs. Monalisha Ratha, and brother-in-law, Mr. Tapan Kar, who have emerged as the two strongest pillars in my life and, particularly, in my career. Their support has been instrumental, and I am deeply thankful for their enduring presence and encouragement.

I am profoundly grateful to my beloved, Ms. Lipsa Rani Nath, a PhD scholar, whose unwavering support has been a constant source of inspiration throughout not only my PhD journey but also my entire academic pursuit. Her tireless efforts to motivate me, coupled with the unwavering confidence she instills in me with the words, "you can do everything," have been instrumental in my academic achievements. Her love and encouragement have been my anchor, and I am truly thankful for her presence in every step of my life.

I extend my gratitude to the esteemed Japanese government for the prestigious MEXT scholarship, which provided invaluable financial support throughout my Ph.D. tenure. I also acknowledge and appreciate the contributions of those individuals whose names may not be explicitly mentioned here but who, directly or indirectly, played a significant role in aiding me to successfully complete this work.

Last but not least, I express my sincere gratitude to Akita University, Japan for allowing me to pursue Ph.D.

Above all, I must, in all humanity, thank "God for his providence", which enabled me to achieve my goal in a determined fashion.

Soumyaranjan Ratha

CONTENTS

ABSTRACT

Nowadays, there is a strong demand for Society 5.0 and IoT to be realized with green IT equipment that has a low environmental impact, and there is also a strong demand for lower power consumption in magnetic devices that perform information recording, video display, sensing, etc. However, the current magnetic field method is used for magnetization reversal in recording devices, the spin injection method is used for magnetization reversal in display devices, and the tunnel magnetoresistance method is used for sensor devices, all of which require current to flow. There are concerns that power consumption will become extremely large as devices become more highly integrated in the future. In order to fundamentally solve these problems, it would be effective to use a completely new drive method and use materials with functions suitable for that new method. At present, efforts are only being made to improve the properties of the materials and the structure of the devices in the current flow driving method, and no fundamental or dramatic solutions have been found.

Ferromagnetic and ferroelectric materials are thought to be able to control the direction of magnetization (M) and electric polarization (P) using an electric field (E) or magnetic field (H), so they are expected to be used as materials for highly functional next-generation electronic devices. In particular, by applying this material to magnetic devices, it becomes possible to drive with low power consumption by applying an electric field and reversing the magnetization. For high-performance magnetic devices, it is essential to use magnetic material thin films with high functionality such as large saturation magnetization (M_s), large perpendicular magnetic anisotropy (K_u), and large magnetic Kerr rotation angle (Θ_k). However, the values of magnetic properties of current ferromagnetic and ferroelectric thin films are still small, and although it is possible to reduce the power consumption of magnetic devices by applying these thin films, it is not easy to improve their performance.

Based on these findings, I searched and produced thin films of highly functional ferromagnetic and ferroelectric materials to enable the realization of high-performance magnetic devices with low power consumption, and selected materials that were found to be suitable for each magnetic device. Finally, I verified the durability of ferromagnetic and ferroelectric thin films in micro-element processing, which is ultimately essential in device packaging, and searched for processing conditions that will cause less damage to the thin films. This paper, which summarizes the results

with the aim of achieving this goal, consisted of six chapters. An overview of each chapter is shown below.

Chapter 1: An introduction and describes the research background as to why power consumption increases with higher integration in magnetic devices that perform information recording, video display, sensing, etc., and the research group's proposal to solve this problem. I presented a new electric field drive method using a $BiFeO_3$-based ferromagnetic/ferroelectric thin film, presented a method for producing high-quality thin films, and the current status of the development of thin film materials using this method, and then discussed the purpose of this research and explained the significance.

Chapter 2: Description on the outline of the production equipment for $BiFeO_3$-based ferromagnetic and ferroelectric thin films, the production method and film-fabrication conditions, the outline of the equipment for evaluating the characteristics of $BiFeO_3$-based ferromagnetic and ferroelectric thin films, the evaluation method and evaluation conditions, and the overview of the microfabrication equipment for magnetic and ferroelectric thin films, the processing methods and processing conditions.

Chapter 3: fabrication of $(Bi,L)(Fe,Co)O_3$ (L = La, Nd, Sm, Eu, Gd, Dy, Er) thin films, and discussed M_s, K_u ($H_{c\perp}/H_{c//}$ and $S_\perp/S_{//}$, which is an index of the magnitude of K_u), and Θ_k. A relatively large M_s was obtained for all the thin films, but among them, the Nd-substituted thin film in particular achieved around 140 emu/cm^3. Relatively large $H_{c\perp}/H_{c//}$ was obtained for all thin films, but especially for the thin film substituted with Sm, it was much larger than 1.0, including $S_\perp/S_{//}$, and was clearly perpendicular magnetic anisotropy. Furthermore, in the thin film substituted with Eu, H_c of 0.5 kOe was obtained. Furthermore, a relatively large Θ_k was obtained for all the thin films, but among them, 0.67° was especially obtained for the thin film substituted with La. The origin of magnetism in $(Bi,L)(Fe,Co)O_3$ thin films is that Co substituted for Fe^{3+} becomes Co^{2+} with a small magnetic moment, becoming ferrimagnetic. It is thought that each lanthanide element has a different effect on the magnetism of Co.

Chapter 4 Discussion of $(Bi,Nd)(Fe,Co)O_3$, $(Bi,La)(Fe,Co)O_3$ and $(Bi,Eu)(Fe,Co)O_3$, I evaluated the micro magnetic properties such as grain size, magnetic domain size, minimum magnetic domain width induced by electric field, and Curie temperature, and I verified the applicability to devices. As a result, the grain size was 100 nm or less, the magnetic domain size was 200 nm or less, the minimum magnetic domain width induced by an electric field was 300 nm or less, and

the Curie temperature was 420 °C or higher for all thin films. We also demonstrated magnetization switching with a width of 500 nm. It was concluded that the method can be applied to high integration.

Chapter 5 Verification of the resistance to micro-element processing required for device formation and the processing conditions with minimal damage in (Bi,Eu)(Fe,Co)O_3 thin films that have micro magnetic properties that can be applied to high integration. As a result, when milling with Ar ions or reactive ion etching with CHF_3, oxygen vacancies were generated in the thin film, which deteriorated the magnetic and electrical properties. On the other hand, reactive ion etching using a mixed gas of CHF_3, and oxygen was able to suppress the generation of oxygen vacancies. From these results, I concluded that it is possible to form devices using $BiFeO_3$-based ferromagnetic and ferroelectric thin films by optimizing the micro-element processing conditions.

Chapter 6 Summarization of the main findings obtained through this research and concluded with a discussion of future challenges.

Keywords: Multiferroics, Thin films, Magnetic Devices, Magnetization, Perpendicular magnetic anisotropy, Ferroelectricity, Microfabrication, Lithography, Dry etching, Reactive ion etching, Bismuth ferrite, XRD, FESEM, EDX, XPS, VSM, MOKE.

Index of Figures

Index of Tables

List of Abbreviations

M	Magnetization
M_S	Saturation Magnetization
H_C	Coercivity
$H_{C//}$	In-plane Coercivity
$H_{C\perp}$	Out-of-plane Coercivity
B	Magnetic Induction
M_r	Retentivity
H	Magnetic Field
E	Electric Field
K_u	Perpendicular Magnetic Anisotropy
Θ_k	Kerr Rotational Angle
$BiFeO_3$	Bismuth Ferrite
T_C	Curie Temperature
XRD	X-ray Diffraction
FESEM	Field Emission Scanning Electron Microscopy
EDX	Energy Dispersive X-ray
XPS	X-ray Photoelectron Spectroscopy
VSM	Vibrating Sample Magnetometer
MOKE	Magneto Optical Kerr Effect
AFM	Atomic Force Microscopy
MFM	Magnetic Force Microscopy
EFM	Electrostatic Force Microscopy
DE	Dry Etching
RIE	Reactive Ion Etching
HDD	Hard Disk Drive
PFM	Piezoresponse Force Microscopy

TMR	Tunneling Magneto Resistance
T_N	Neel Temperature
p-DC	Pulsed DC
RF	Radio Frequency
PVD	Physical Vapor Deposition
VHF	Very High Frequency
MEMS	Micro Electromechanical System

CHAPTER - 1
Introduction

1.1. Introduction to Magnetic Devices

Magnetic devices are the most cutting-edge technology currently available. They represent the future of technology. The characteristics that these future technologies are expected to possess are really remarkable, including the ability to convert energy more effectively and to store data more quickly. Nevertheless, the dilemma of energy consumption is a significant barrier that stands in the way of our progress toward this magnetic future [1, 2, 3, 4, 5].

Imagine living in a world where magnets make everything work. The power of magnets is used by these gadgets to do things like store data or make electricity. That sounds cool, right? No doubt about it, but there is a catch: they can be very greedy when it comes to energy. Let us break it down. Strong magnetic fields are what cause the problem with how much energy future magnetic devices will need. For these gadgets to work right, these fields are like the fuel that powers them. Creating and keeping these strong magnetic fields going, on the other hand, takes a lot of energy. It's like having a fast car that uses a lot of gas. Our magnetic gadgets need energy to keep doing amazing things. As we try to make magnetic systems that are stronger and more efficient, the need for energy keeps going up. A lot of scientists and engineers are working hard to figure out how to make these gadgets use less energy. Finding the right mix between power and saving is a lot like making sure our magnetic wonders can work their magic without using up all of our energy.

This report focuses on three critical elements comprising magnetic devices: the read head of hard disk drives (HDDs), the write head of Racetrack memory, and the write head of a Spatial Optical Modulator (SOM).

1.1.1. Write Head of Racetrack Memory: Energy Conundrum Navigation

Concerning Racetrack memory, the optimal write head selection remains debatable. Conventional approaches such as writing by coils (figure 1) or employing spin current exhibit potential, but they are accompanied by substantial limitations [6, 7]. The substantial energy consumption incurred by these approaches presents a challenge to the Racetrack memory's overall efficacy. In addition,

substantial manufacturing expenses are expected, which gives rise to apprehensions regarding the economic viability of extensive implementation.

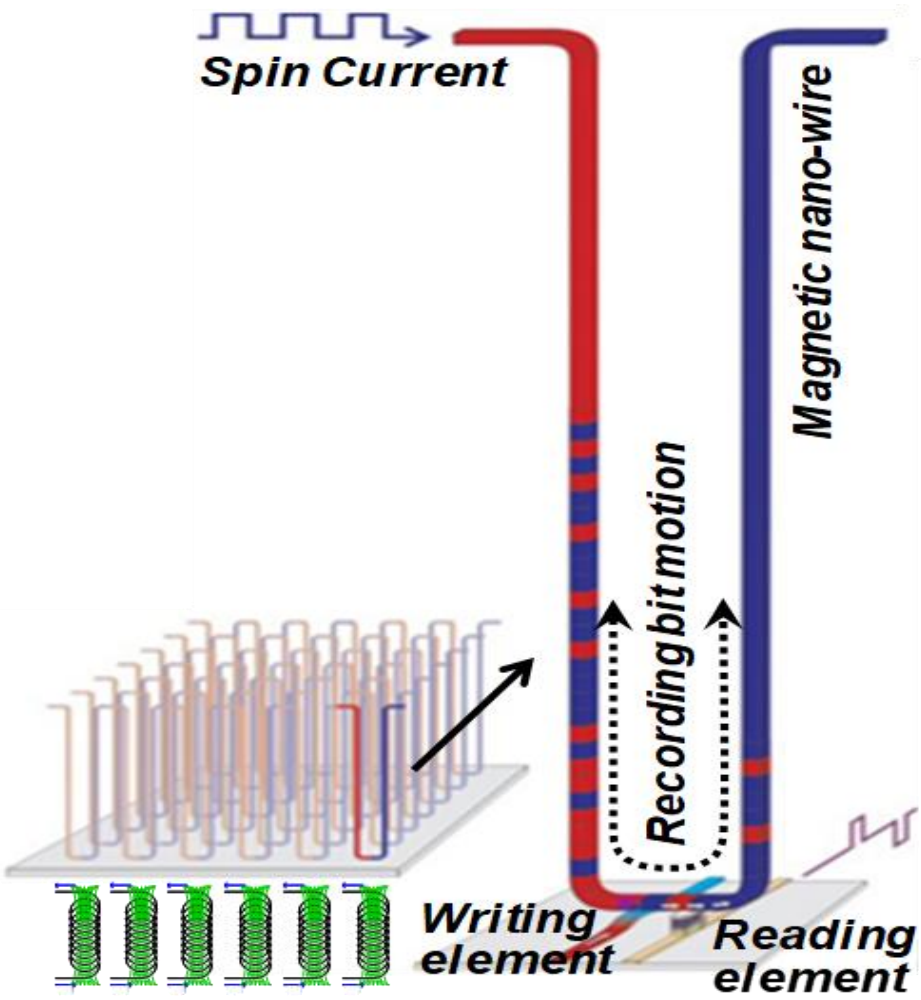

Figure 1. Racetrack memory and the conventional writing element (coil)

1.1.2. Write Head of Spatial Optical Modulators

Current Spatial Optical Modulators (SOMs) write data using spin current, a technique notorious for its substantial energy consumption [8, 9, 10]. Moreover, the requirement for a significant quantity of array as shown in figure 2 for data storage results in additional energy requirements and escalated production expenses. Striking a balance between attaining high-performance optical

modulation and reducing the energy consumption and manufacturing costs linked to SOMs presents a formidable obstacle.

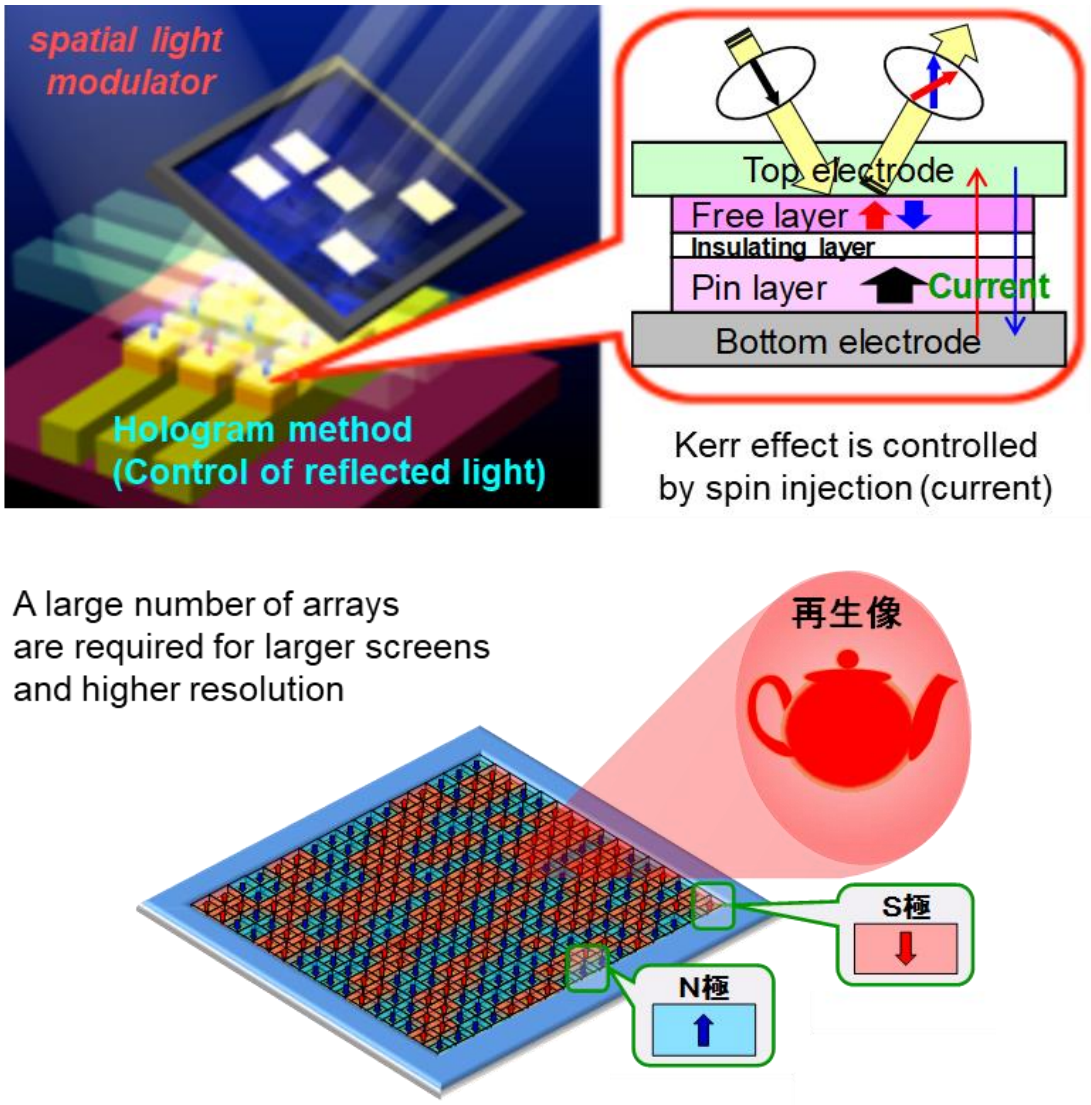

Figure 2. Spatial optical modulator, its writing element (spin injection method)

1.1.3. Read Head of Hard Disk Drive

In order to retrieve information from Hard Disk Drives (HDDs), Tunneling Magnetoresistance (TMR) is utilized as shown in figure 3; however, the resultant signal may lack the desired level of robustness. This poses a challenge with regard to the quickness and dependability of data retrieval. However, there is ongoing research focused on developing methods to optimize the output signal

of the TMR in order to enhance the overall performance of HDD read heads and guarantee precise and efficient data retrieval [11].

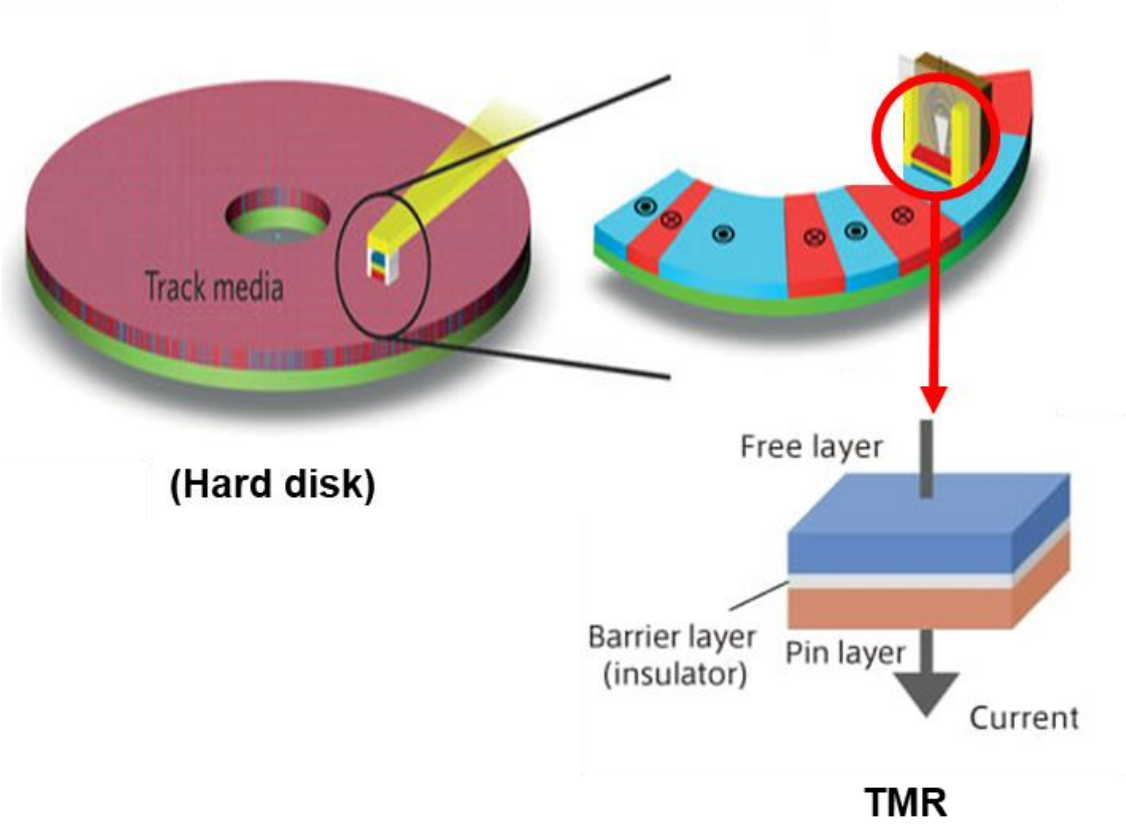

Figure 3. Hard disk drive (HDD) and its reading element (TMR)

1.2. Introduction to Multiferroics

The study of multiferroic materials has become an intriguing and vibrant area of research in the fields of condensed matter physics and materials science. These materials have the exceptional capacity to simultaneously display various ferroic orders, particularly ferroelectricity and ferromagnetism, shown in figure 4. The simultaneous existence of these orders has sparked considerable scientific attention and investigation, primarily because to the possibility of groundbreaking technological advancements in various fields, including electronics, information storage, and energy conversion.

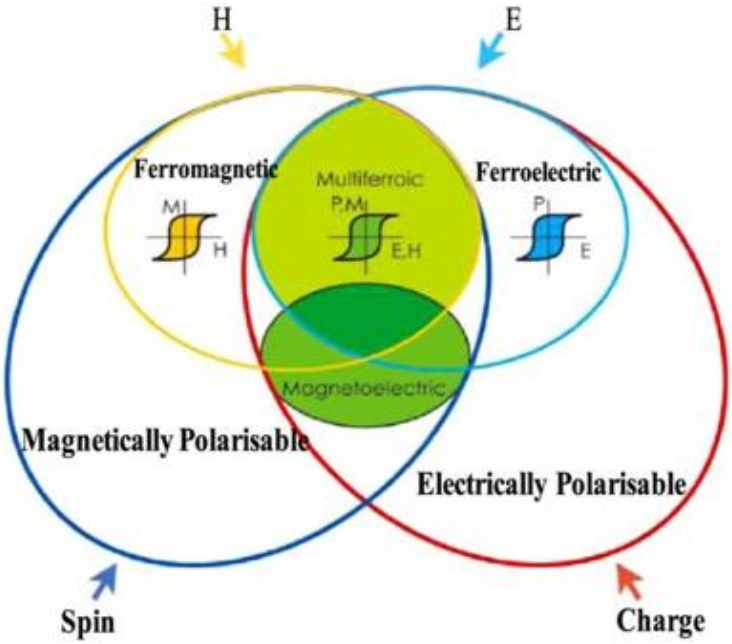

Figure 4. Schematic diagram of multiferroic materials

1.2.1. Fundamental Principles of Multiferroicity

Ferroelectricity: The Core of Electric Polarization

Ferroelectricity is a primary type of ferroic order that underlies the multiferroic behavior seen by these materials. Ferroelectricity is characterized by the emergence of an inherent electric polarization in a material. The polarization is a result of the movements of charged ions within the crystal structure, which causes the creation of electric dipoles [12, 13].

The movement of ions and the resulting polarization

A ferroelectric substance is characterized by a crystal lattice composed of positively charged cations and negatively charged anions. The movement of these ions from their balanced positions leads to the formation of a large-scale electric dipole moment. Barium titanate ($BaTiO_3$) is the most renowned instance of a ferroelectric substance, characterized by its perovskite crystal structure. The titanium ions (Ti^{4+}) in $BaTiO_3$ have the ability to move inside the lattice, resulting in the formation of dipoles.

Symmetry Breaking and Domain Structure

Ferroelectricity is characterized by the disruption of inversion symmetry, which occurs when the crystal structure does not possess a center of symmetry. The presence of broken symmetry leads to the formation of domains, which are distinct regions inside the material where the polarization is oriented in various directions. The emergence of these domains is a result of the disrupted symmetry and has consequences for the overall behavior of ferroelectric materials.

Phase Transitions and Landau Theory

Ferroelectric materials frequently experience changes in their phase as a result of temperature variations. These transitions entail modifications in the alignment of electric dipoles and are accompanied by changes in the symmetry of the crystal structure. The Landau theory offers a thermodynamic framework for comprehending ferroelectric phase transitions, in which the spontaneous polarization serves as the order parameter.

Ferromagnetism: Alignment of Magnetic Moments

Ferromagnetism is the second fundamental ferroic order observed in multiferroic materials, which is defined by the alignment of magnetic moments inside the material. Ferromagnetic materials have a parallel orientation of their magnetic moments, resulting in a macroscopic magnetic polarization.

Spin and Magnetic Moments

The fundamental basis of magnetism is in the characteristic of electron spin. Electron spin is a quantum characteristic that can be understood as an inherent rotational momentum. The magnetic behavior observed in materials is a result of the magnetic moment associated with electron spin.

Exchange Interactions and Curie Temperature

The orientation of magnetic moments is determined by exchange interactions, which result from the exchange of electrons between neighboring atoms. Ferromagnetic materials exhibit a propensity for parallel alignment, as it results in a lower energy state. The Curie temperature (T_c) is the temperature at which ferromagnetic order begins to appear.

Spin-Orbit Coupling and Magnetic Domains

Spin-orbit coupling, the interaction between the spin of an electron and its orbital motion, can play a role in the creation of magnetic moments. Strong spin-orbit coupling in certain materials can result in the emergence of magnetic moments, even without the presence of an external magnetic field. Ferromagnetic materials frequently display magnetic domains characterized by distinct orientations, which are separated by domain walls.

1.2.2. Mechanism of multiferroicity

Coupling mechanisms

The coexistence of ferroelectricity and ferromagnetism in multiferroic materials prompts inquiries into the underlying mechanics behind this captivating phenomenon. Multiple factors contribute to the interconnection of electric and magnetic characteristics in these materials:

Direct Coupling through magnetic ions

Within certain multiferroic materials, there exists a direct correlation between the magnetic moments of certain ions and the electric polarization. The orientation of magnetic moments affects the organization of charges in the crystal structure, leading to an overall electric polarization. An exemplary instance is $BiFeO_3$, in which the ferroelectric and magnetic states are interconnected via the iron (Fe) ions.

Spin-Orbit Interaction

Spin-orbit coupling, a phenomenon that connects the spin of electrons to their orbital motion, can have a substantial impact on multiferroicity. The interplay between electric and magnetic properties emerges due to the connection of electron spin and orbital angular momentum.

Charge-Magnetic Coupling

The interaction between electric charge and magnetic properties is an additional factor that contributes to the phenomenon of multiferroic activity. Variations in the distribution of electronic charge are directly connected to changes in magnetic order, leading to the simultaneous presence of ferroelectric and ferromagnetic characteristics.

Geometric Frustration

The presence of geometric frustration, which arises from the arrangement of atoms in the crystal lattice, can play a role in the development of multiferroicity. Complex magnetic structures that coexist with ferroelectricity can arise from frustrated magnetic groupings. The rivalry among various magnetic interactions inside the lattice contributes to the formation of multiferroic characteristics.

1.2.3. Types of multiferroics

Typically, multiferroic materials are classified into two primary categories depending on how ferroelectricity and ferromagnetism coexist [14]:

Type-I multiferroics

Type-I multiferroic materials have simultaneous ferroelectric and ferromagnetic ordering in their lowest energy state. A prime example of a material in this category is $BiFeO_3$, in which the magnetic moments of iron ions are closely correlated with the electric polarization.

Type-II multiferroics

Unlike type-I multiferroics, type-II multiferroics do not exhibit both orders simultaneously in their lowest energy state. The multiferroic state is attained by means of an external stimulus, such as the application of an electric or magnetic field. $TbMnO_3$ and $HoMn_2O_5$ are classified as type-II multiferroics.

Out of the many different multiferroic materials, bismuth ferrite (BFO) is particularly remarkable and distinct. The unique combination of ferroelectric and magnetic properties, along with its perovskite crystal structure, gives BFO exceptional versatility and potential for revolutionary applications in the fields of electronics, spintronics, and multifunctional devices.

1.3. Introduction to Bismuth Ferrites

Bismuth ferrite, also known as $BiFeO_3$ or BFO, is an exceptional multiferroic compound owing to its dual-phase nature, which enables it to manifest antiferromagnetism (G-type) and ferroelectricity [15]. The crystal structure of BFO exhibits a perovskite-like configuration, consisting of oxygen atoms bridging the two lattice sites occupied by bismuth (Bi) and iron (Fe) ions as shown in figure 5. The distinctive multiferroic characteristics of the compound are due to this intricate arrangement.

The origin of the ferroelectricity in BFO may be traced back to the movement of oxygen ions inside the crystal lattice, which ultimately results in the formation of spontaneous electric dipoles. A net dipole moment is produced as a consequence of the off-center displacement of the bismuth and oxygen ions, which is the source of this polarization. In the case of BFO, the temperature at which this ferroelectric polarization goes through a phase transition is referred to as the ferroelectric Curie temperature (T_c), and it takes place at an extremely high temperature of 1120 K [16]. One of the factors that leads to the strong ferroelectric behavior of bismuth ferrite is the complicated interaction between crystal structure and electrical configurations. The ferromagnetic feature of bismuth ferrite is explained by the magnetic ordering of iron ions. For example, BFO displays antiferromagnetic (G-type) ordering, in which adjacent spins are antiparallel to one another. A Neel temperature (T_N) of 640 K is required for this magnetic ordering to take place. Because of its complicated spin and orbital interactions, BFO exhibits a precise equilibrium between antiferromagnetism and ferroelectricity, making it a unique contender for multifunctional applications. Dual ferroic bismuth ferrite has several applications due to its versatility. BFO is

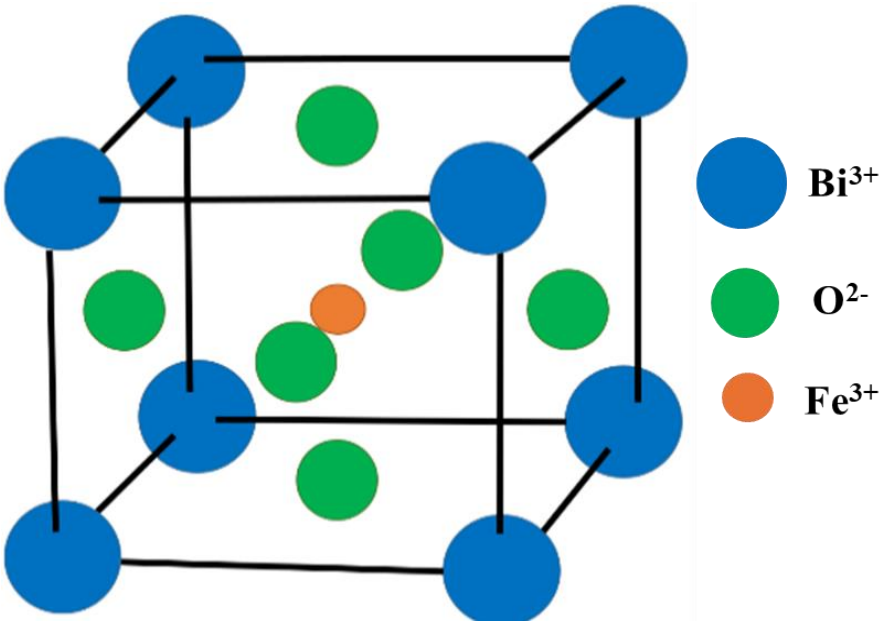

(Perovskite $BiFeO_3$structure)

Figure 5. Perovskite crystal structure of Bismuth Ferrite ($BiFeO_3$)

suitable for non-volatile memory, sensors, and energy harvesting because of its ferroelectric and antiferromagnetic characteristics. Applications in a wide temperature range are possible due to its high Curie temperature. Bismuth Ferrite is being investigated for spintronics, magneto-optical devices, and next-generation electronics.

In order to include Bismuth Ferrite (BFO) into magnetic devices, it is important to make any necessary adjustments to the antiferromagnetic properties that are intrinsic to the material. One of the most important techniques is element substitution, which is responsible for changing the antiferromagnetic nature of pure BFO into a ferrimagnetic condition that is more conducive to its use. The change in question involves the strategic substitution of components within the crystal lattice, with the goal of enhancing the magnetic characteristics of BFO so that it can be utilized more effectively in a variety of magnetic devices. It is well known that $(Bi,Ba)FeO_3$ (BBFO) [17], which is a derivative of BFO, demonstrates both ferromagnetism and ferroelectricity within a single phase, even at temperatures that are considered to be ambient. This makes it a prominent contender in this territory. However, in order to fully utilize the potential of BBFO in magnetic devices, there is continuing research that aims to improve its magnetic properties. These features include saturation magnetization (M_s), perpendicular magnetic anisotropy (PMA), and the magneto-optical Kerr rotation angle (Θ_k). These developments are essential for unlocking the full applicability of BBFO across a wide range of device applications. They also represent a significant step forward in the evolution of multifunctional materials within the realm of magnetic technology.

1.4. Application of BFO in Magnetic Devices

Within the domain of magnetic devices, the essential aspect that determines their functionality is the process of magnetization reversal. Bismuth ferrite (BFO) thin films, which are multiferroic, provide a highly efficient solution to this problem by allowing for the smooth alteration of magnetization using an electric field (figure 6). This innovative method not only greatly simplifies the structure of the gadget, but also eliminates the requirement for new materials, making it a cost-efficient alternative. The use of BFO based multiferroic thin films is advantageous due to their capacity to efficiently achieve magnetization reversal, leading to a significant transformation in the field of magnetic device design and manufacturing [18, 19, 20, 21, 22, 23].

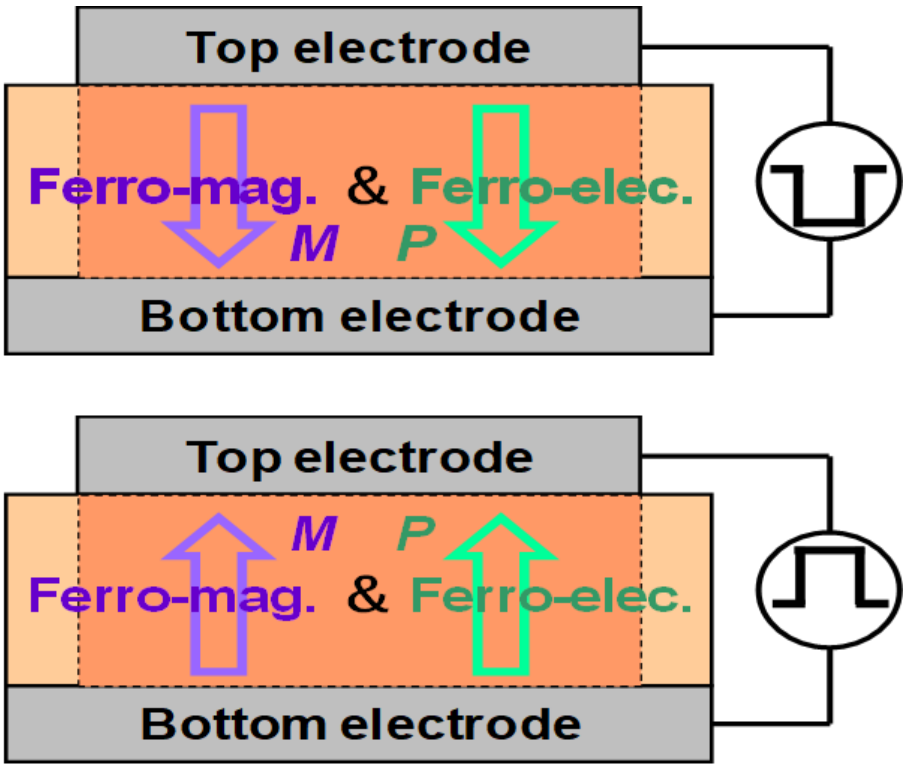

Figure 6. Schematic diagram of magnetization reversal by applied electric fields.

1.5. Previous Results

As part of our continuous endeavors to improve the film quality of $BiFeO_3$ (BBFO) for advanced applications in high-performance magnetic devices, we previously investigated the advantages of using pulsed DC reactive sputtering instead of RF sputtering as shown in figure 7. This method resulted in a significant enhancement in the magnetic saturation (M_s) value, increasing it from 60 to 90 emu/cm^3. Although this accomplishment is noteworthy, it did not meet the criteria for high-performance magnetic nano devices due to several key factors. These factors include a relatively low in-plane magnetic anisotropy (measured as the ratio of coercivity between the alignment of the film plane perpendicular and parallel to the applied field, $H_{c\perp}/H_{c//} = 0.8$), a modest Θ_k value of 0.03˚, and a transition temperature (T_c) of 350 ˚C [24]. Consequently, we tackled these difficulties by only using cobalt (Co) substitution in the B-site, in $Bi(Fe,Co)O_3$ thin films. Nevertheless, this method solely led to magnetic anisotropy within the plane, failing to attain the required enhancements. We achieved a significant advancement by successfully achieving perpendicular magnetic anisotropy (PMA) in thin films of $(Bi,La)(Fe,Co)O_3$ [25], shown in figure 8. These films

have a magnetization (M_s) value of 75 emu/cm^3, an out-of-plane coercivity ($H_{c\perp}$) of 4.0 kOe, a Θ_k value of 0.67˚, and a high Curie temperature (T_c) of 420 ˚C. We initiated a thorough investigation to explore the possibility of improving magnetic properties such as M_s, PMA, T_c, and Θ_k. We conducted an analysis where we replaced various lanthanides, such as lanthanum (La), neodymium (Nd), samarium (Sm), europium (Eu), gadolinium (Gd), dysprosium (Dy), and erbium (Er), in the A-site, all at concentrations that were optimal. The goal was to methodically investigate the influence of these substitutions on the attributes, with the intention of enhancing the performance of magnetic nano devices.

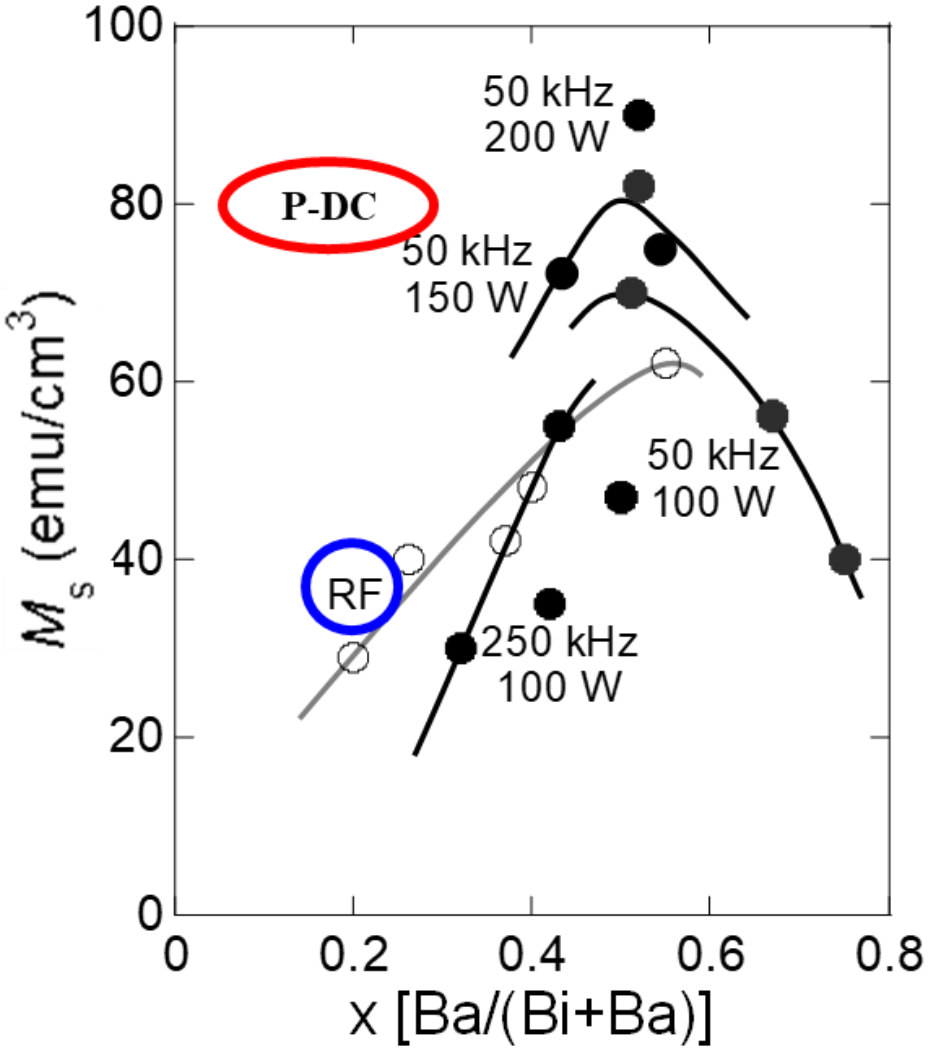

Figure 7. Magnetic properties in BBFCO thin films

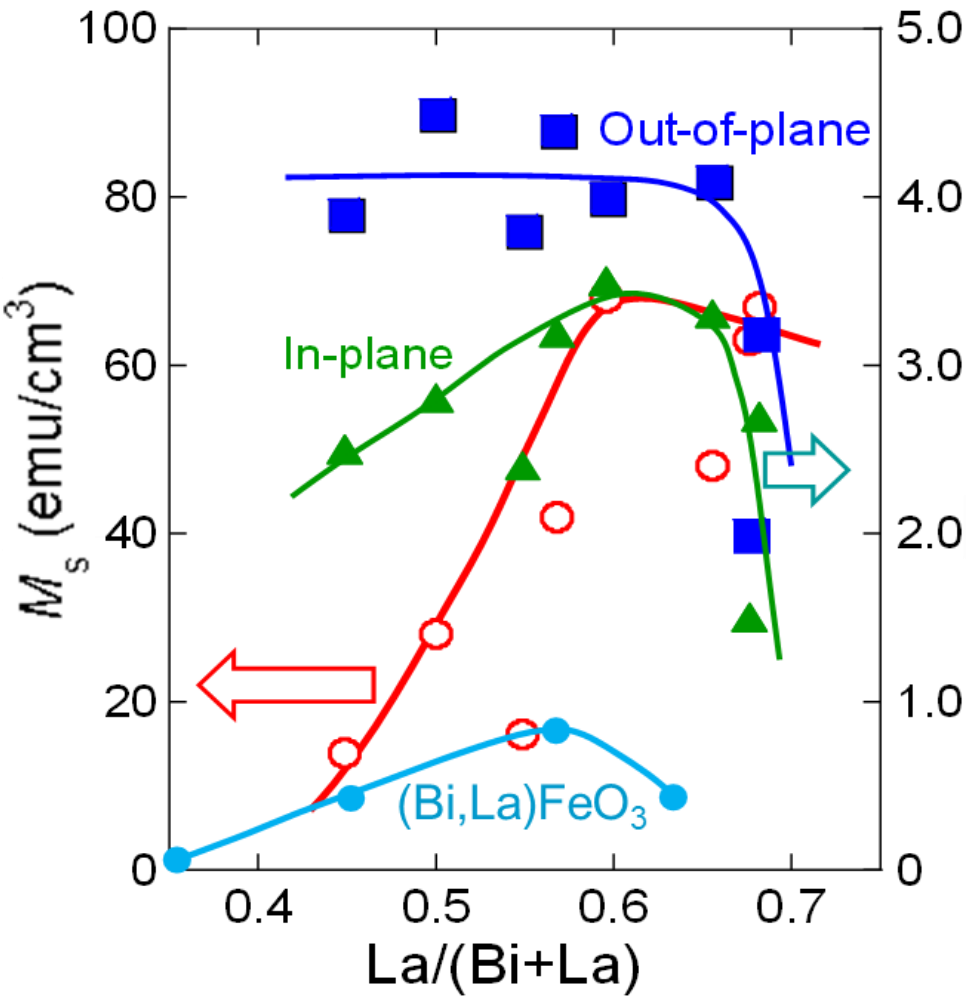

Figure 8. Magnetic properties in BLFO and BLFCO thin film

CHAPTER-2
Experimental Techniques

2.1. Introduction to Sputtering

Technological developments in materials science and nanotechnology have been fueled by the need to produce high-quality thin films with previously unheard-of precision and control. With its own set of features, sputtering has become a game-changer in the multitude of techniques accessible, revolutionizing the deposition of thin films. This scientific investigation explores the complexities of sputtering and clarifies why it is better than traditional techniques for producing thin-film quality that is superior [26].

Sputtering produces films with superior purity, homogeneity, and adherence above typical thin film deposition processes. Sputtering is excellent for a variety of substrates since it operates at lower temperatures than evaporation, which can damage sensitive materials. Sputtering's directed nature allows for detailed nanostructures, which are useful in microelectronics, photovoltaics, and medicinal devices. Sputtering is also known for its precise film thickness control. Researchers and engineers can accurately measure nanoscale thicknesses using tailored deposition rates and real-time monitoring and feedback systems. Thin film qualities determine performance in sophisticated semiconductor devices and sensors; hence this level of control is essential [27].

Sputtering Mechanism:

Physical vapor deposition (PVD) techniques like sputtering work by moving high-energy ions toward a target material and transferring their kinetic energy. This causes atoms or molecules to be ejected. Multiple sputtering systems exist for the purpose of depositing thin films. The dc diode sputtering system serves as the fundamental model for sputtering systems, with all subsequent systems being enhanced iterations of the dc diode sputtering system [28].

1. ***DC diode Sputtering***

The system has two planar electrodes, with one serving as the anode and the other as the cold cathode. The cathode serves as a base for the target material, and it is also equipped with a water-cooling system on its opposite side. Simultaneously, the anode serves as the base position for positioning the substrate. The application of argon gas and a sequence of voltage and resistance occurs between the diode and cathode. Highly charged Ar ions are accelerated to forcefully

dislodge particles from the target, resulting in the formation of a thin layer on the substrate. Positively charged Ar ions collide with the cathode, causing the ejection of cathode electrons or the sputtering of the target by transferring momentum to them. Electrons and negative ions, which have been released, are propelled by the electric field, and directed towards the anode, where they deposit onto the developing film.

2. ***RF Radio Sputtering:***

The DC diode has been modified to create the RF radio sputtering system, in which an insulator is employed as the metal target. Sputtering is unable to sustain the glow discharge in this system due to the accumulation of positive ions that create a surface charge on the front side of the insulator. To maintain the luminosity, the power source for the direct current diode is substituted with the radio frequency power supply. The term used to describe this phenomenon is RF radio sputtering.

3. ***Magnetron Sputtering:***

This technique is an advanced method of depositing material by creating and confining a gaseous plasma in a region that contains the target. The high-energy ions cause the erosion of the target surface within the plasma, leading to the release of atoms. Subsequently, free atoms travel the vacuum and adhere to the target substrate, resulting in the formation of a thin film. Generating gaseous plasma requires the use of a high voltage application. The electrons within the gas undergo acceleration away from the cathode and subsequently collision with adjacent atoms. An electrostatic repulsion arises from the collision that expels electrons from the sputtering gas atoms, transforming them into ions. Currently, the ions with a positive charge swiftly move towards the cathode and forcefully crash with the target surface. These impacts can result in the ejection of surface atoms into the vacuum environment, carrying sufficient kinetic energy to reach the substrate and create thin films. To maximize the number of collisions with high energy and increase the rate at which particles are deposited, it is crucial to select a sputtering gas with the largest molecular weight available, such as xenon or argon. To achieve reactive sputtering, the sputtering chamber can also utilize gases such as nitrogen or oxygen. Magnetron sputtering offers several advantages over physical vapor deposition methods due to its independence from the melting and evaporation of the target material. Materials of any melting temperature can be deposited. The source material can be easily scaled and positioned anywhere in the sputtering changer to meet the

specific coating or substrate needs. In addition, it is possible to achieve alloys and complex film deposition.

Pulsed – DC (p-DC) Reactive sputtering with Very VHF Plasma:

The introduction of p-DC reactive sputtering in the field of thin film deposition techniques signifies a significant advancement in terms of both effectiveness and accuracy. This method, based on the fundamental principles of magnetron sputtering, incorporates a pulse direct current (p-DC) component that not only aligns with the current mechanisms but also enhances the entire process to a higher level. This study also examined the unique characteristics of p-DC reactive sputtering that distinguish it from other methods. It emphasizes its ability to reduce arc current, provide precise temperature control, and improve crystallization as shown in Figure 9. The sputtering machine (Eiko, ES-360-AK) used for our study is shown in figure 10.

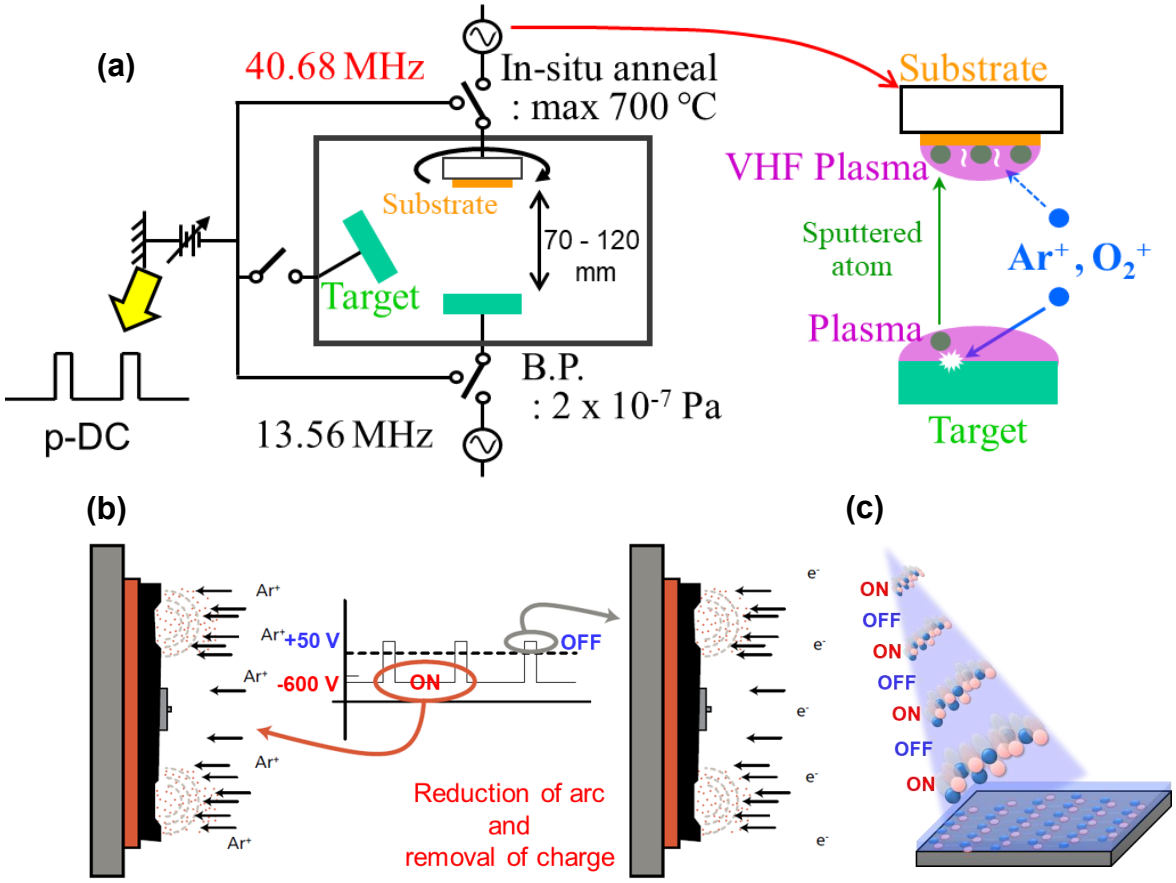

Figure 9. (a) Schematic diagram of sputtering, (b) and (c) schematic diagram of p-DC

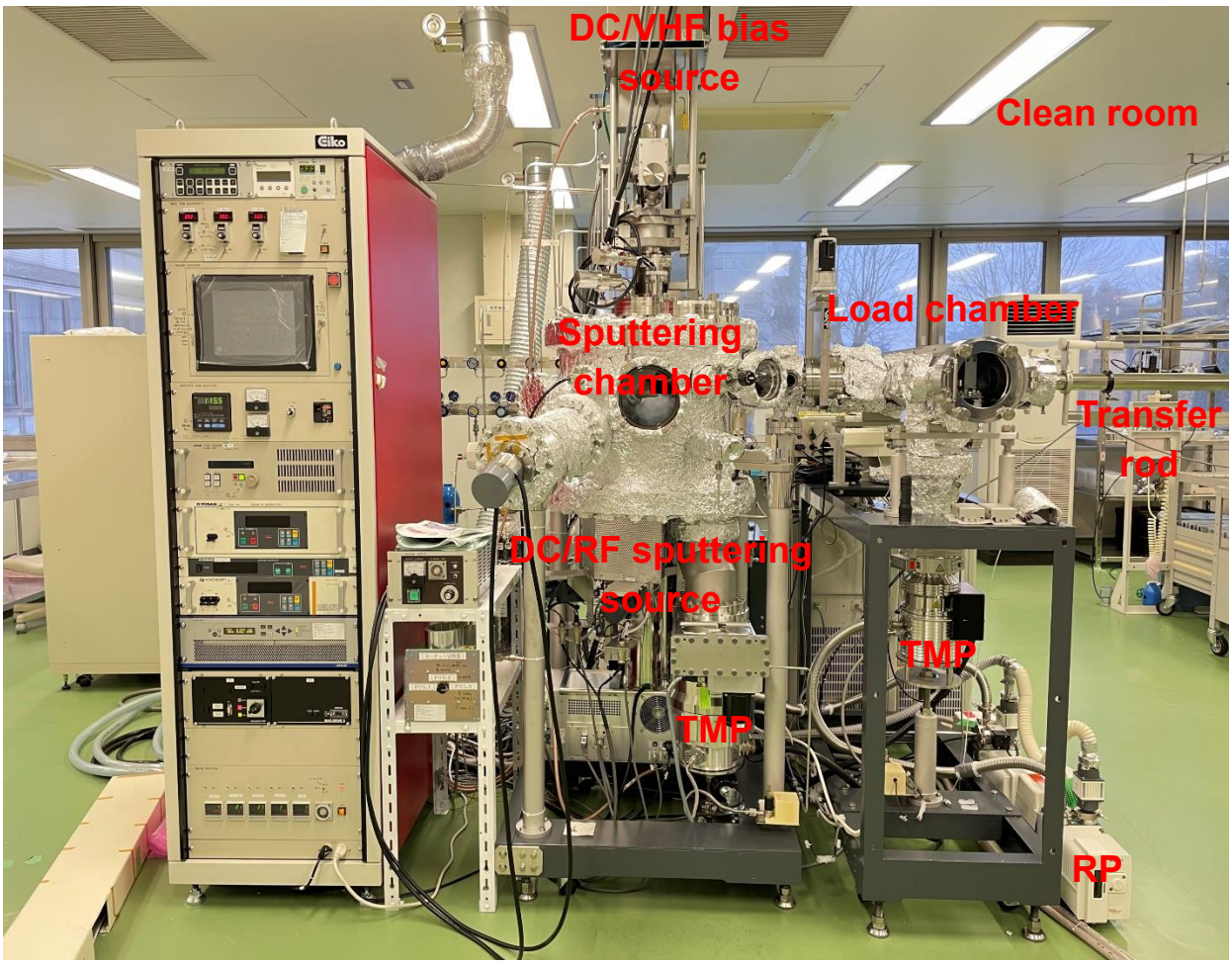

Figure 10. Image of sputtering machine

2.2. Synthesis of High-Quality Film Samples

UHV sputtering apparatus (Eiko, ES-360-AK) was used to deposit Ta (5 nm)/Pt (100 nm)/(Bi,*L*)(Fe,Co)O_3 (*L*: Lanthanides) (200 nm) multilayers onto a thermally oxidized Si wafer. After dry-etching for cleaning of the substrate surface, the Ta seedlayer with 50 W normal DC power, Pt underlayer with 100 W RF power and (Bi,*L*)(Fe,Co)O_3 layer with 150 W pulse-DC power were deposited. To achieve the crystal grain formation of the $BiFeO_3$ phase, reactive pulsed DC (p-DC) sputtering of the (Bi,*L*)(Fe,Co)O_3 thin films was carried out with a 5 W electric power and very high frequency (VHF) (40.68 MHz) plasma irradiation [29]. A frequency of 100 kHz was set for the pulsed DC operation.

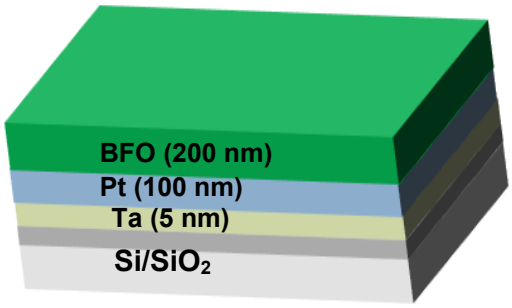

Figure 11. Schematic diagram of fabricated BFO based thin films with substrate, underlayers and electrodes.

2.3. Film Characterizations

2.3.1. X-Ray Diffraction (XRD)

X-ray Diffraction (XRD) is a crucial technique in materials science and crystallography, offering unprecedented insights into the atomic and molecular structures of crystalline materials. X-ray diffraction (XRD) is a highly advanced analytical technique that originated from the observation of the diffraction phenomenon by Max von Laue in 1912. It is used to determine the internal arrangement of atoms in a substance.

Working principle of XRD

The fundamental basis of XRD is in the interaction between X-rays and crystalline formations. Monochromatic X-rays experience diffraction when they hit a crystalline sample because of the periodic arrangement of atoms in the crystal lattice. Bragg's Law states that when X-rays are dispersed, they undergo constructive interference at certain angles, resulting in a diffraction pattern that reveals the crystal's internal arrangement. Subsequently, the diffraction pattern is captured by a detector, and mathematical techniques are utilized to convert this pattern into a three-dimensional map of electron density. This map offers comprehensive data regarding the spatial arrangement of atoms within the crystal lattice, enabling researchers to infer crystallographic factors such as the size of the unit cell, the symmetry of the crystal, and the existence of impurities or defects. XRD is a non-destructive and extremely sensitive method used to investigate the properties of crystalline materials.

The relationship between them can be expressed by Bragg's law given as relation (figure 12).

$$2dSin\theta = n\lambda$$

Where n is an integer, λ is the wavelength of X-ray, d is the lattice inter-atomic spacing, and θ is the diffraction angle [30].

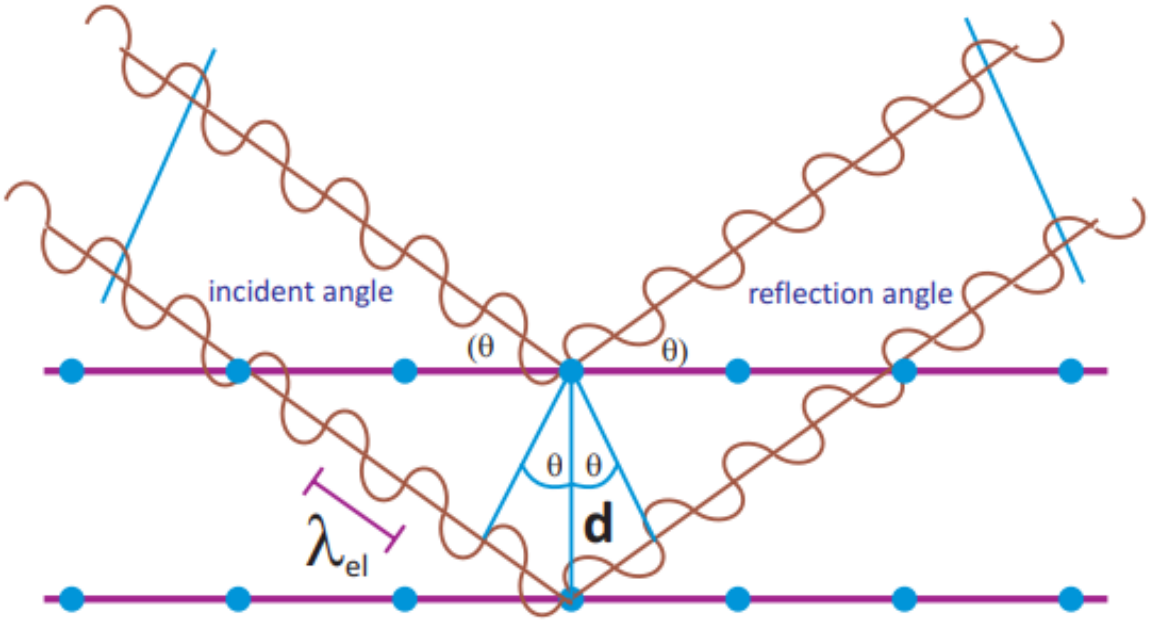

Figure 12. Schematic diagram of Bragg's diffraction

In this study, we have used the instrument BRUKER, D8 ADVANCE X-ray Diffractometer (Figure 13) for the determination of the XRD pattern of prepared thin film samples. The instrument was operated at 40mA and 40kV. The samples were scanned from Bragg's angle 20˚ to 80˚. The measurement was carried out using a target of Cu-Kα (λ= 1.5418Å) X-Ray beam with a Ni filter and the detector maintaining a step size of 0.05° at a scan rate of 2.5°/min.

Figure 13. Image of XRD machine

2.3.2. Field Emission Scanning Electron Microscopy (FESEM)

Field Emission Scanning Electron Microscopy (FESEM) is an advanced imaging technology that provides exceptional resolution and allows for detailed examination of the nanoscale structure of materials. FESEM is based on the principles of electron microscopy, however it stands out by using a field emission electron source. FESEM, in contrast to traditional SEM, utilizes a sharp metal tip or a field emitter to produce a tightly focused electron beam, instead of relying on

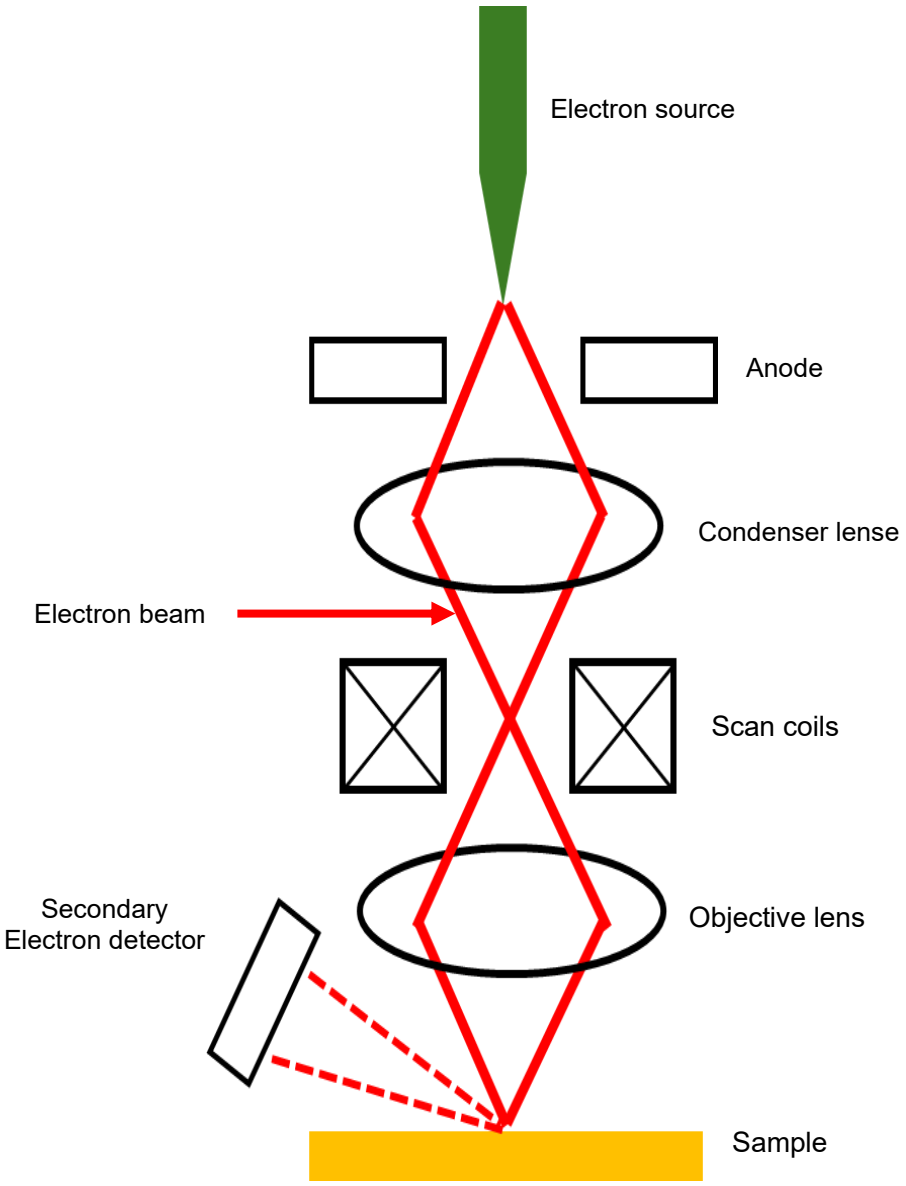

Figure 14. Schematic diagram of FESEM instrument

Figure 15. Image of FESEM instrument

electrons generated from a heated tungsten filament. The field emission process allows for the generation of electron beams with very small diameters, resulting in spatial resolutions at the sub-nanometer level. FESEM, or Field Emission Scanning Electron Microscopy, is a highly advanced technique that combines powerful detectors and excellent imaging capabilities. It allows for a thorough analysis of the surface characteristics, structure, and composition of specimens. The core concept of FESEM is based on utilizing the quantum mechanical phenomenon of field emission to attain unparalleled imaging resolutions, enabling a thorough comprehension of materials at the nanoscale. The schematic diagram of the FESEM is shown in figure 14. The FESEM instrument (JEOL, JSM-7800) used in our study (figure 15).

2.3.3. Energy Dispersive X- ray (EDX)

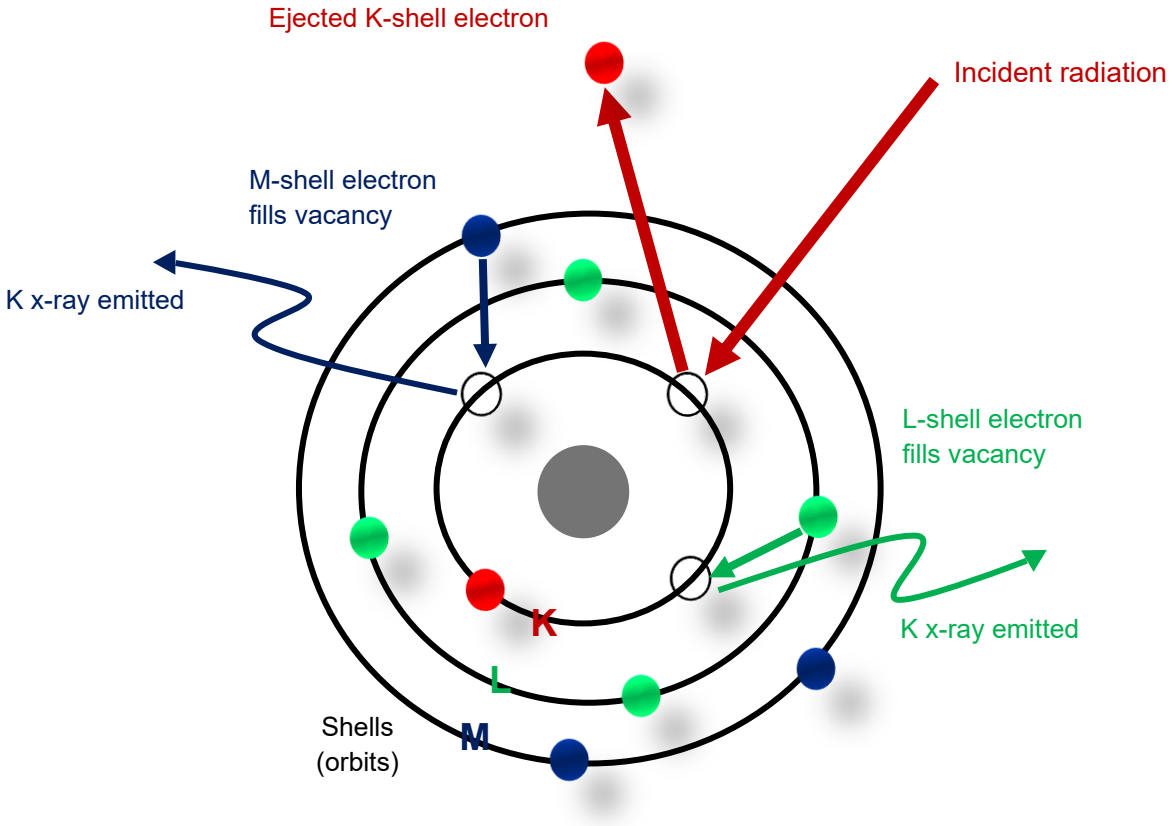

Figure 16. Schematic diagram of X-ray emission in EDX

Energy-Dispersive X-ray Spectroscopy (EDX) is an essential analytical technique commonly combined with electron microscopy to perform elemental analysis of materials at the micro and

nanoscale. EDX, when used alongside SEM, allows for the detection and measurement of elements in a sample by capturing the emitted X-rays that occur when the electron beam interacts with the specimen (refer figure 16). The underlying idea of EDX is based on the relationship between the energy of emitted X-rays and the elemental content of the material. When the incident electrons collide with the sample, they cause the ejection of inner-shell electrons. This leads to further relaxation processes, resulting in the emission of X-rays that are particular to the elemental elements. EDX captures and analyzes X-rays to produce spectra that disclose the elemental composition and distribution within the examined area.

2.3.4. Vibrating Sample Magnetometer (VSM)

A Vibrating Sample Magnetometer (VSM) is a sophisticated and adaptable apparatus extensively employed in the domains of material science and physics to explore the magnetic characteristics of materials. This instrument is highly effective in providing significant insights into the behavior of magnetic materials. It enables researchers to analyze important parameters such as magnetic susceptibility, saturation magnetization, and hysteresis loops. The VSM functions by detecting the alteration in vibration frequency of a minute magnetic specimen when subjected to or modified by an external magnetic field.

The hysteresis loop is a key characteristic of magnetic materials that describes the correlation between magnetic induction (B) and magnetic field strength (H) as shown in figure 17. The VSM possesses exceptional capacity to measure and analyze hysteresis loops with utmost accuracy. In a standard VSM experiment, a specimen is placed on a vibrating platform inside a consistent magnetic field. The sample's vibration frequency is methodically recorded as the external magnetic field is adjusted, due to the magnetic response induced by the field variations. The purpose of this data is to create the hysteresis loop, which visually represents the magnetic properties of the material as they change in different settings.

The hysteresis loop acquired via VSM measurements is essential for comprehending the magnetic characteristics of various materials. It offers crucial data regarding a material's magnetic stability, coercivity, remanence, and other vital properties. Scientists and engineers utilize this data to evaluate the appropriateness of materials for different applications, such as in the creation of magnetic devices, memory storage, and other technological progressions. VSM also provides the capability to investigate the temperature dependency of magnetic characteristics, in addition to

conducting hysteresis loop research. This feature is extremely helpful for understanding the thermal stability, phase transitions, and curie temperature of magnetic materials.

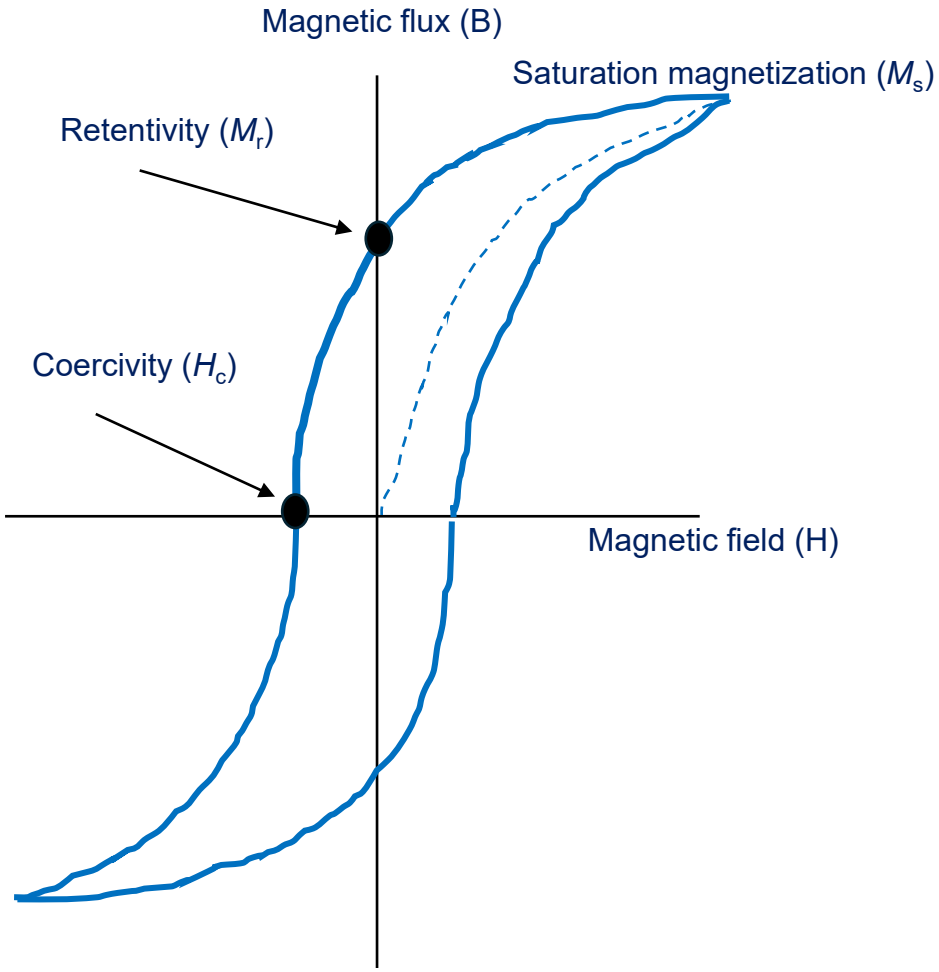

Figure 17. Schematic diagram of magnetic hysteresis curve.

In this study, the Toei VSM-5S (figure 19) emerged as a crucial tool for precise magnetic property measurements. The amazing capacity to increase the magnetic field up to 20 kOe allowed for thorough evaluations of both in-plane and out-of-plane magnetization in thin films. The VSM allowed for temperature-dependent studies across a wide range, spanning from 0 ˚C to a maximum of 500 ˚C. A notable characteristic worth mentioning is the ability to modulate the magnetic field rotationally, which enables precise measurements at different angles and enhances the range of

magnetic property evaluations in various field applications. The schematic diagram of VSM is shown in figure 18.

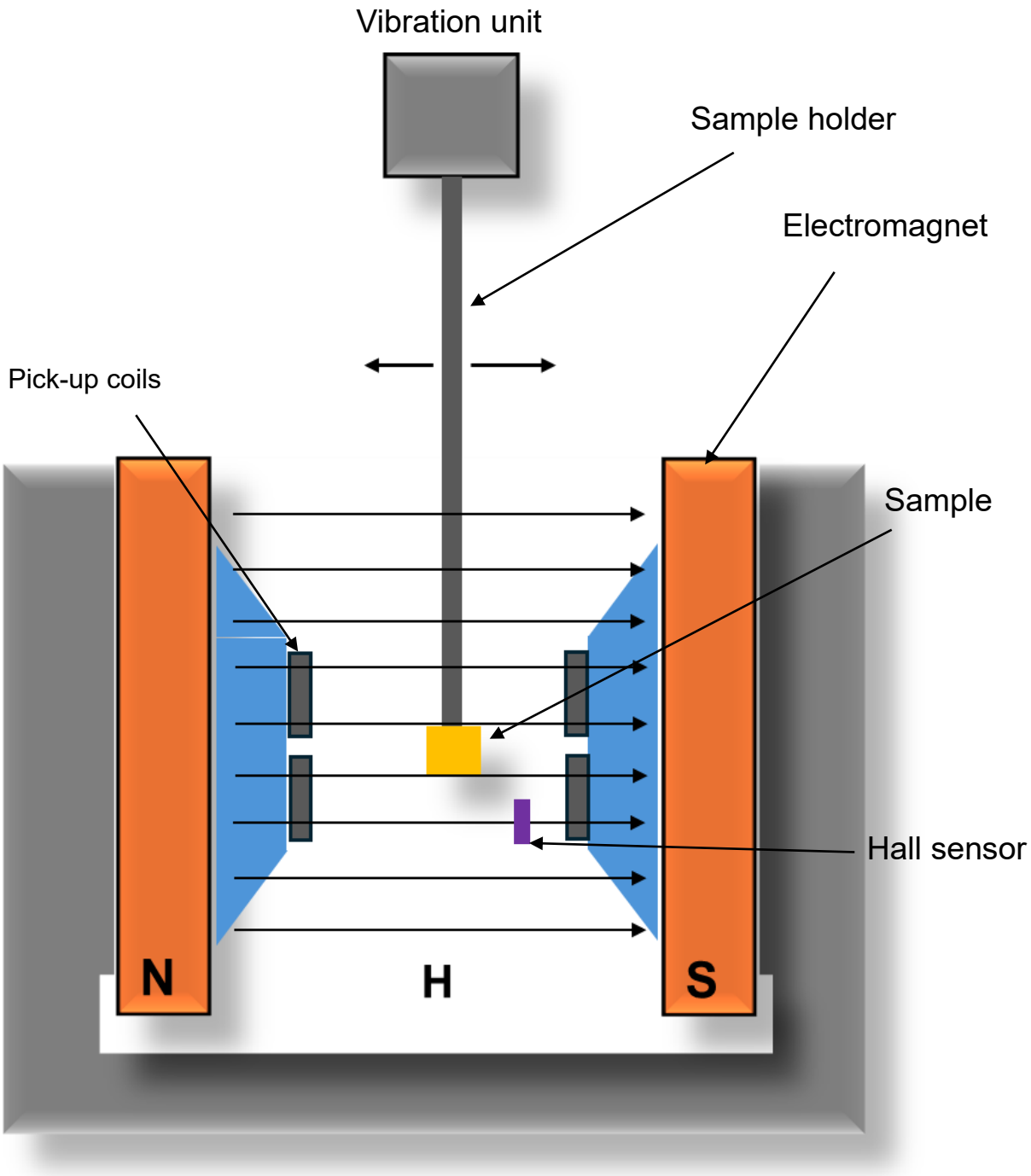

Figure 18. Schematic diagram of VSM instrument

Figure 19. Image of VSM instrument.

2.3.5. Magneto – Optic Kerr Effect (MOKE)

The Magneto-Optical Kerr Effect (MOKE) is a very effective and non-invasive method extensively utilized in the realm of condensed matter physics and materials research to study the magnetic characteristics of surfaces and thin films. MOKE offers significant insights into the kinetics of magnetization and the magnetic anisotropy of materials. This method exploits the interaction between light and magnetization, providing a distinctive way to investigate the magnetic properties of materials with great sensitivity. Figure 20 shows the schematic diagram of MOKE.

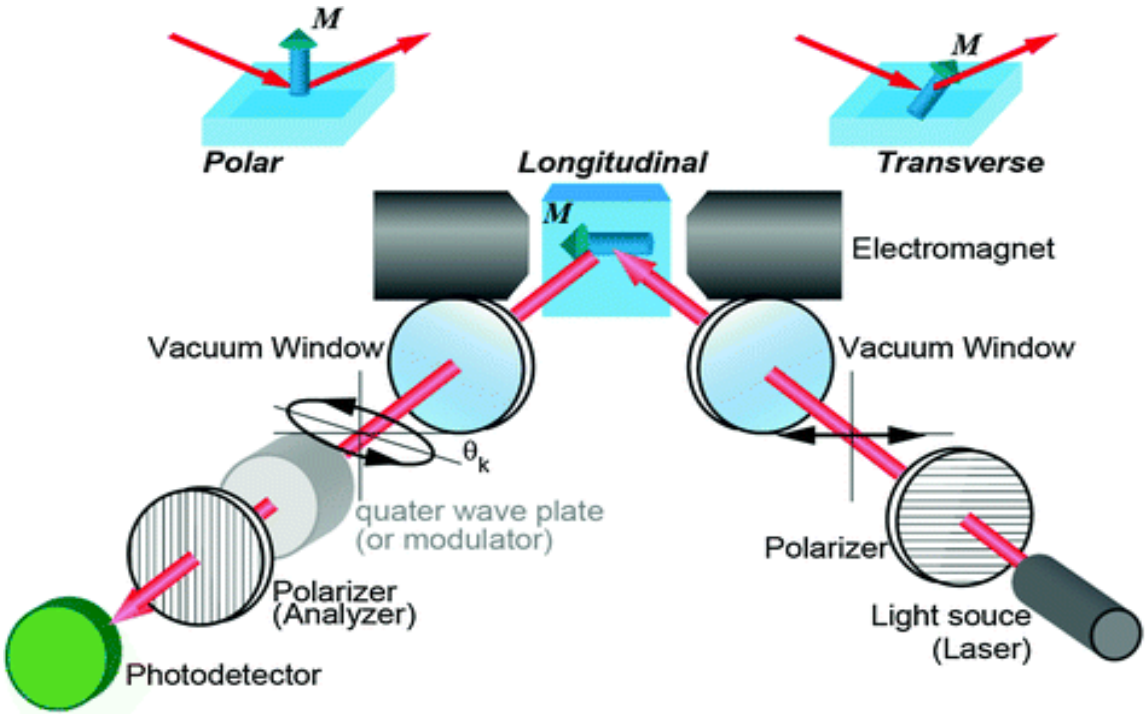

Figure 20. Schematic diagram of MOKE instrument

(**Image courtesy:** T. Nakagawa, *surface magneto optic kerr effect*, 2018)

The working principle of MOKE is as follows:

The underlying idea of MOKE is that the polarization state of reflected light undergoes changes upon interaction with a magnetized surface. The basic procedure entails illuminating a magnetic sample with polarized light and then examining the alterations in the polarization state of the reflected light. MOKE can be classified into two primary categories: longitudinal MOKE (LMOKE) and transverse MOKE (TMOKE).

LMOKE: In LMOKE, the incident light is oriented in the same direction as the magnetism. When the polarized light comes into contact with the magnetic sample, it experiences a rotation in its polarization state, which is referred to as the Kerr rotation angle. The extent of this rotation is

closely correlated with the magnetization of the sample. Subsequently, a detector gauges the Kerr rotation, yielding insights into the magnetic characteristics of the substance.

TMOKE: In TMOKE is a phenomenon where light is directed at a right angle to the direction of magnetism. The light that is reflected undergoes a modification in its elliptical shape, which is referred to as the Kerr ellipticity. Like LMOKE, the Kerr ellipticity is directly proportional to the magnetization of the sample.

MOKE can measure magnetic properties like VSM. But it has merits as well as demerits against VSM.

Merits of MOKE against VSM

- Measurement time of hysteresis curve is very short. MOKE takes several seconds whereas VSM takes several minutes.
- Cutting of measuring samples is not required. Any size of sample can be measured.
- Analysis of magnetic domain is possible in MOKE.
- Local hysteresis curve can also be measured. Minimum size of several μm can be measured in MOKE.

Demerits of MOKE against VSM

- Measurement with various directions is difficult.
- Measurement of the absolute value of magnetization is impossible.
- Kerr effect depends on materials.
- Kerr effect depends on wavelength of laser.

In this study, MOKE measurement equipment; NEOARK, BH-P920- EM (refer figure 21) with the magnetic field perpendicular to film plane was used to measure the magneto-optical Kerr rotation angle (Θ_k-H) curves. A maximum magnetic field of 10 kOe can be applied to this equipment.

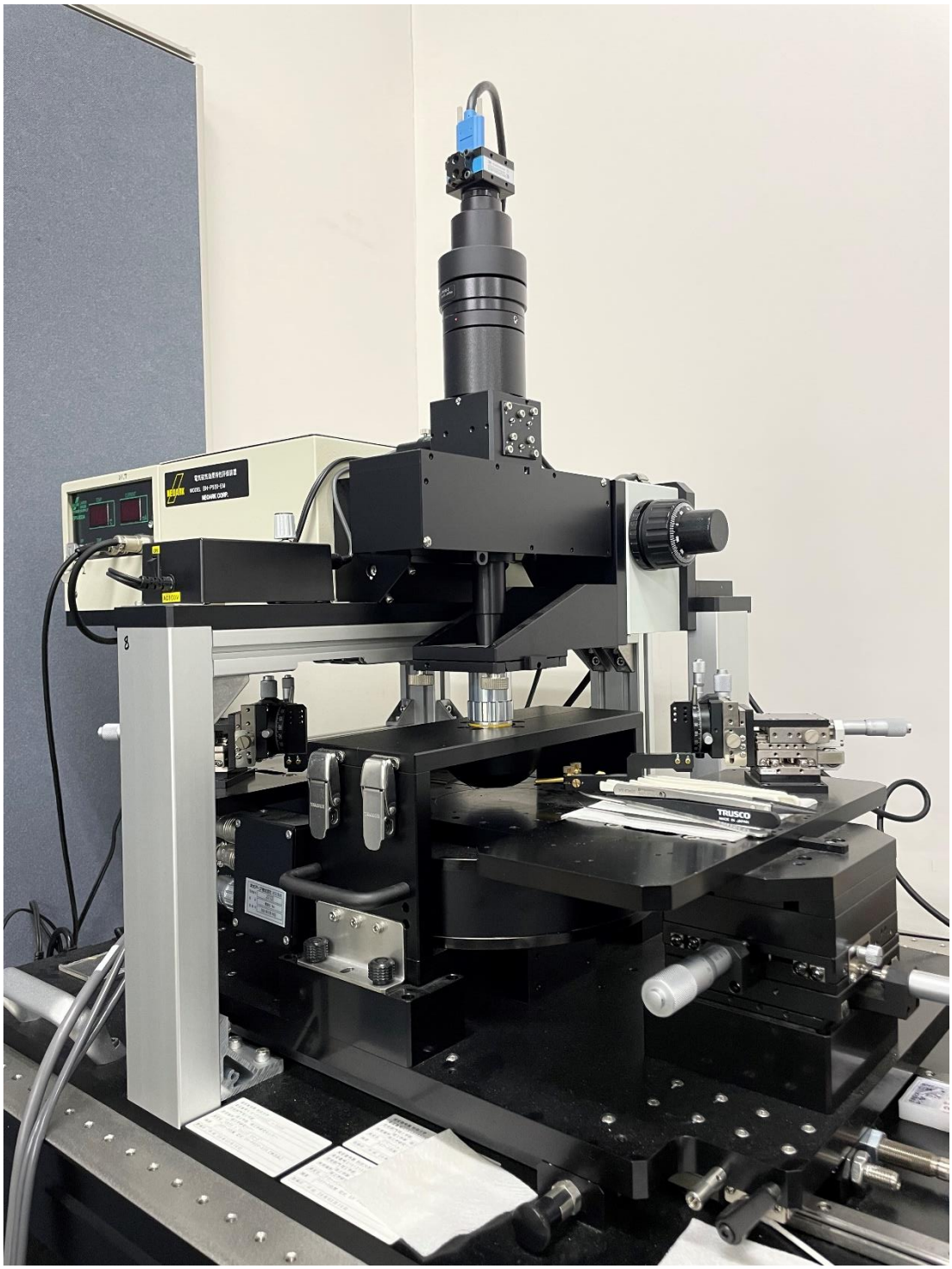

Figure 21.Image of MOKE instrument

2.3.6. Atomic Force Microscopy (AFM)

Atomic Force Microscopy (AFM) is a precise imaging technique that provides high-resolution study of surfaces. It is a non-optical method that serves as a powerful instrument for surface measuring. AFM enables accurate and non-invasive assessments of the surface properties of a sample, including topography, electrical conductivity, magnetic behavior, chemical composition, optical characteristics, mechanical attributes, and more, with exceptional resolution.

Working Principle of AFM

The fundamental operational principle of a conventional AFM system with optical feedback is scanning an AFM probe, equipped with a sharp AFM tip, in a raster pattern across the surface of a material. The AFM tip is typically composed of either silicon or silicon nitride and is incorporated in close proximity to the unfixed end of a pliable AFM cantilever. A piezoelectric ceramic scanner is responsible for regulating the horizontal and vertical position of the AFM probe in relation to the surface. As the Atomic Force Microscope (AFM) tip scans across objects of varying heights, the deflection of the AFM cantilever undergoes alterations. The laser beam, which is reflected off the back side of the AFM cantilever, is used to monitor and measure the deflection. It is then directed into a photodetector that can detect the position of the beam with high accuracy. A feedback mechanism regulates the vertical movement of the scanner to ensure a consistent deflection of the AFM cantilever, hence maintaining a constant contact force. The AFM tip records the coordinates it tracks during the scan, which are then used to create a three-dimensional topographic representation of the surface. Figure 22 shows the schematic diagram of AFM. The AFM instrument (SII, SPI3800N) used in our study is shown in figure 23.

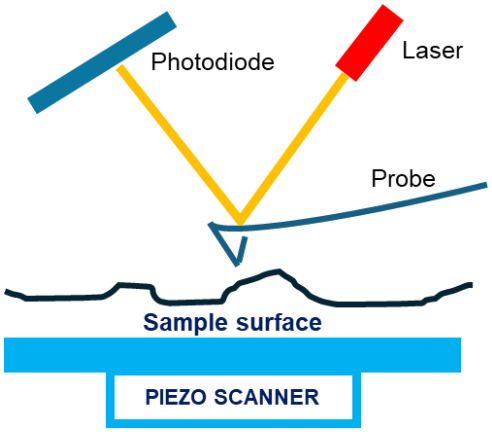

Figure 22. Schematic diagram of AFM

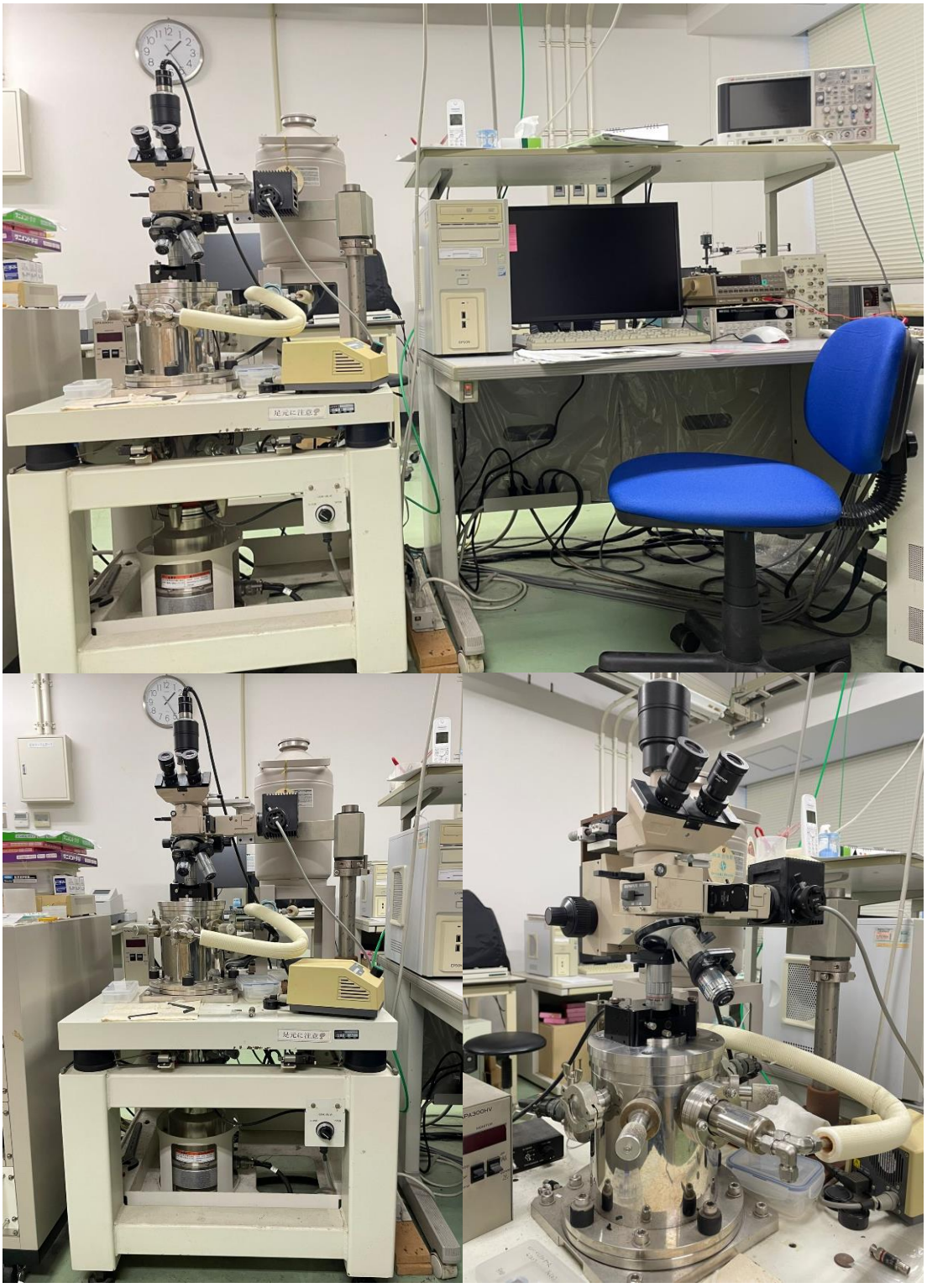

Figure 23. Image of AFM instrument

AFM Operation Modes

The Atomic Force Microscope utilizes two primary methods for imaging surface topography: Static or Contact Mode and Dynamic Mode. The Dynamic Mode of Atomic Force Microscopy (AFM) can be classified into two categories: Tapping or Intermittent Contact Mode and Non-Contact Mode, based on the forces involved in the contact between the AFM tip and the surface.

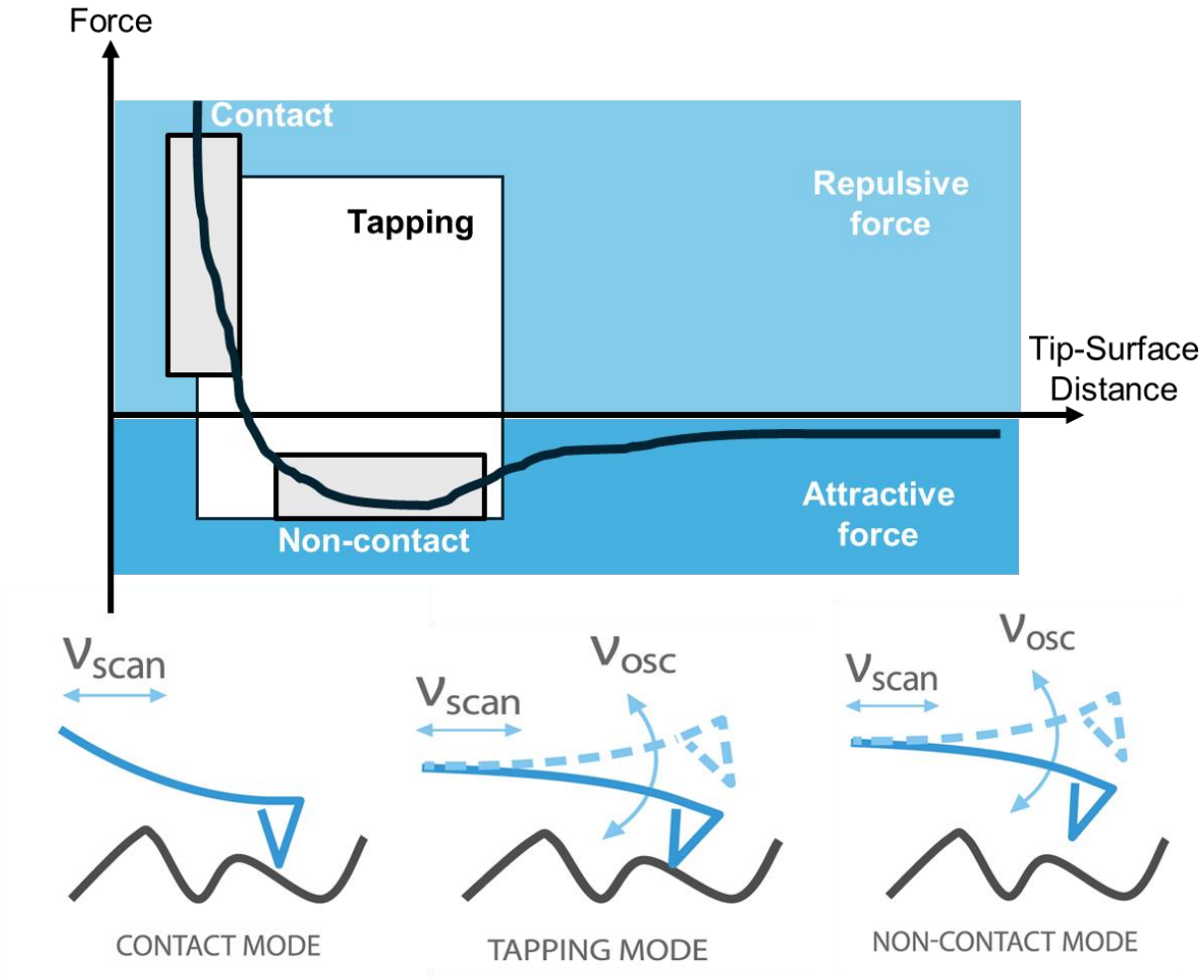

Figure 24. Interaction forces in AFM at different modes

In Contact Mode, the AFM probe tip is moved around the sample surface while ensuring continuous contact with it (figure 24). The purpose of the feedback system is to ensure a consistent deflection of the AFM cantilever, which in turn maintains a constant contact force. The interactions between the atomic force microscopy (AFM) tip and the surface exhibit a repulsive nature, as depicted in Figure 24. Soft atomic force microscopy (AFM) cantilevers, with force constants of

1N/m or less, are commonly employed to prevent wear and surface damage to the AFM tip, while simultaneously enhancing sensitivity. One of the primary disadvantages of Contact Mode operation is that the AFM tips on soft AFM cantilevers are prone to both lateral forces and adhesion to the surface contamination layer that is often found on most surfaces in ambient air. These lead to visual distortions. Furthermore, the application of sideways pressures can cause harm to both the AFM probe tip and delicate materials.

In Tapping Mode, the AFM probe cantilever is vibrated by a piezoelectric actuator at or close to its fundamental resonance frequency, typically ranging from several tens to several hundred kilohertz. The AFM probe is positioned in close proximity to the sample surface, with the tip of the probe making modest contact near the lower end of the AFM cantilever oscillation (Fig. 24), causing a reduction in the amplitude of its oscillation. The feedback loop ensures a consistent amplitude of oscillation for the AFM cantilever, hence maintaining a constant contact force. The dominant forces governing the contact between the AFM tip and the surface are repulsive. Stiff atomic force microscopy (AFM) cantilevers, with force constants ranging from 10 to 100N/m and high resonance frequencies exceeding 190kHz, are employed for typical Tapping Mode operation. These AFM cantilevers are not prone to adhesion to the surface when conducting measurements in the surrounding air. Softer atomic force microscopy (AFM) cantilevers with force constants below 10N/m, and occasionally as low as sub-0.1N/m, are utilized to measure soft samples such as living cells.

In Non-Contact Mode, the AFM cantilever is vibrated at or close to its resonance frequency with a smaller amplitude (1nm or less) compared to Tapping Mode. The AFM probe tip is maintained at a distance ranging from several nanometers to several tens of nanometers away from the surface in the area where attractive interaction forces occur (Fig. 24). In certain instances, the feedback loop sustains a consistent oscillation frequency of the AFM cantilever, hence maintaining a constant contact force (FM-AFM). This technique enables more accurate force manipulation and provides exceptionally detailed images in a liquid medium. The primary benefit of Non-Contact Mode is its ability to minimize the level of interaction between the tip and the surface of the sample. Minimal contact forces contribute to the preservation of AFM tip sharpness and the attainment of high resolution. The drawback lies in the difficulty of maintaining the AFM tip in the attractive

regime. Close proximity between the tip and surface requires the use of advanced feedback controls to achieve optimal performance.

2.3.7. Magnetic Force Microscopy (MFM)

Magnetic Force Microscopy (MFM) is a cutting-edge imaging technology that has become crucial in the examination of magnetic structures at the nanoscale. Magnetic force microscopy (MFM) is a technique that utilizes atomic force microscopy (AFM) to investigate local magnetic fields at the nanoscale. It involves using an AFM tip coated with a magnetic material to obtain high-resolution images that depict the magnetic properties of the samples. Magnetic Force Microscopy (MFM) enables researchers to observe and chart magnetic domains and interactions with amazing precision, rendering it an indispensable instrument in disciplines including materials science, nanotechnology, and magnetic data storage. Figure 25 shows the schematic diagram of MFM.

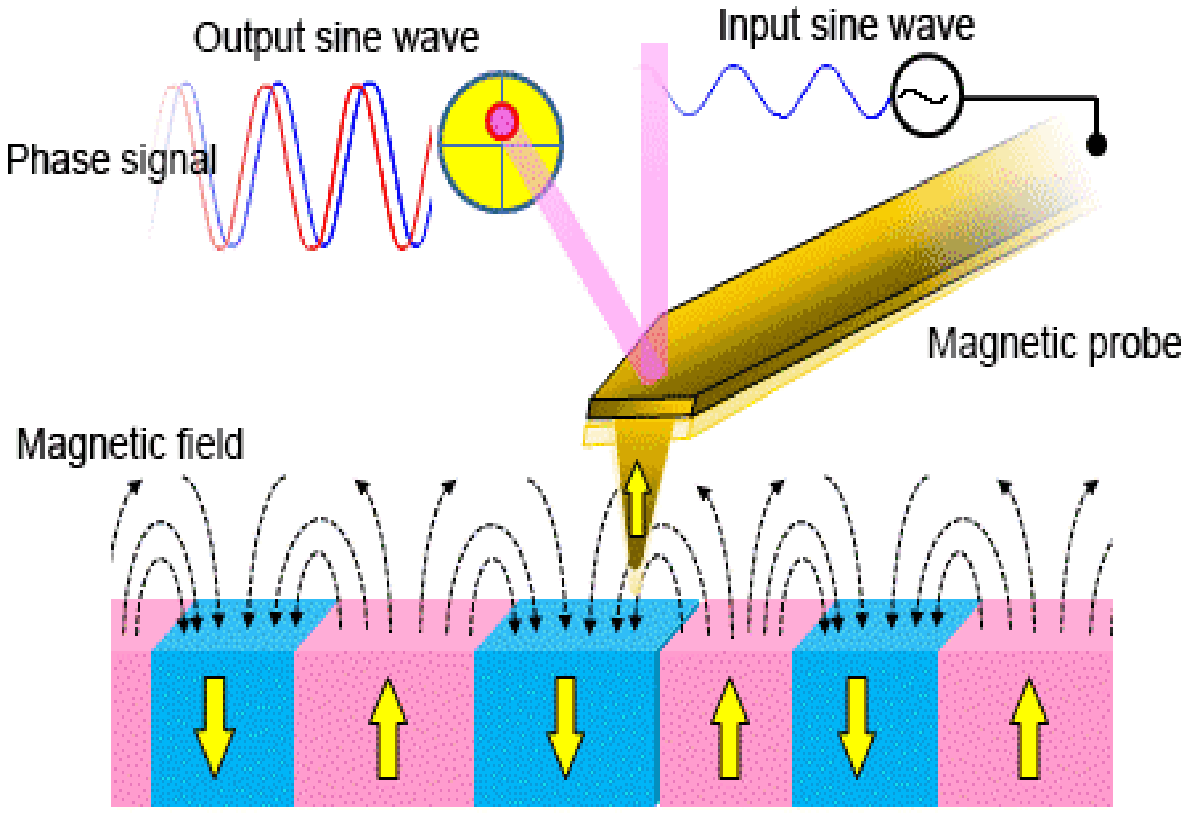

Figure 25. Schematic diagram of MFM

(**Image courtesy:** S. V. Kontomaris et al., atomic force microscopy on biological materials related to pathological conditions, 2019)

2.4.8. Electrostatic Force Microscopy (EFM)

Electrostatic force microscopy (EFM) is a technique used to measure the electrical properties of a sample surface. It does this by measuring the electrostatic force that occurs between the surface and a biased atomic force microscopy (AFM) tip. EFM utilizes voltage to create a potential difference between the tip and the sample, while the cantilever oscillates over the surface without making physical contact. While scanning the surface of the sample, the existence of electrostatic forces causes a modification in the amplitude and phase of oscillation in the vertical deflection signal (figure 26). Hence, the resultant EFM amplitude and phase images encompass data regarding electrical characteristics such as the surface potential and/or the distribution of charge on the sample surface. In EFM, the electrostatic force between the biased tip and the sample is the important force for imaging the electrical characteristics of the sample surface. Furthermore, apart from the electrostatic force, there are also short-range van der Waals forces that occur between the tip and the surface of the sample. The van der Waals forces are utilized for the purpose of quantifying the surface topography.

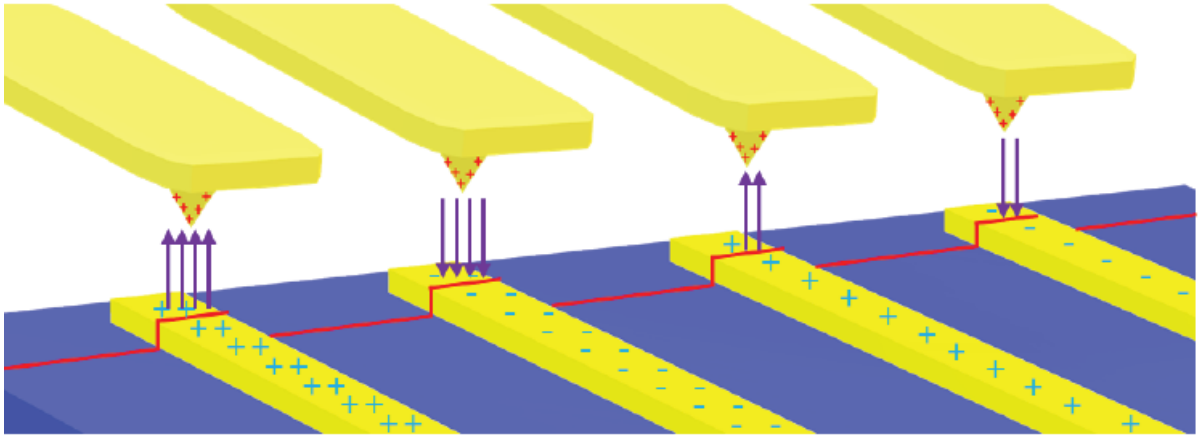

Figure 26. Electrostatic force acting between a metal-coated tip and locally charged domains on the sample surface.

(**Image courtesy:** www.parksystems.com)

2.3.9. X-ray Photoelectron Spectroscopy (XPS)

X-ray Photoelectron Spectroscopy (XPS), alternatively referred to as Electron Spectroscopy for Chemical Analysis (ESCA), is a highly effective method for analyzing the surface properties of materials, widely utilized in the fields of materials science, chemistry, and physics. X-ray photoelectron spectroscopy (XPS) allows researchers to examine the surface of a material and determine its elemental makeup, chemical state, and electronic structure. X-ray Photoelectron Spectroscopy (XPS) is a technique that uses X-ray light to stimulate electrons and examine the emitted photoelectrons. The schematic diagram of generation of photoelectron is shown in figure 27. This method is highly beneficial for studying the surface chemistry of various materials.

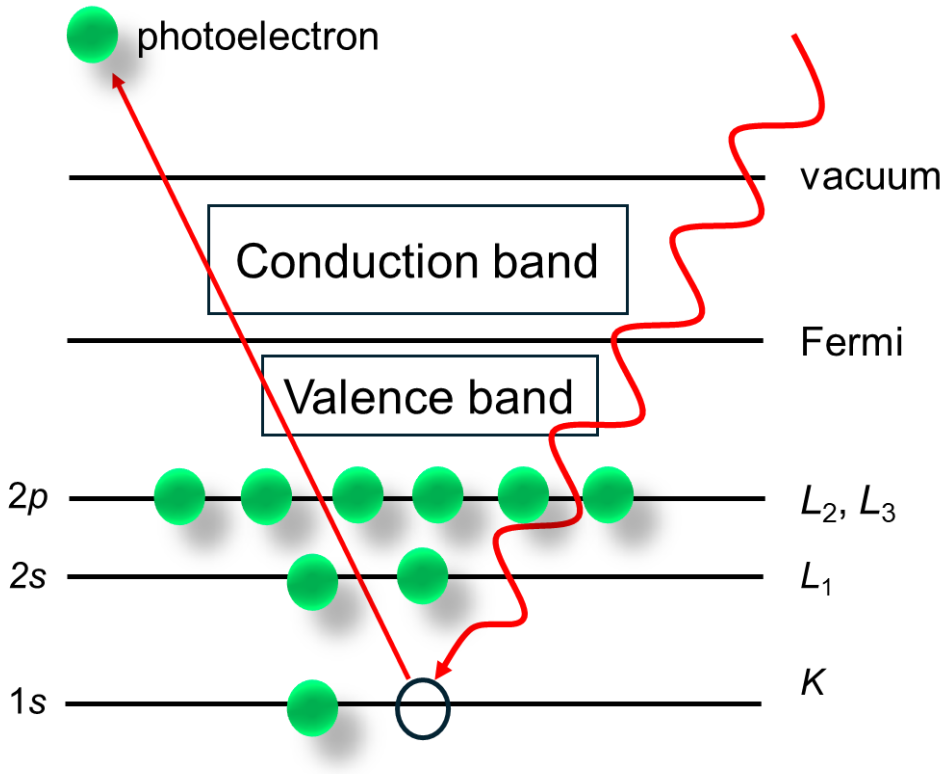

Figure 27. Schematic diagram of generation of photoelectron in XPS

X-ray Photoelectron Spectroscopy (XPS) begins by exposing the surface of a specimen to monochromatic X-ray photons, which have energy that usually range from a few hundred to several thousand electron volts. The energy exceeds the binding energy of electrons in the inner shells of the sample. When incident X-ray photons contact with atoms near the surface, inner-shell electrons are expelled through the photoelectric effect. The kinetic energy of the released photoelectrons is exactly proportional to the difference between the energy of the X-ray photon

and the binding energy of the electrons. Afterwards, the photoelectrons that are released are guided towards an electron energy analyzer, which separates them according to their kinetic energy, enabling the formation of a photoelectron energy spectrum. The resultant spectrum, which

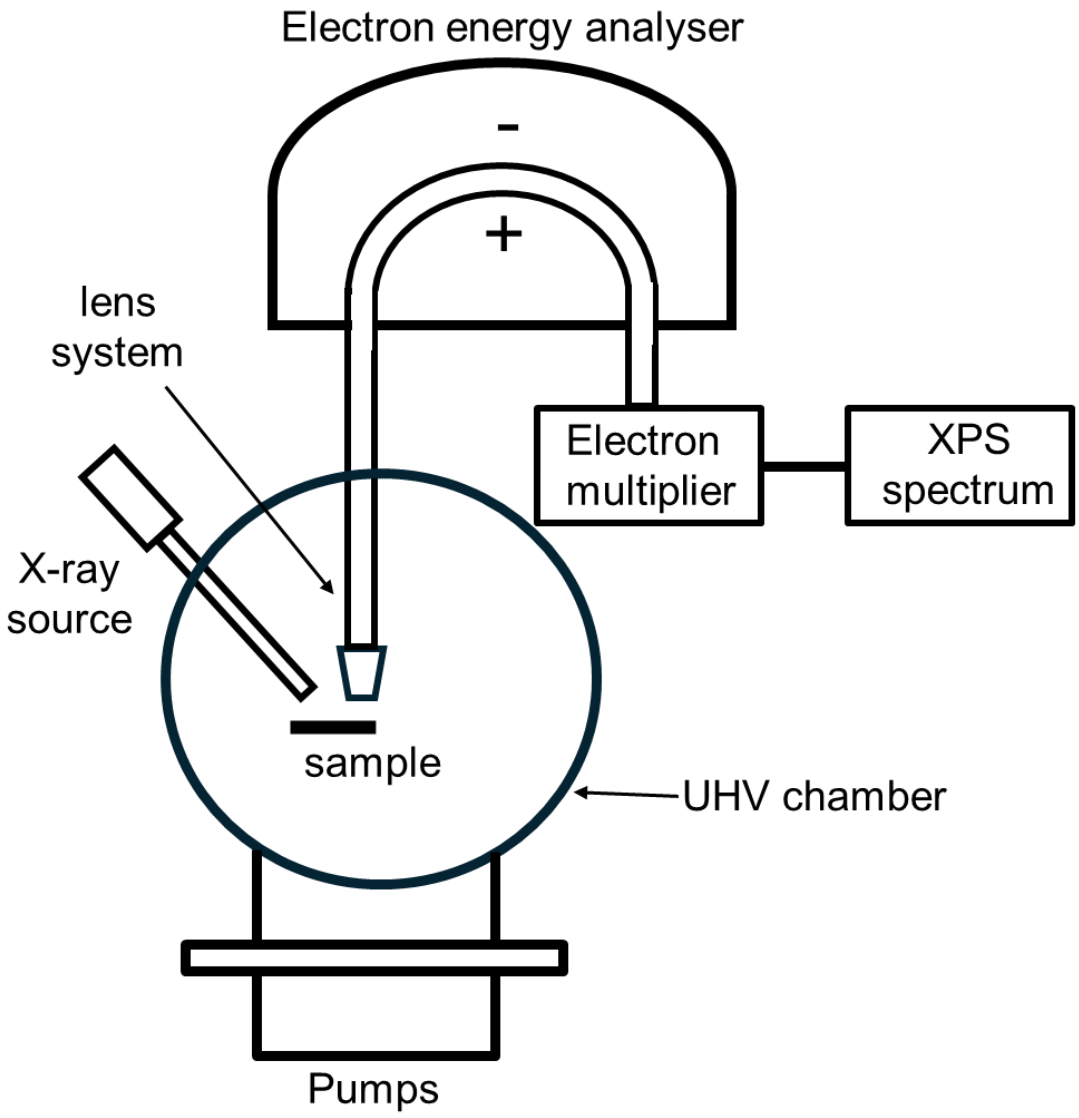

Figure 28. Schematic diagram of XPS Instrument

illustrates the quantity of photoelectrons in relation to their kinetic energy, displays distinct peaks that correspond to individual components present in the sample. The locations of these peaks yield useful insights into the electron binding energies, hence providing significant information regarding the elemental composition. In addition, XPS provides information about the chemical state of elements by identifying specific binding energies related to various chemical environments. Utilizing ion bombardment for progressive material removal facilitates depth profiling, enabling

researchers to examine the elemental composition at different depths. Figure 28 shows the schematic diagram of XPS instrument.

2.3.10. Ferroelectric Tester

A Ferroelectric Tester is a crucial tool for examining and characterizing ferroelectric materials, enabling researchers to quantitatively measure and evaluate the polarization-electric field (PE) curves. Ferroelectric materials provide distinctive characteristics, such as inherent polarization, which are crucial for diverse technology implementations, including non-volatile storage, sensors, actuators, and capacitors. The Ferroelectric Tester is essential for comprehending and enhancing the efficiency of these materials by accurately recording the complicated correlation between polarization and electric field intensity. Figure 29 shows the schematic diagram of a ferroelectric tester. In my study, I have used TOYO, FCE-1E ferroelectric tester.

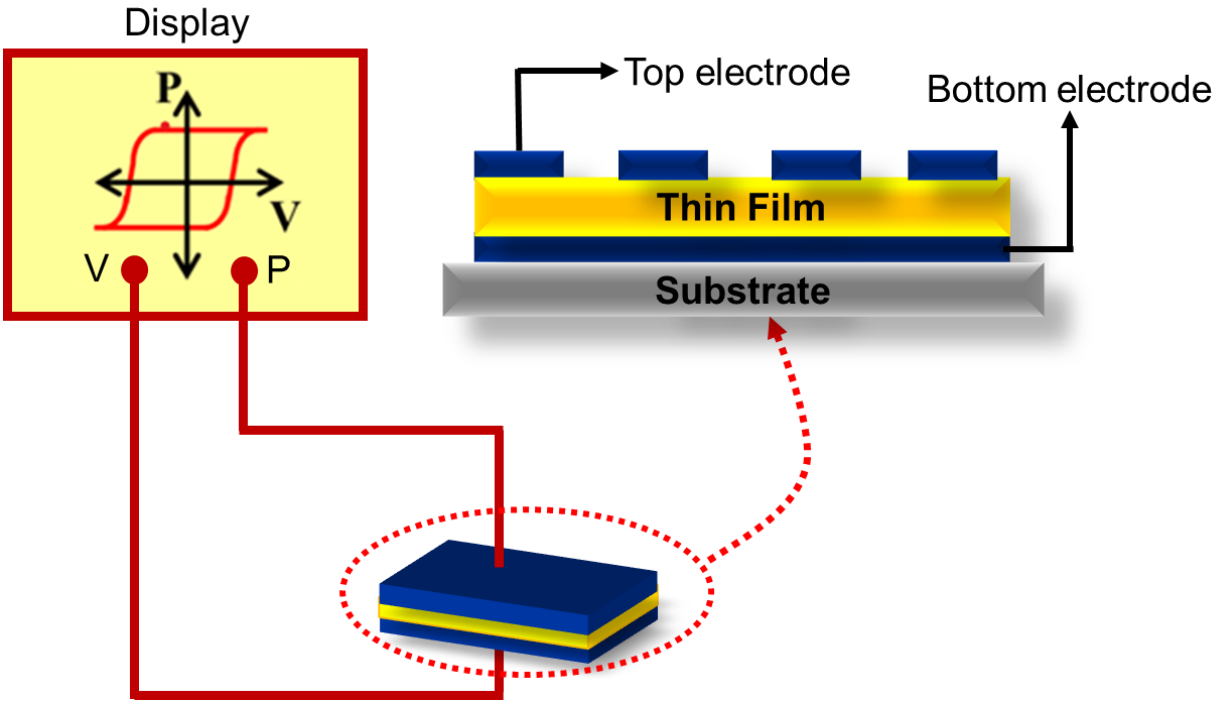

Figure 29. Schematic diagram ferroelectric tester set up.

A carefully prepared ferroelectric specimen, typically in the shape of a thin layer or solid material, is affixed and electrically linked to the Ferroelectric Tester. The Ferroelectric Tester applies a regulated electric field to the sample, inducing the alignment of the material's polarization in the direction of the field. This arrangement leads to an overall macroscopic polarization within the material. The instrument quantifies the induced polarization of the ferroelectric sample in relation

to the applied electric field. A PE curve is constructed by systematically altering the electric field intensity and documenting the related polarization values. This graph depicts the ferroelectric hysteresis loop, which represents the correlation between polarization and electric field as the field is applied and then removed in cycles.

2.3.11. Piezoresponse Force Microscopy (PFM)

Piezoresponse force microscopy (PFM) is an atomic force microscopy (AFM) technique that investigates electromechanical material properties at the nanoscale scale, in addition to analyzing the sample's topography. By utilizing a conductive tip to physically scan the surface, the application of an alternating current voltage induces an electromechanical reaction in piezoelectric materials. This reaction allows for the identification and analysis of specific differences in both piezoelectric and ferroelectric properties at a local level.

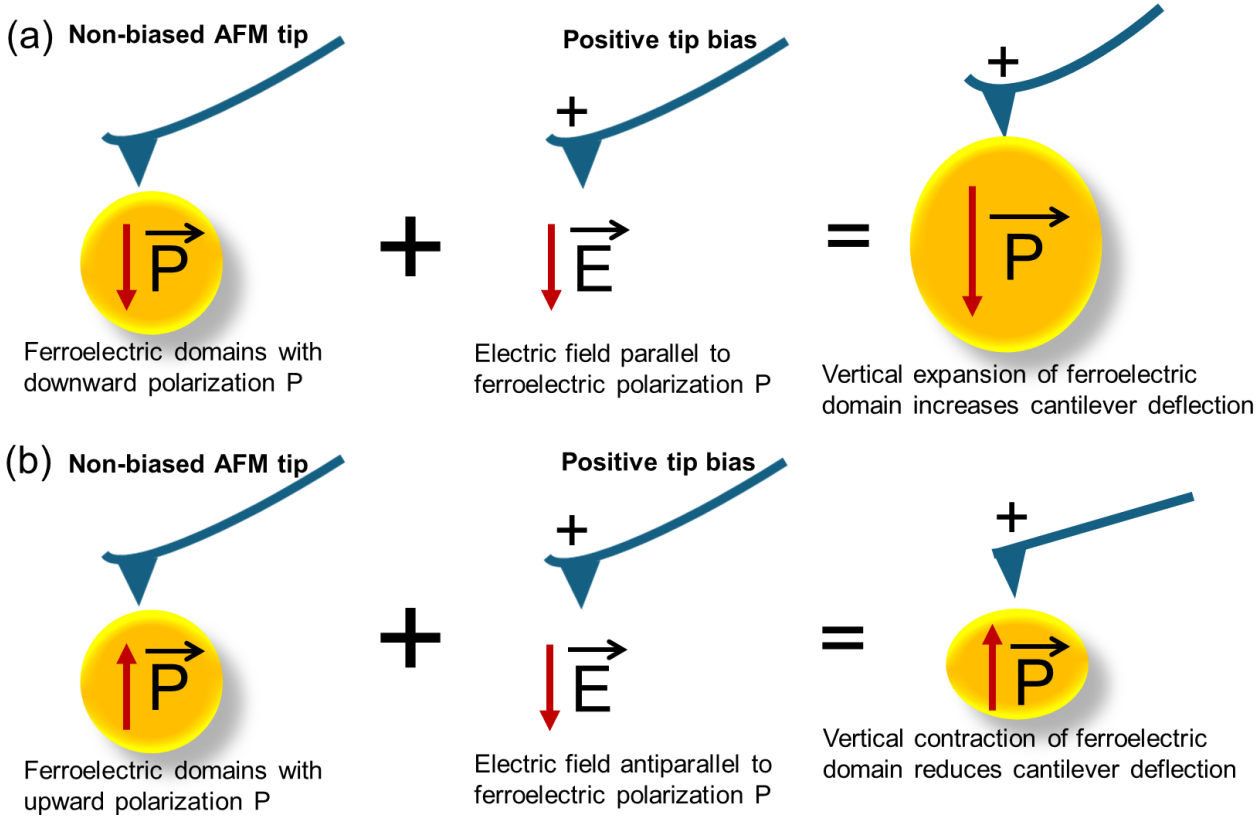

Figure 30. Fundamental principle of PFM, ferroelectric domains with (a) downward polarization and (b) upward polarization.

PFM involves the use of a conductive AFM tip that is placed in contact with the surface of ferro- or piezoelectric materials. A predetermined voltage is then delivered between the sample surface and the AFM tip. The voltage creates an external electric field in the sample. The sample undergoes local expansion or contraction based on the direction of the electric field due to the presence of the inverse piezoelectric effect in piezoelectric materials. For instance, if the electrical polarization of a ferroelectric domain underneath the tip is directed at a right angle to the surface of the sample and in the same direction as the applied electric field, the domain will undergo a vertical expansion, as depicted in figure 30 (a). As the AFM tip makes contact with the surface of the sample, the expansion of this domain causes the AFM cantilever to bend upwards, resulting in an increase in deflection. If the initial domain polarization is antiparallel to the applied electric field, the domain will contract, resulting in a reduced cantilever deflection, as illustrated in figure 30 (b). Hence, the alteration in the cantilever's deflection provides insights on the orientation and comparative strength of the ferroelectric polarization in the area underneath the tip.

2.4. Thickness Measurement

Figure 31. Image of thickness measurement instrument by using line profiles.

During my research, I utilized line profile analysis to measure the precise thickness of the thin films being studied. I performed comprehensive evaluations of the thin films using the ACCRETECH SURFCOM 1400D (figure 31), a high-precision measurement device.

2.5. Etching

Microfabrication is an important technique in the manufacturing of small-scale structures and devices, which are vital for the advancement of sophisticated technologies like microelectronics, sensors, and microelectromechanical systems (MEMS). Etching is a crucial method in microfabrication that is used to define and shape structures at the micro- and nanoscale. Etching is a method that removes material from a substrate in a selective manner, enabling the exact creation of patterns and features.

There are two main methods of etching that are often employed: wet etching and dry etching, which is often referred to as plasma or dry chemical etching. Every approach possesses its own benefits and uses, although they all strive towards the shared objective of attaining exceptional accuracy in the process of material removal.

2.5.1. Wet Etching

Wet etching is based on the chemical reactivity that occurs between the etchant solution and the substance on the substrate. The selection of etchant is dictated by the composition of the material undergoing etching.

For example, in silicon micromachining, a widely used etchant is a combination of hydrofluoric acid (HF), nitric acid (HNO_3), and acetic acid (CH_3COOH), commonly known as buffered oxide etchant (BOE). The reaction involving silicon can be expressed in the following manner:

$$Si + 6HF \longrightarrow H_2SiF_6 + 2H_2O$$

The reaction leads to the creation of a soluble compound called hexafluorosilicic acid, which efficiently eliminates silicon from the affected regions. Figure 32 shows the RIE instrument (SAMCO: RIE-10NR-0U), used in my study.

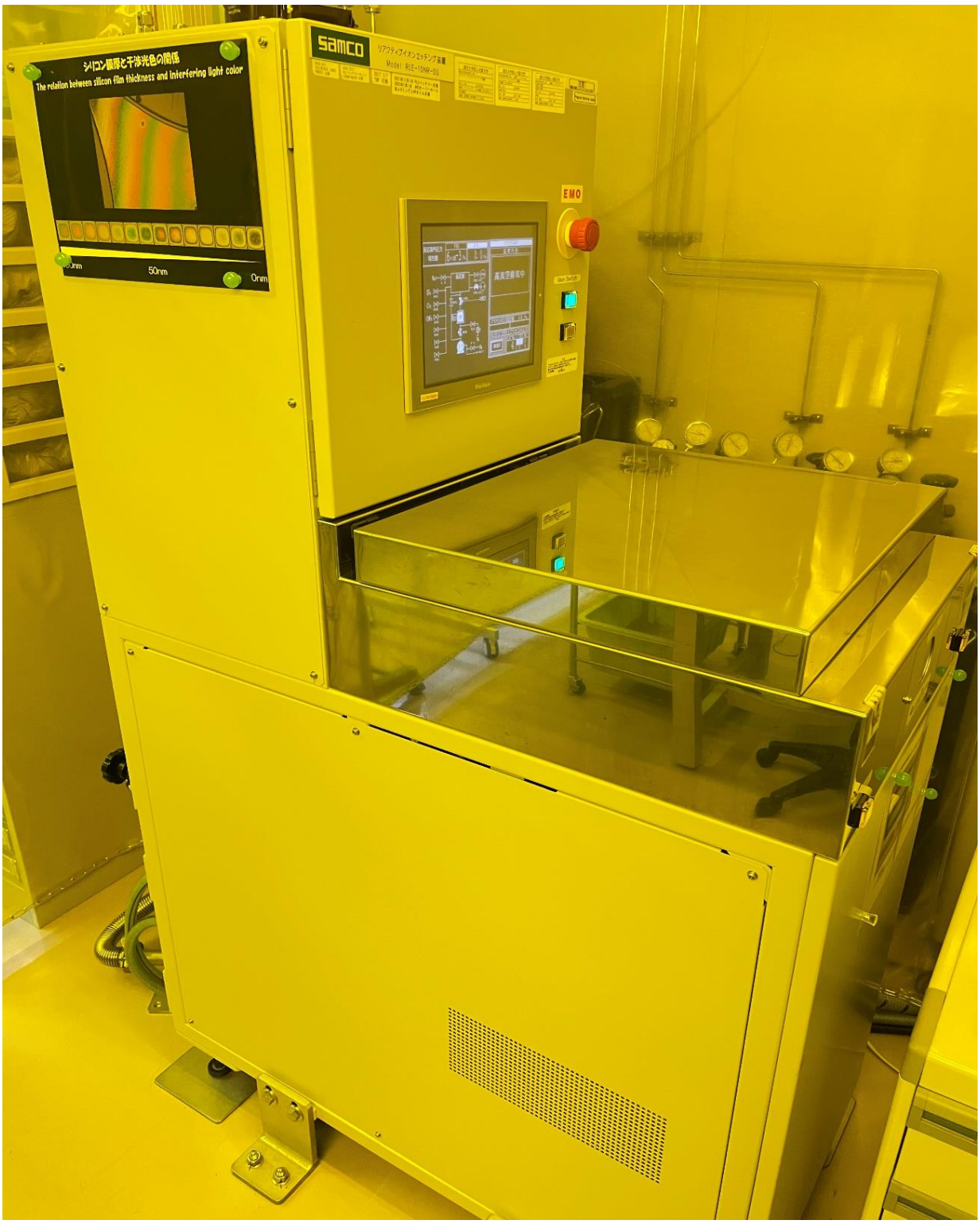

Figure 32. Image of reactive ion etching instrument.

Again, wet etching is classified as 2 types.

- Isotropic Etching

Isotropic etching occurs evenly in all directions, leading to the removal of material in an approximately spherical shape. Isotropic etching's attribute renders it appropriate for generating concave or rounded characteristics.

- Anisotropic Etching

Anisotropic etching is a process that eliminates material in a selective manner along specified crystallographic planes, resulting in clearly defined and frequently perpendicular sidewalls. This form of etching is essential for producing accurate and structures with a high aspect ratio.

2.5.2. Dry Etching (DE)

Dry etching, also known as plasma etching, is a crucial method in microfabrication that exhibits notable differences from wet etching. The process entails utilizing plasma, which is a gas that has been ionized and contains reactive components, to specifically eliminate material from the substrate. Dry etching offers significant benefits in creating accurate and regulated patterning in micro- and nanoscale devices.

Plasma, the fourth phase of matter, is formed by subjecting a gas to an electric field, resulting in ionization. This plasma consists of electrons, ions, and neutral species, and it exhibits a high level of reactivity. The reactive species present in the plasma undergo chemical reactions with the material on the substrate, resulting in its elimination. Fluorine (F) and chlorine (Cl) are commonly used as plasma etchants. When these two elements are mixed, they produce extremely reactive fluorine and chlorine radicals. Plasma etching provides a notable benefit in terms of its exceptional level of control. By accurately adjusting parameters like gas composition, pressure, power, and temperature, specified etching rates and selectivity can be achieved.

Dry etching is intrinsically anisotropic, indicating that material is selectively eliminated in particular directions. The anisotropic property of this material enables the formation of vertical sidewalls, which is a crucial necessity in numerous microfabrication procedures. Figure 33 shows the DE instrument, used in my study.

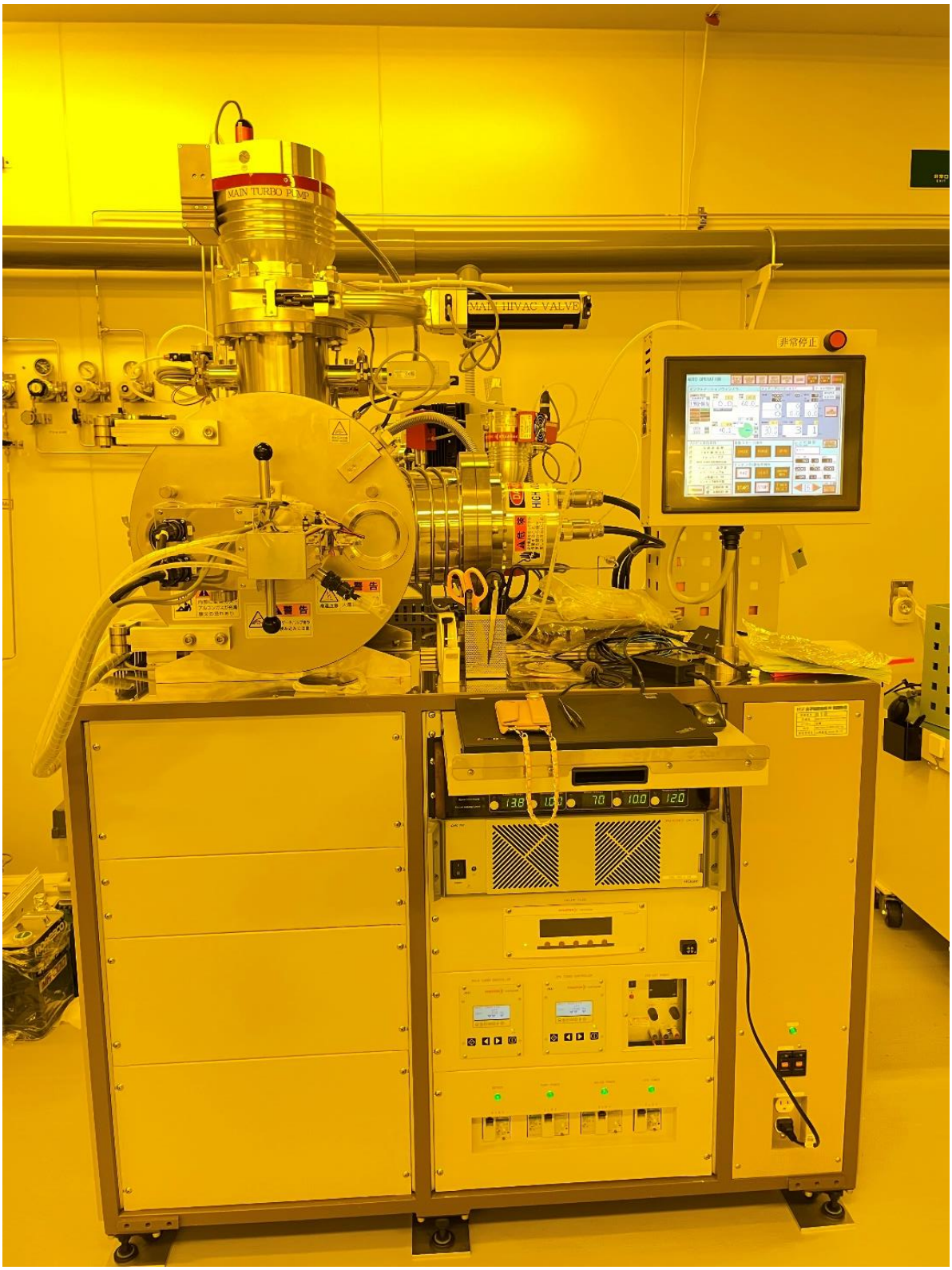

Figure 33. Image of dry etching instrument.

2.6. Photolithography

Photolithography is an advanced method of creating small-scale patterns on surfaces, which is crucial for current technology and allows for the production of elaborate designs at the micro- and nanoscale. Photolithography is extensively used in the production of microelectronics, integrated circuits, and microelectromechanical systems (MEMS). It allows for the accurate replication of complex designs onto semiconductor wafers. Essentially, the technique is applying a light-sensitive substance called photoresist onto a surface, then selectively exposing it to ultraviolet light using a photomask, and finally generating the desired pattern through chemical reactions. Photolithography's intricate and precise nature establishes it as a crucial component in the development of sophisticated microscale devices, driving the limits of miniaturization and technological advancement.

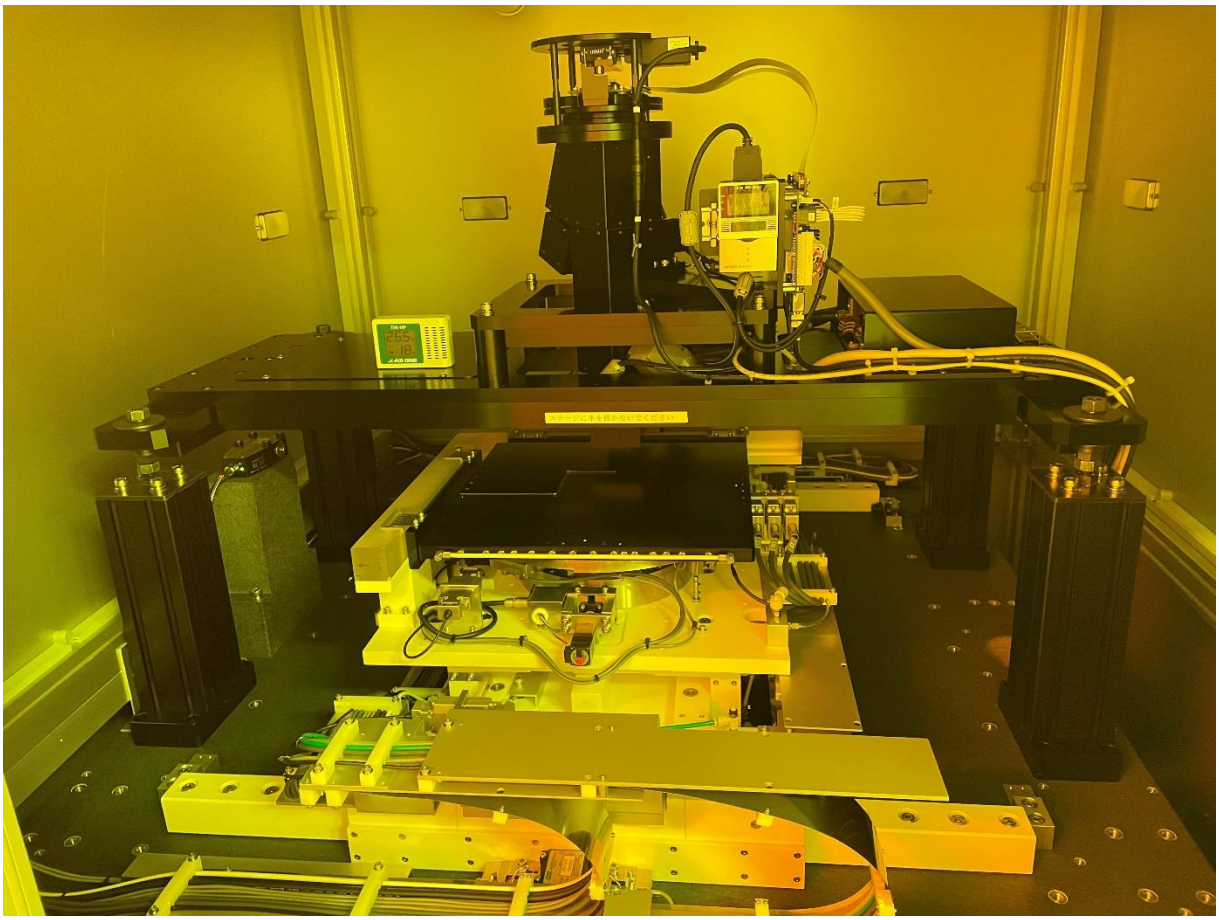

Figure 34. Image of photolithography instrument.

Photolithography proceeds through a carefully coordinated sequence of stages. The procedure starts with preparing the substrate and applying a layer of photoresist. It then goes through soft baking, aligning a mask, exposing it to UV light, post-exposure baking, development, and ultimately, further stages such as etching or deposition to transfer the pattern onto the substrate. The meticulous control of light and chemical reactions during these stages leads to the formation of intricate patterns with exceptional precision. The adaptability and precision of photolithography have driven progress in semiconductor manufacturing, allowing for the creation of smaller and more powerful electronic components that form the foundation of modern technological developments. Photolithography instrument (PMT Corporation: PLS-1000) was used for my study.

CHAPTER – 3

Experimental results

Improved Physical Properties in (Bi,*L*)(Fe,Co)O_3 (*L*: La, Nd, Sm, Eu, Gd, Dy, Er) Multiferroic Thin Films

3.1. Crystallographic Study using X-ray Diffraction

Figure 35 illustrates the X-ray diffraction (XRD) patterns of thin films made up of (Bi,*L*)(Fe,Co)O_3, with *L* representing different lanthanides, across a broad scanning range. Significantly, because of the prominent Si (400) peak at around 69°, the profile provided only covers up to 65° in the vicinity of this peak. The figure includes the XRD profile of (Bi,La)(Fe,Co)O_3 thin films [25] for reference. Furthermore, it is noticed that the Pt underlayer demonstrates a strong (111) orientation. The asterisks indicate the minute and pointed peaks that correlate to the Si/SiO2 substrate.

The examination of the XRD profiles indicates the presence of a noticeable (006) peak, which is visually represented by a conspicuous red shaded area located directly before the Pt peak. The presence of a (001) orientation in the thin films indicates a crystalline structure. The lack of any other distinguishable peaks related to bismuth ferrite (BFO) suggests the absence of secondary components, confirming the presence of a structure composed of a single phase. The overwhelming data indicates that when lanthanides (*L*= La, Nd, Sm, Gd) are added to (Bi, *L*)(Fe,Co)O_3 thin films, the Bi atoms in the BFO phase are substituted.

Nevertheless, the XRD examination reveals a significant variation in the (Bi,*L*)(Fe,Co)O_3 thin films, where *L* represents Eu, Dy, and Er. Significantly, the absence of a prominent peak at (006) indicates that the BFO thin films with europium, dysprosium, and erbium replacements are not completely crystalline. The complexities of this occurrence will be further elaborated in future conversations. This departure motivates additional investigation into the crystalline properties of these substituted BFO thin films. The next sections will explore the reasons for this different behavior exhibited in the XRD profiles.

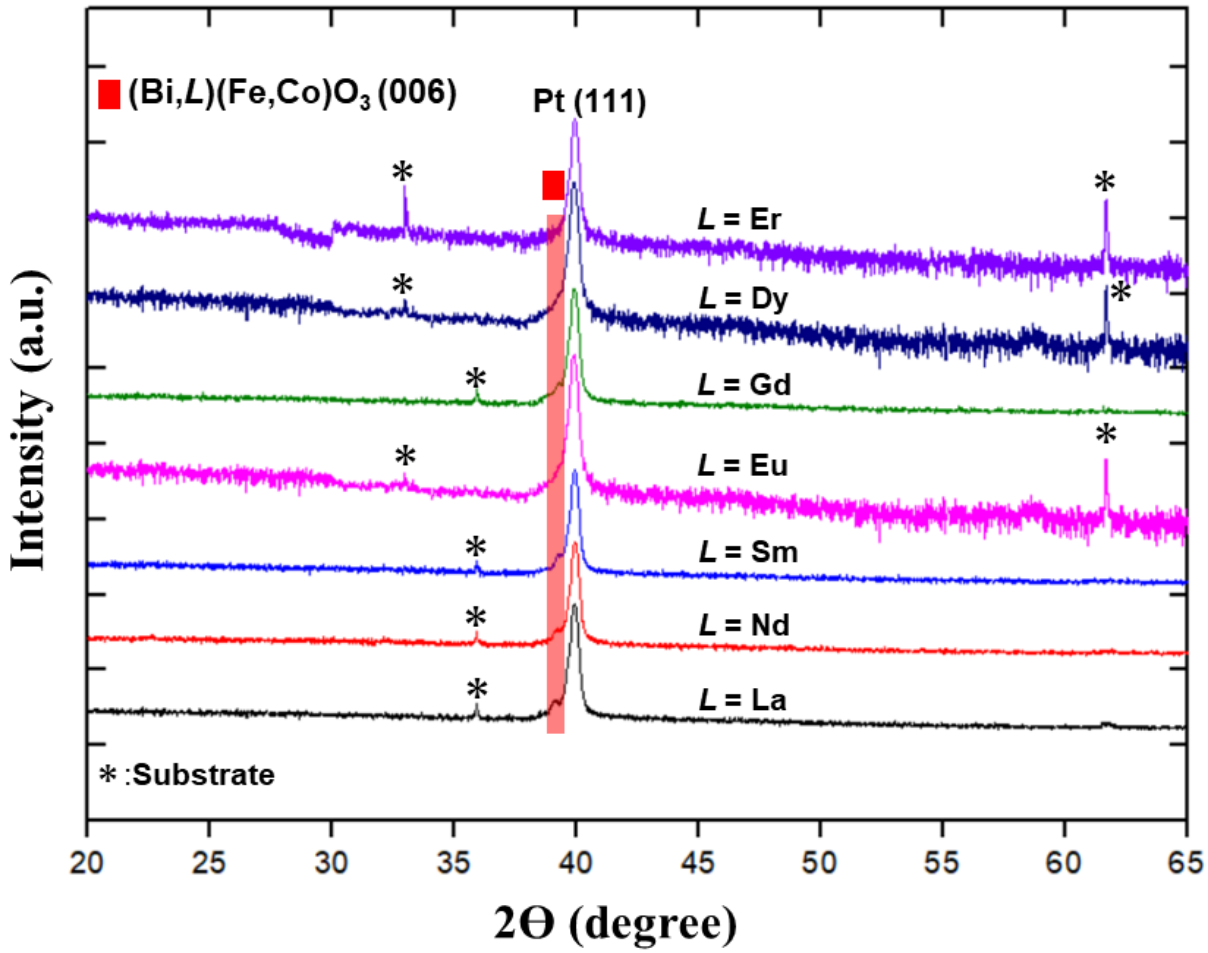

Figure 35. XRD profile of (Bi,*L*)(Fe,Co)O_3 (*L*: Lanthanides) thin films with a layer of Ta/Pt layer, prepared by p-DC reactive sputtering.

3.2. Microstructural Analysis

3.2.1. Surface Morphology by FESEM

A detailed analysis of the structural properties of thin films composed of bismuth ferrite (BFO) was conducted using scanning electron microscopy (SEM), as depicted in Figure 36. The image displayed exhibits particles on the film, which function as an indicator of the refined focusing achieved throughout the imaging procedure. High-resolution scanning electron microscopy (SEM) images were acquired, providing precise information about the geometry and microstructure of the film surface. The scans showed that the (Bi,*L*)(Fe,Co)O_3 (*L*= La, Nd, Sm, Gd) thin films had a

continuously smooth surface with clearly visible characteristics, such as distinct grains and grain boundaries.

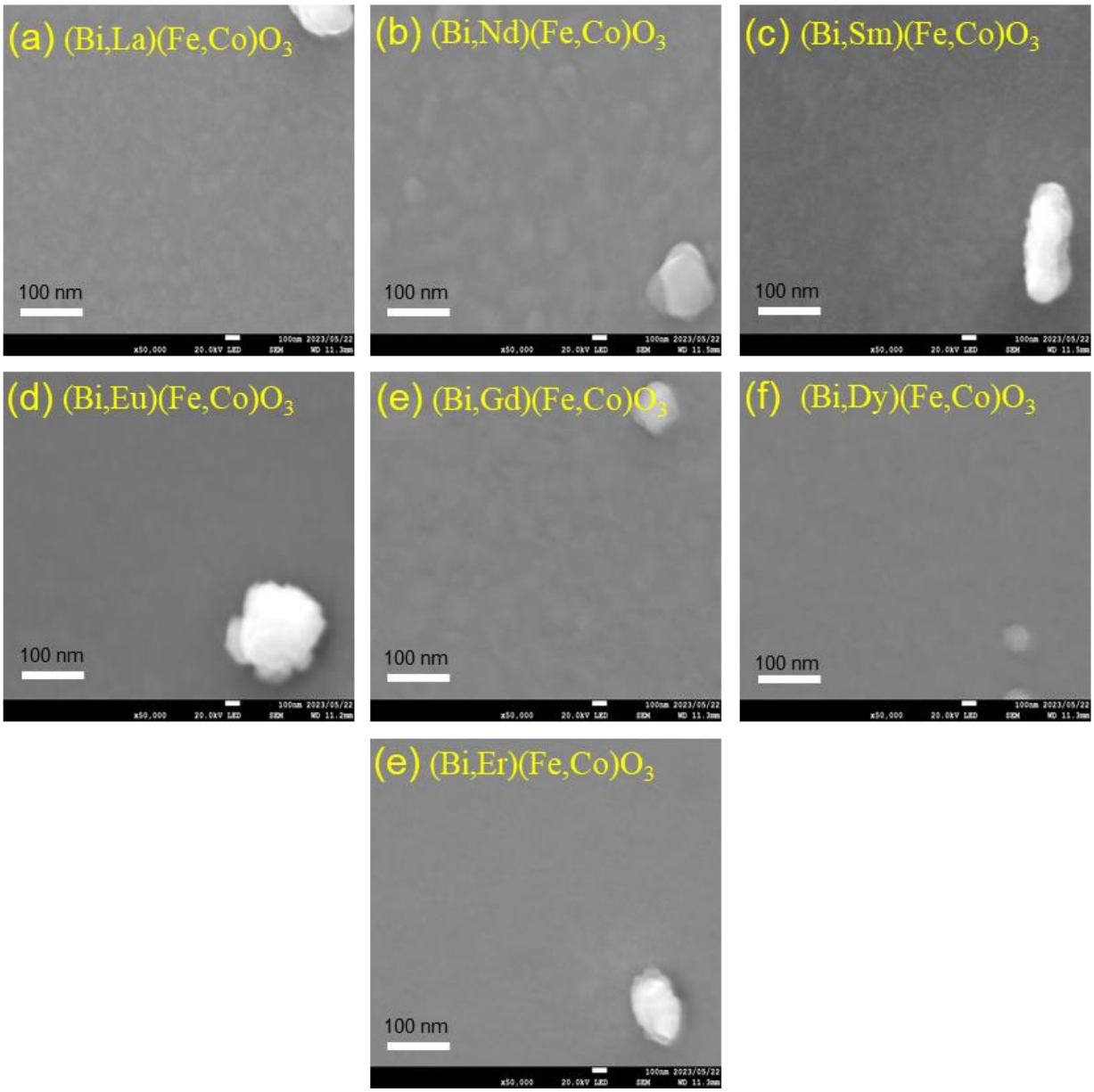

Figure 36. SEM images of the (Bi,*L*)(Fe,Co)O_3 (*L*: Lanthanides) thin films prepared by p-DC reactive sputtering.

The grain structures displayed distinct clarity and consistent dispersion throughout the samples. Significantly, there was a noticeable lack of contrast variation, with the exception of the differentiation between the grains and their respective boundaries in these scanning electron

microscope (SEM) images. The thin film's composition was constantly confirmed by doing further research using Energy Dispersive X-ray Spectroscopy (EDS) at magnifications ranging from x50000 to x250000. This rigorous examination highlights the lack of any additional stage in the SEM pictures and suggests a uniform elemental composition without significant variations.

Conversely, the scanning electron microscopy (SEM) analysis of (Bi,*L*)(Fe,Co)O_3 (*L*= Eu, Dy, Er) thin films showed blurred boundaries between grains, suggesting an unfinished crystalline arrangement. The observation is consistent with the results obtained from X-ray diffraction (XRD) investigations, which together indicate a unique crystalline behavior in BFO thin films when europium, dysprosium, or Erbium is used as a substitute element. The presence of structural differences, which may be observed at both small and large scales, highlights the complex impact of lanthanides on the structural stability of BFO thin films. This necessitates thorough examination and clarification in future studies.

The thorough assessment of dopant replacement in our thin films goes beyond the examination of X-ray diffraction (XRD), embracing a synergistic utilization of energy-dispersive X-ray spectroscopy (EDS) data. We wanted to thoroughly examine the existence and distribution of dopants by carefully collecting EDS data at various locations throughout the thin films and using different levels of magnification. The included scanning electron microscopy (SEM) images, taken at various levels of magnification, serve as prime examples of this scientific technique.

The presence of particles in the SEM images not only acts as a visual element, but also indicates the accuracy gained through fine-tuning the focus during the imaging process. This approach guarantees the dependability and precision of our observations. Our SEM examination, performed at various magnifications ranging from x50000 to x250000, demonstrated a noteworthy uniformity in the composition of the film as shown in figure 37. The lack of noticeable variations in contrast in SEM pictures further emphasizes the consistent and uniform nature of the thin film formations.

Importantly, the confirming quality of EDS results acquired from different levels of magnification confirms the lack of secondary phases within the SEM images. The careful implementation of this approach not only confirms the replacement of dopants but also acts as a reliable tool to test the overall structural soundness of the thin films. The thorough procedures, which utilize many analytical techniques, enhance the dependability and trustworthiness of our results, establishing a

strong basis for understanding the complex structural characteristics of our (Bi,*L*)(Fe,Co)O_3 thin films.

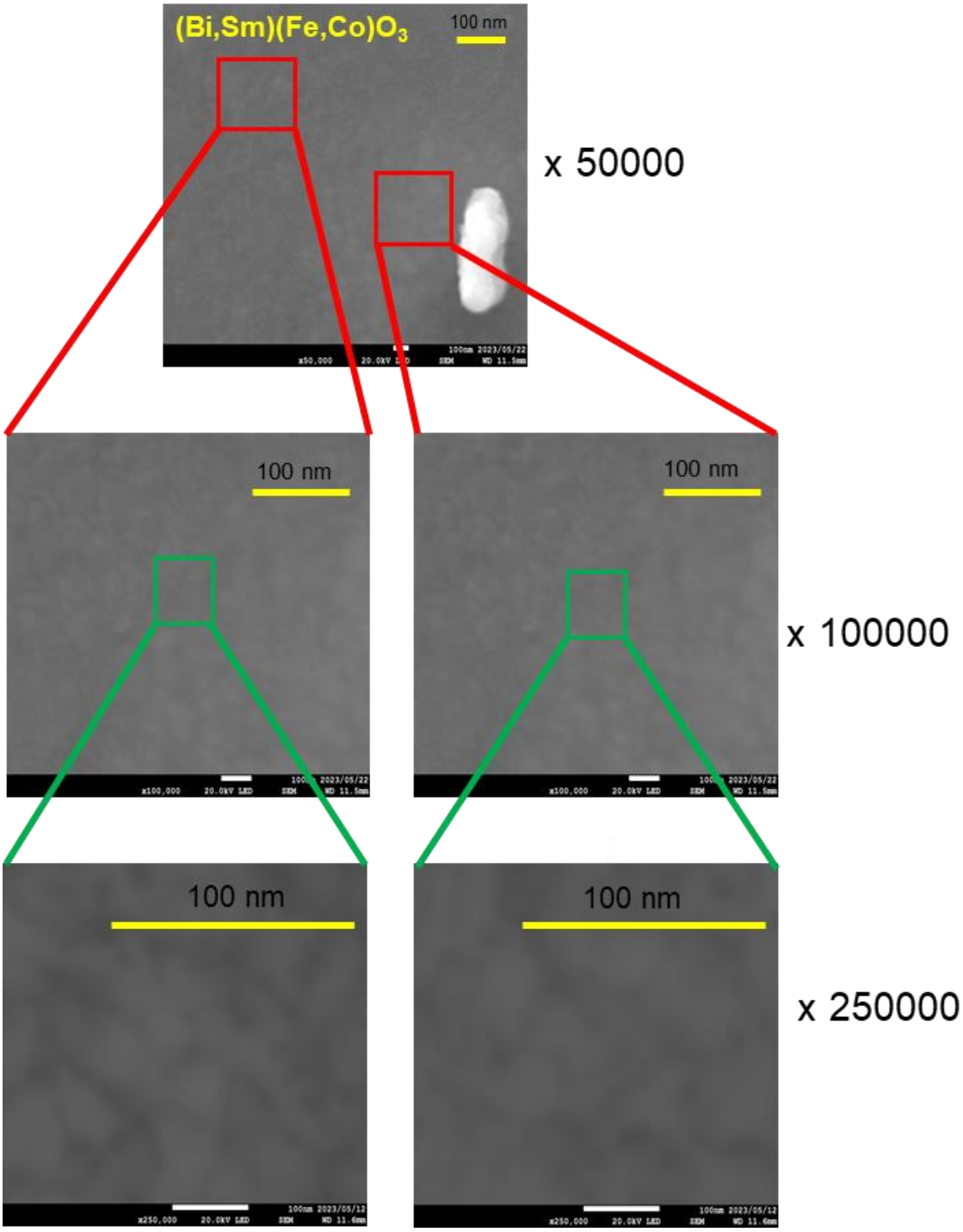

Figure 37. SEM images of the (Bi,Sm)(Fe,Co)O_3 thin films, at different magnifications showing the uniformity.

3.2.2. Elemental Composition Analysis by using EDX

Optimizing the substituent components is crucial for enhancing the magnetic properties of multiferroic thin films made from $BiFeO_3$. A precise methodology was employed to improve the magnetic characteristics by stabilizing the proportion of lanthanides in the A-site at around 50 at% [25]. The purpose of this strategic modification in the lanthanide composition was to attain an ideal equilibrium for advantageous magnetic properties in the (Bi,*L*)(Fe,Co)O_3 thin films.

In addition, the introduction of roughly 25 at% of cobalt substitution in the B-site resulted in a significant influence on magnetic characteristics [31]. The intentional replacement technique exhibited substantial improvements in many magnetic parameters, as thoroughly shown in Table 1. Cobalt plays a crucial function in the B-site, significantly impacting and enhancing the magnetic properties of the (Bi,*L*)(Fe,Co)O_3 thin films. The precise adjustment of both the concentrations of lanthanides on the A-site and cobalt on the B-site highlights the complexity involved in customizing the magnetic properties of these thin films with multiple ferroic properties. This sets the groundwork for further investigation and comprehension in the field of advanced materials science.

Table 1. Percentage of dopant concentration in A-site and B-site of (Bi,*L*)(Fe,Co)O_3 (*L*: Lanthanides) thin films.

Sample name	at % of A-site dopant	at % of B-site dopant
(Bi,La)(Fe,Co)O_3	51	24
(Bi,Nd)(Fe,Co)O_3	45	23
(Bi,Sm)(Fe,Co)O_3	48	25
(Bi,Eu)(Fe,Co)O_3	49	24
(Bi,Gd)(Fe,Co)O_3	52	24
(Bi,Dy)(Fe,Co)O_3	51	25
(Bi,Er)(Fe,Co)O_3	47	23

3.3. Magnetic Properties

3.3.1. Magnetic Hysteresis (*M-H*) Curve by VSM

Figure 38 illustrates the magnetic properties of (Bi,*L*)(Fe,Co)O_3 (*L*: Lanthanides) thin films using in-plane (blue) and out-of-plane (green) magnetic hysteresis curves. The figure includes the *M-H* curve of the (Bi,La)(Fe,Co)O_3 thin film [25]for reference. Distinctive characteristics, such as clearly defined hysteresis loops and relatively high saturation magnetization (M_s) values, are consistently present in all (Bi,*L*)(Fe,Co)O_3 thin films.

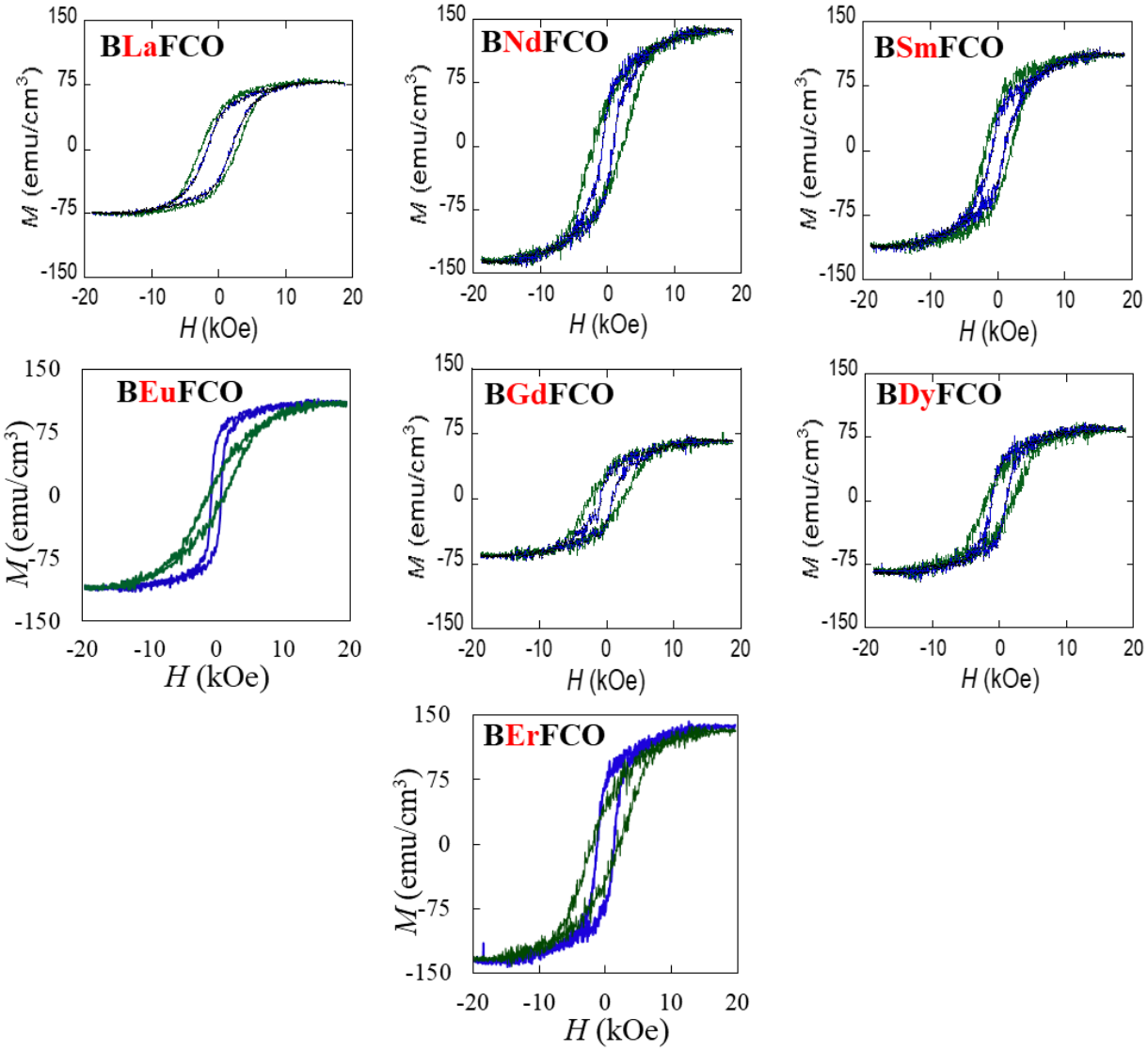

Figure 38. In-plane (blue) and out-of-plane (green) magnetic hysteresis curves of (Bi,*L*)(Fe,Co)O_3 (*L*: Lanthanides) thin films prepared by p-DC reactive sputtering.

Remarkably, the thin films (BNdFCO), (BErFCO), and (BEuFCO), which are substituted with lanthanoid elements, demonstrate remarkably high M_s values. These values are notably prominent, exceeding those observed in the (Bi,La)(Fe,Co)O_3 (BLaFCO) thin film, as documented in our prior investigation. The significant improvement in M_s demonstrates the positive impact of Nd, Er, and Eu replacements on the magnetic characteristics of the thin films.

Moreover, it is worth mentioning that thin films of (BNdFCO) demonstrate elevated M_s values, while thin films of (BEuFCO) exhibit extremely low coercivity, suggesting improved stability in the magnetization state. In addition, the BNdFCO thin film exhibits a notably high perpendicular magnetic anisotropy (PMA). In the following discussion, we will provide a thorough explanation of the PMA phenomenon. This will help us understand the complex relationship between the composition and magnetic properties in (Bi,*L*)(Fe,Co)O_3 systems. Specifically, we will focus on the magnetic behaviors and superior characteristics displayed by certain lanthanide-substituted thin films.

3.3.2. Perpendicular Magnetic Anisotropy Study (PMA) by VSM

Figure 39 provides a detailed analysis of the relationship between coercivity (H_c) and squareness (S) in different orientations of each (Bi,*L*)(Fe,Co)O_3 thin film, with respect to the angle between the film plane and the applied magnetic field. At 0°, the measurements of H_c and S are taken in the direction parallel to the plane ($H_{c//}$ and $S_{//}$), whereas at 90°, they reflect the features perpendicular to the plane ($H_{c\perp}$ and $S_{\perp}$). The magnetic anisotropy of thin films can be determined by observing the H_c and S values of the Stoner-Wohlfarth single-domain particle. These values are represented by dotted lines, which provide a reference for understanding the relationship between the magnetic field angle and the easy or hard axis.

Significantly, the coercivity (H_c) displayed a consistent upward trend with the angle, reaching its highest point at 90° for all (Bi,*L*)(Fe,Co)O_3 thin films. This is consistent with the expected behavior in Stoner-Wohlfarth single-domain particles, where the axis of ease at 90 degrees shows a similar trend, showing a widespread perpendicular magnetic anisotropy (PMA) in all thin films.

Interestingly, the squareness (S) of BNdFCO, BSmFCO, and BGdFCO thin films exhibited a dependence on the angle, reaching its maximum value at 90°. Conversely, a reverse pattern was noted for BDyFCO, BErFCO, and BEuFCO thin films, with a reduction in S, reaching its minimum

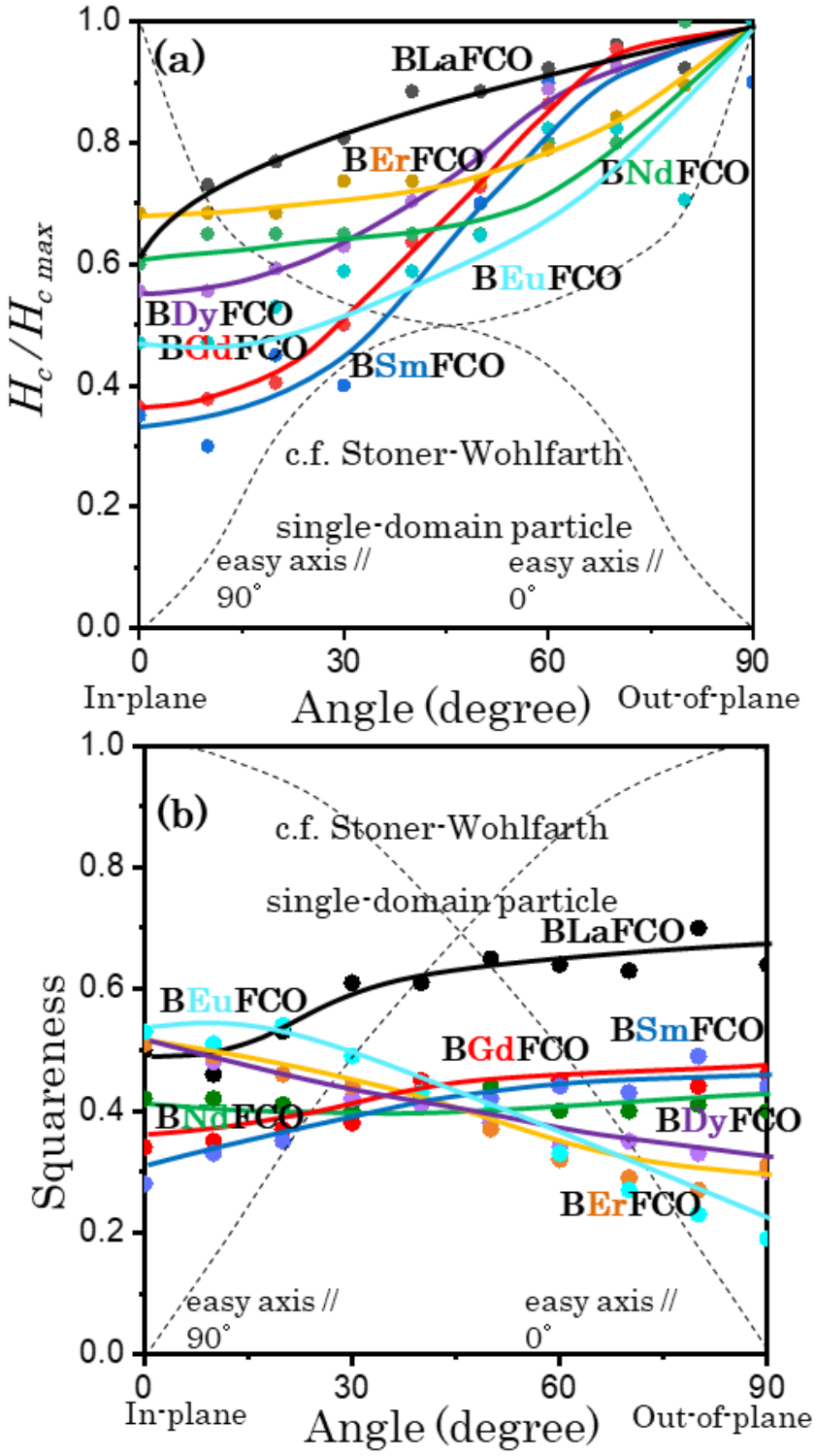

Figure 39. Dependence of coercivity (a) and squareness (b) on the angle between the film plane and magnetic field of VSM measurement in (Bi,*L*)(Fe,Co)O_3 (*L*: Lanthanides) thin films prepared by p-DC reactive sputtering.

at 90°. The results indicate that thin films of BNdFCO, BSmFCO, and BGdFCO demonstrate perpendicular magnetic anisotropy (PMA), whereas BDyFCO, BErFCO, and BEuFCO thin films exhibit in-plane magnetic anisotropy.

The in-plane magnetic anisotropy seen in the later group of thin films may be explained by the ambiguous crystalline structure and the lack of a distinct (001) orientation, as depicted in Figure 35. A comprehensive comprehension of the interplay between film orientation, crystalline structure, and magnetic characteristics is crucial in the study of thin film magnetism.

3.3.3. Magneto-Optical Kerr Angle by MOKE

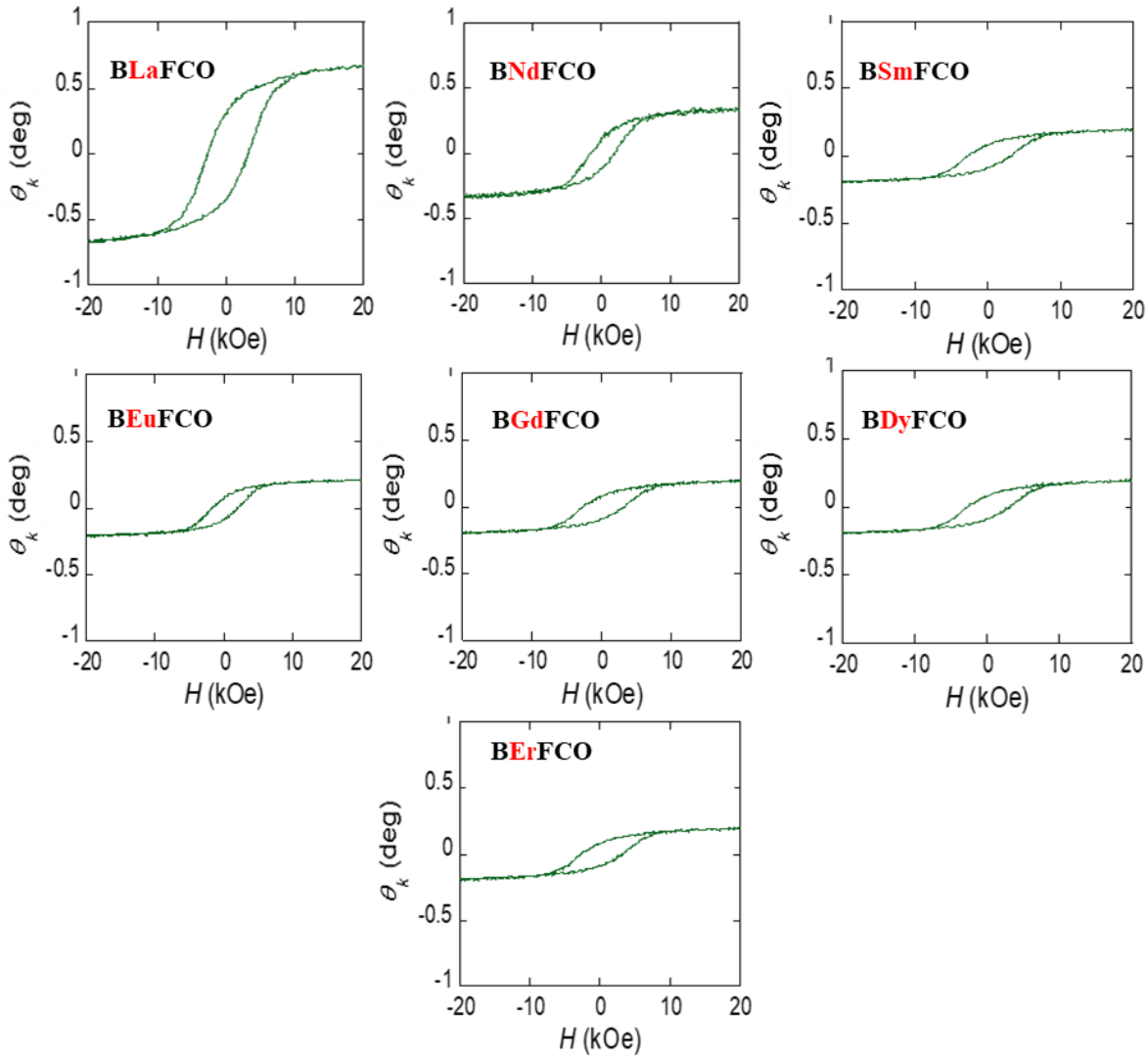

Figure 40. Magneto-optical Kerr loop of (Bi,*L*)(Fe,Co)O_3 (*L*: Lanthanides) thin films

Figure 40 presents an analysis of the magnetic characteristics of thin films of (Bi,*L*)(Fe,Co)O_3, where *L* represents Lanthanides. The analysis is conducted using Θ_k-*H* curves, which are obtained using Magneto-Optical Kerr Effect (MOKE) equipment, specifically the NEOARK BH-P920-EM model. The magnetic field is oriented perpendicular to the plane of the film during these tests. The obtained θ_k-*H* curves of all (Bi,*L*)(Fe,Co)O_3 thin films demonstrate distinct hysteresis loops, indicating strong magnetic behavior. Moreover, a constant and significant Kerr rotation angle (Θ_k) was detected in all cases, indicating the films' proficiency in altering the polarization of light when subjected to a magnetic field.

The (Bi,La)(Fe,Co)O_3 thin film is notable for its outstanding performance, as it achieves an extraordinarily high thermal conductivity value of 0.67°. The observed value in this case is significantly double the size of the values observed in all other (Bi,*L*)(Fe,Co)O_3 thin films. The exceptional performance of (Bi,La)(Fe,Co)O_3 in terms of Kerr rotation angle indicates an increased sensitivity to magnetic fields and highlights the unique magnetic properties displayed by this particular composition. An analysis of the subtle variations in Θ_k-*H* curves offers useful information about the magneto-optical characteristics of these thin films. This contributes to a thorough comprehension of their prospective uses in sophisticated magnetic devices and technologies.

3.4. Ferroelectric Curve (P-E) Study by Ferroelectric Tester

Figure 41 illustrates the ferroelectric characteristics of thin films composed of (Bi,*L*)(Fe,Co)O_3 (*L*: Lanthanides). The ferroelectric polarization-electric field (*P*-*E*) curves were obtained by measuring the films using a ferroelectric tester. The P-E curve of the reference (Bi,La)(Fe,Co)O_3 thin film [25] is included for the purpose of comparison. It is worth mentioning that all thin films display hysteresis loops in the ferroelectric curves when subjected to low electric fields, which indicates strong and durable ferroelectric behavior. The resistance of each thin film, which was measured in the megaohm range (MΩ) at a voltage of 5V (as specified in Table 2), provides evidence for the simultaneous existence of both ferromagnetic and ferroelectric features in these materials.

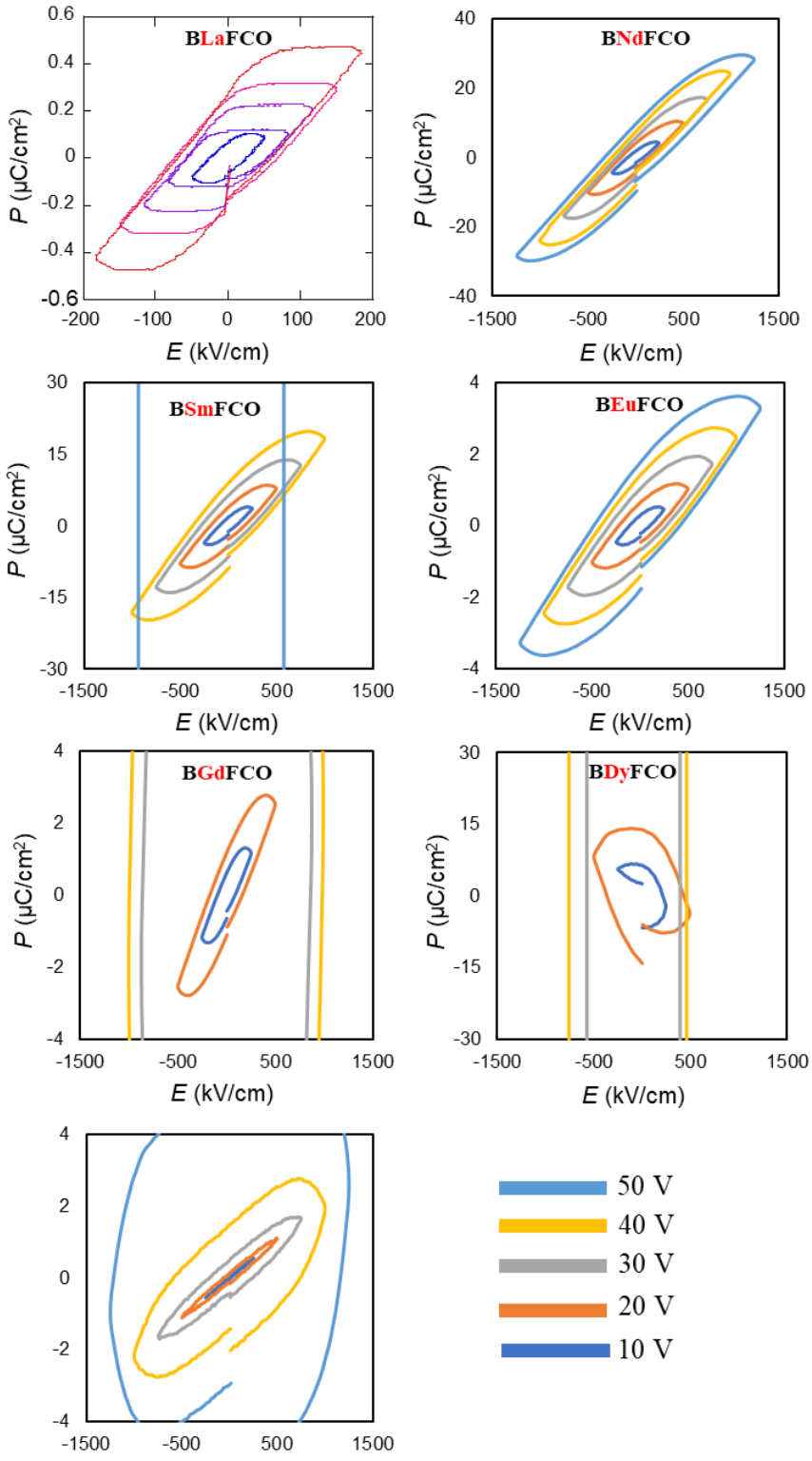

Figure 41. Ferroelectric curves with various applied voltages of the (Bi,*L*)(Fe,Co)O_3 (*L*: Lanthanides) thin films

Table 2. Resistance measured at 5 V and breakdown voltage of (Bi,*L*)(Fe,Co)O_3 (*L*: Lanthanides) thin films prepared by p-DC reactive sputtering.

Name of the thin film	Resistance (at 5V)	Breakdown Voltage
(Bi,Nd)(Fe,Co)O_3	71 MΩ	> 50V
(Bi,Sm)(Fe,Co)O_3	42 MΩ	50V
(Bi,Eu)(Fe,Co)O_3	60 MΩ	> 50V
(Bi,Gd)(Fe,Co)O_3	42 MΩ	30V
(Bi,Dy)(Fe,Co)O_3	54 MΩ	30V
(Bi,Er)(Fe,Co)O_3	4 MΩ	40V

Nevertheless, when the applied electric field intensifies, some thin films exhibit significantly pronounced hysteresis, indicating the deterioration of their insulating characteristics and leading to a substantial rise in leakage current at the breakdown voltage. The breakdown voltages, as indicated in Table 2, demonstrate variability across the films, with notably low breakdown voltages reported in the case of (Bi,*L*)(Fe,Co)O_3 thin films where *L* = Gd, Dy, Er. The increased leakage current is caused by the existence of defects or pinholes, perhaps in the form of oxygen vacancies.

The occurrence of pinholes is closely connected to the oxidation propensity of the substituted lanthanides, as inferred from the analysis of Gibbs' free energy [32]. The oxidation propensity of an element can be comprehended by considering the ideas of Gibbs free energy, which is a thermodynamic parameter that incorporates both enthalpy and entropy changes in a chemical reaction. Regarding the propensity for oxidation, the alteration in Gibbs free energy (ΔG) offers understanding into the possibility and naturalness of the oxidation procedure. A negative change in Gibbs free energy (ΔG) signifies a spontaneous reaction, indicating a greater propensity for oxidation. The relative order of oxidation propensity among elements can be determined by comparing their ΔG values, with larger negative values indicating a higher probability of oxidation. Elements with higher electronegativity or stronger electron-attracting properties typically have larger negative ΔG values, indicating a greater tendency to undergo oxidation. Therefore, this thermodynamic approach allows for a methodical comprehension of the oxidation propensity, relying on the energy alterations linked to electron transfer phenomena.

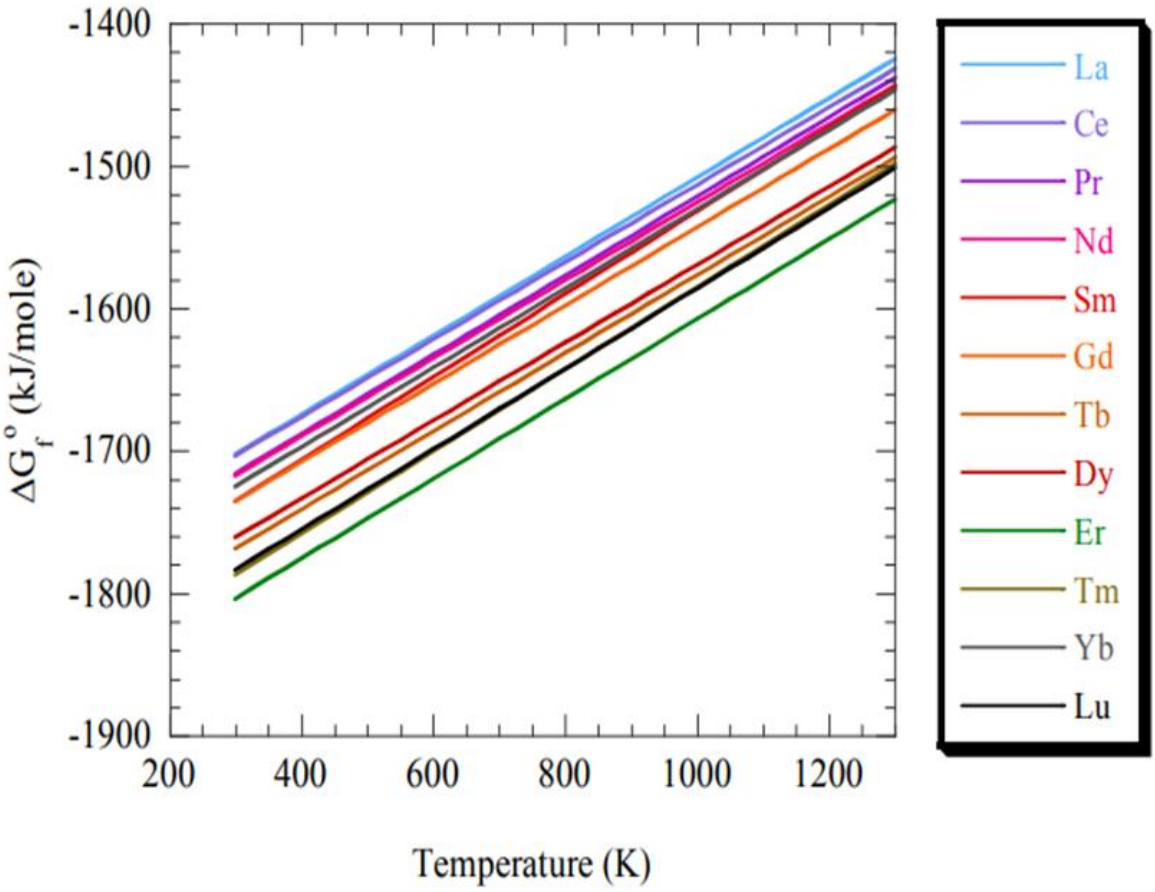

Figure 42. Ellingham diagrams of representative for the lanthanide oxides high-κ dielectrics showing the free energy of formation as a function of temperature. Free energy of formation determined on a per mole basis. [32]

The oxidation propensity of the lanthanides follows the order (from figure 42):

Er > Dy > Gd > Eu > Sm > Nd > La.

This order is important for stabilizing the face-centered oxygen in the perovskite unit cell. The elevated propensity for oxidation exhibited by Er, Dy, and Gd, when compared to other lanthanides like Sm, Nd, and La, implies that oxygen atoms may have a greater inclination towards lanthanides with higher oxidation tendencies. Consequently, this could result in the creation of Er-O, Dy-O, and Gd-O phases instead of the intended perovskite phase as shown in figure 43. As a result, the creation of oxygen vacancies and defects/pinholes follows. Electrons can readily pass through these defects or pinholes, leading to undesired leakage current.

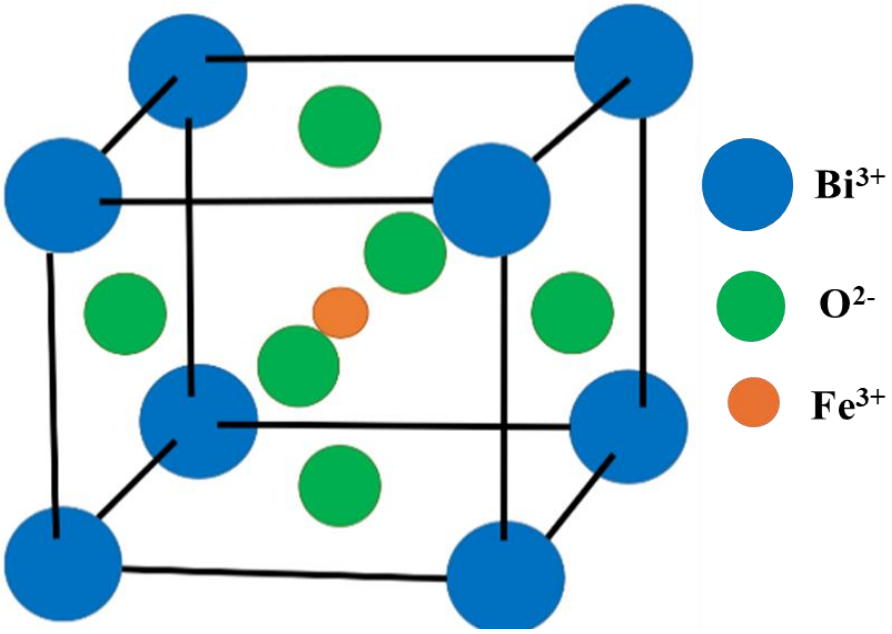

(Perovskite $BiFeO_3$ structure)

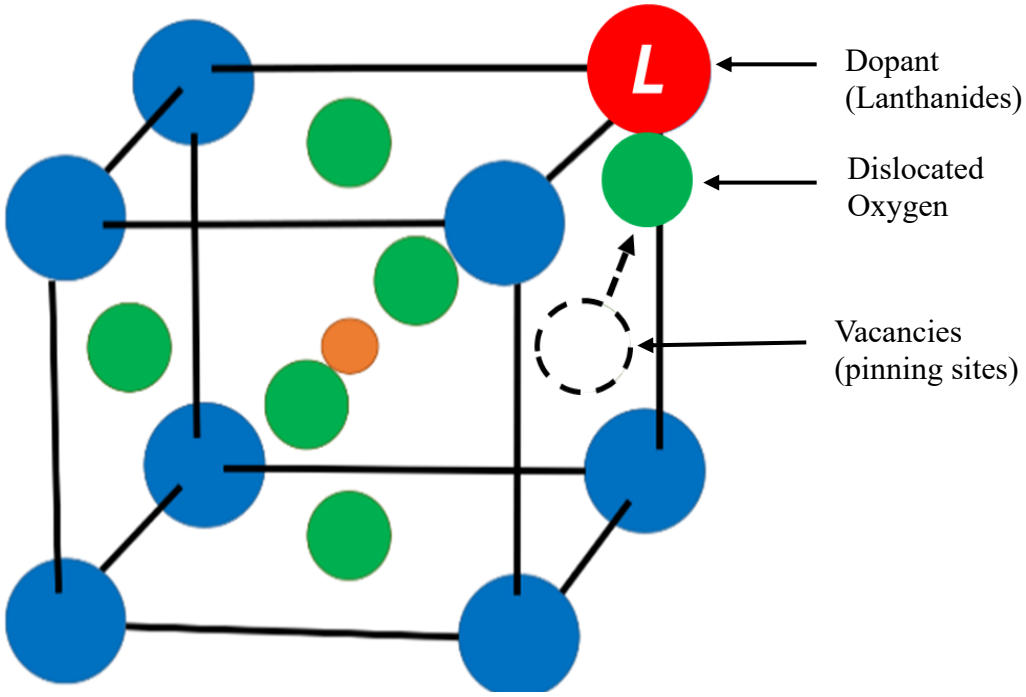

Figure 43. $BiFeO_3$ perovskite structure without any substitution and after substitution.

The presence of defects and pinholes in (Bi,*L*)(Fe,Co)O_3 thin films with *L* = Dy, Er can explain the observed phenomena, including the significant ferroelectric hysteresis loop, high leakage

current at high voltage, unclear crystalline structure, and in-plane magnetic anisotropy. The presence of defect/pinholes is confirmed by X-ray photoelectron spectroscopy (XPS) examination.

During our work, we aimed to establish a connection between the ferroelectric properties of (Bi,*L*)(Fe,Co)O_3 thin films and the tendency of the lanthanides present to create oxygen vacancies. We specifically focused on comparing two films, BErFCO and BEuFCO. Our theory suggested that the thin film containing a dopant with a higher oxidizing tendency would have a reduced concentration of oxygen vacancies. Based on the Ellingham diagram, we concluded that Er exhibits a greater propensity for oxidation in comparison to Eu. Therefore, according to our premise, the thin film BErFCO, which clearly shows a ferroelectric curve, is expected to have a reduced amount of oxygen vacancies as a result of the stronger oxidizing properties of Er. In contrast, BEuFCO, which has a suboptimal ferroelectric curve, may possess a greater abundance of oxygen vacancies due to the diminished propensity of Eu for oxidation.

X-ray Photoelectron Spectroscopy (XPS) was employed to undertake a comprehensive examination of the chemical surroundings of oxygen. The objective was to determine the degree of oxygen deficit in two separate thin films: BErFCO and BEuFCO. In Figure 44, the O 1s peaks indicate the presence of two distinct oxygen states: vacancy oxygen (O_V) and lattice oxygen (O_L). By carefully analyzing the O 1s level spectra, two distinct Gaussian components are identified, each with binding energies of 532 and 530 eV, respectively. The 530 eV peak is ascribed to O^{2-} ions present in the original structure of bismuth ferrite (BFO) (O_L), whereas the 532 eV peak belongs to O^{2-} ions located in areas of oxygen deficiency within the BFO lattice matrix (O_V). The quantification of oxygen vacancies was accomplished by computing the integral of the curves following fitting using the Pseudo-Voigt function, which combines Gaussian and Lorentzian functions. A comparative evaluation was performed to determine the estimated percentage of oxygen vacancies in (Bi,Er)(Fe,Co)O_3 and (Bi,Eu)(Fe,Co)O_3 thin films.

The analysis revealed a greater abundance of oxygen vacancies (O_V) in BErFCO compared to BEuFCO. This observation clearly implies that the BErFCO thin film has a larger number of pinning sites, indicating a higher concentration of oxygen vacancies compared to the BEuFCO thin film.

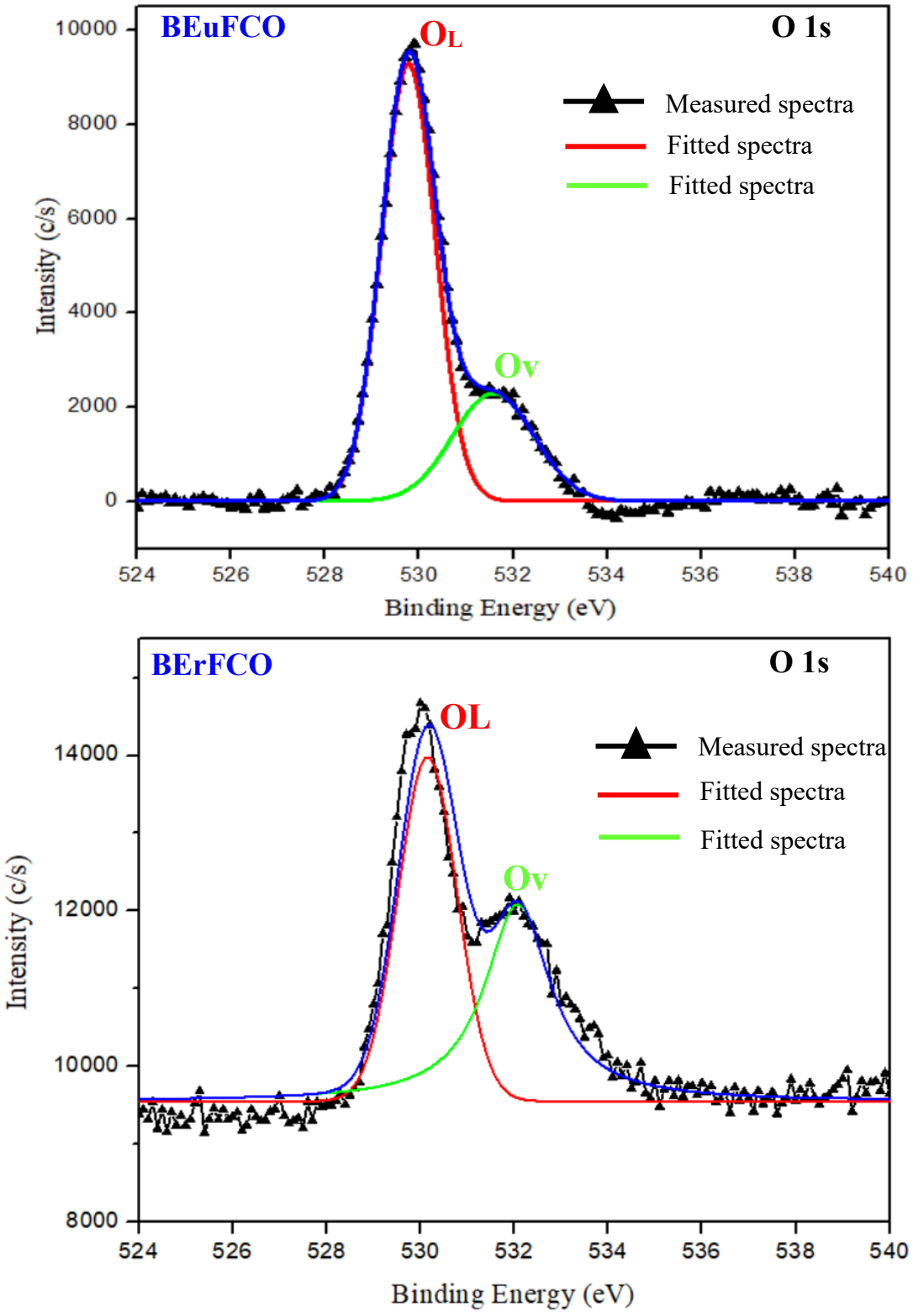

Figure 44. Comparison of oxygen vacancies between Er (high oxidizing tendency) and Eu (high oxidizing tendency) substituted BFO based thin films by XPS.

This thorough XPS study offers a comprehensive and quantitative comprehension of the oxygen-deficient areas in the thin films, elucidating the intricate interaction between lanthanide dopants, oxygen vacancies, and the consequent characteristics of the bismuth ferrite-based thin films.

3.5. Conclusion of Chapter 3

Table 3. Magnetic properties (M_s, $H_{c\perp}$, $H_{c\perp}/H_{c//}$, $S_\perp/S_{//}$, Θ_k) of (Bi,*L*)(Fe, Co)O_3 (*L*: Lanthanides) thin films prepared by p-DC reactive sputtering.

Substitution element	La	Nd	Sm	Eu	Gd	Dy	Er
$Co^{2+}/(Fe^{3+}+Co^{2+})$	0.28	0.25	0.25	0.25	0.24	0.27	0.24
M_s (emu/cm^3)	80	140	110	110	65	75	135
$H_{c\perp}$ (kOe)	2.6	2.1	1.9	0.8	2.2	2.7	1.9
$H_{c\perp}$ / $H_{c//}$	1.6	2.6	2.1	1.5	2.8	1.7	1.5
$S_\perp$ / $S_{//}$	1.3	1.0	1.4	0.3	1.4	0.6	0.6
Θ_k (°@750 nm)	0.67	0.34	0.21	0.21	0.19	0.23	0.23

Multiferroic thin films with good magnetic properties were successfully fabricated. All the improved magnetic properties are listed in table 3. The thin films of (Bi,*L*)(Fe,Co)O_3 (*L*: Lanthanides) had a relatively high M_s, $H_{c\perp}$, $H_{c\perp}/H_{c//}$, $S_\perp/S_{//}$ and Θ_k. Especially, (Bi,Nd)(Fe,Co)O_3 thin film shows a very high M_s of 140 emu/cm^3, a high $H_{c\perp}/H_{c//}$ and $S_\perp/S_{//}$ of 2.6 and 1.0. From these results, (Bi,Nd)(Fe,Co)O_3 thin film is suitable for realization of magnetic nano devices such as high density memory device driven by electric field. An improved Θ_k of 0.67°, $H_{c\perp}/H_{c//}$ of 1.6 and $S_\perp/S_{//}$ of 1.3 was observed in (Bi,La)(Fe,Co)O_3 thin film. From this result, (Bi,La)(Fe,Co)O_3 thin film is suitable for realization of magnetic nano devices such as high-definition display device driven by electric field. (Bi,Eu)(Fe,Co)O_3 thin film shows a very low coercivity of 0.5 kOe, high M_s of 110 emu/cm^3. From this result, (Bi,Eu)(Fe,Co)O_3 thin film is suitable for nano sensor devices applications because of its high sensitivity to external magnetic field.

The combination of information obtained from ferroelectric polarization-electric field (*P*-*E*) curves and X-ray Photoelectron Spectroscopy (XPS) investigations strongly supports the idea that the increased tendency to oxidize has a significant influence on the formation of secondary phases,

leading to the disruption of the perovskite phase in (Bi,*L*)(Fe,Co)O_3 thin films. The significant occurrence of oxygen vacancies, as detected by XPS, is identified as a crucial element that leads to a series of unfavorable outcomes. These consequences encompass not only the generation of secondary phases but also encompass expressions such as reduced crystallization, decreased perpendicular magnetic anisotropy (PMA), and increased leakage current. The complex interaction among lanthanide dopants, oxygen vacancies, and the resulting material properties is revealed, emphasizing the crucial influence of oxidation tendencies in shaping the structural and functional traits of these sophisticated thin films.

CHAPTER – 4
Investigation on Potential to use in Nano Devices

Investigating the Nano Device Potential using BFO-Based Thin Films: Assessing the Full Potential of Nano Devices: A Thorough Examination of Thin Films of $(Bi,Nd)(Fe,Co)O_3$, $(Bi,La)(Fe,Co)O_3$, and $(Bi,Eu)(Fe,Co)O_3$.

Based on the acquired data, it is important to mention that $(Bi,Nd)(Fe,Co)O_3$ demonstrates significant saturation magnetization (M_s) and positive perpendicular magnetic anisotropy (PMA), making it a suitable candidate for nano device applications. Moreover, $(Bi,La)(Fe,Co)O_3$ exhibits a significantly high perpendicular magnetic anisotropy constant (Θ_k), hence enhancing its potential in the field of nanoscale devices. On the other hand, $(Bi,Eu)(Fe,Co)O_3$ demonstrates a very low coercivity (H_c), indicating interesting potential for targeted use in the field of nano devices.

In order to determine the suitability of these thin films for nano devices, an extensive examination was conducted, exploring key characteristics such as grain and magnetic domain size, Curie temperature, magnetization switching behavior, and the piezoelectric effect. By carefully analyzing these crucial factors, our objective is to offer a detailed comprehension of the distinctive attributes that render these thin films as highly favorable options for advanced nano device applications.

4.1. Nanoscale Characterization by Using AFM and MFM

The Importance of Small Grain and Domain Sizes in Magnetic Nano Devices

The investigation and application of small grain and domain sizes in magnetic nano devices are crucial factors based on the fundamental principles of nanomaterial science and device engineering. The significance of very small scales in magnetic nano devices is influenced by several critical parameters, which determine their performance and application.

1. ***Improved Magnetic Properties***

At the nanoscale, the decrease in grain and domain sizes frequently results in an augmentation of the surface-to-volume ratio. This effect, known as magnetic amplification, can intensify magnetic interactions, leading to improved magnetic characteristics such as higher saturation magnetization

and enhanced coercivity. As a result, magnetic nano devices that have reduced grain and domain sizes demonstrate higher magnetic performance, which is a crucial characteristic for effective device operation.

2. ***Decreased Energy Consumption***

The use of small grain and domain sizes results in a decrease in the amount of energy needed for magnetization operations. Minimizing energy consumption is crucial in magnetic nano devices to provide efficient operations, especially in applications where power economy is a significant factor, such as data storage and processing.

3. ***Enhanced Switching Dynamics***

Reduced grain and domain sizes impact the switching dynamics of magnetic moments. Decreased magnetic domain size facilitates quicker response times during the process of magnetization reversal. This characteristic is particularly beneficial for high-frequency applications, where quick and effective switching is crucial.

4. ***Increased Density and Miniaturization***

The capacity to produce magnetic nano devices with diminutive grain and domain sizes enables the achievement of greater device packing densities. Miniaturization is essential for achieving tiny and lightweight gadgets, which is a significant objective in modern technology due to the increasing demand for such products. The compact dimensions facilitate the incorporation of magnetic capabilities into nanoscale components, hence facilitating the advancement of sophisticated and space-saving technology.

5. ***Multifunctionality and Integration***

Nanoscale materials possess distinct and frequently adjustable characteristics. The small sizes of grains and domains in magnetic nano devices allow for the incorporation of numerous capabilities, such as the combination of ferromagnetism with other physical phenomena like ferroelectricity. This creates opportunities for the advancement of versatile devices with unique and customized characteristics, broadening the range of uses in fields like spintronics and quantum computing.

Ultimately, the significance of having small grain and domain sizes in magnetic nano devices lies in their capacity to amplify magnetic characteristics, decrease energy usage, enhance switching

dynamics, allow for greater device packing densities, and enable multifunctionality. These characteristics collectively contribute to the creation of magnetic nano devices that are more efficient, smaller in size, and adaptable, with a wide range of applications in modern technology.

Analysis of AFM and MFM reveals nanostructural and magnetic characteristics of $(Bi,Nd)(Fe,Co)O_3$, $(Bi,La)(Fe,Co)O_3$, and $(Bi,Eu)(Fe,Co)O_3$ thin films.

The topographic and magnetic domain properties of the studied thin films, specifically $(Bi,Nd)(Fe,Co)O_3$, $(Bi,La)(Fe,Co)O_3$, and $(Bi,Eu)(Fe,Co)O_3$, were thoroughly examined using atomic force microscopy (AFM) and magnetic force microscopy (MFM), as illustrated in Figure 45. The AFM images offer vital information on the surface morphology, showcasing clear and well-defined grain boundaries in $(Bi,Nd)(Fe,Co)O_3$ and $(Bi,La)(Fe,Co)O_3$. This observation indicates a remarkably ordered arrangement of atoms in these films, which aligns with the results obtained from X-ray diffraction (XRD) and scanning electron microscopy (SEM) images.

However, in the case of $(Bi,Eu)(Fe,Co)O_3$, the grain boundaries are less prominent, suggesting a somewhat lower degree of crystallinity. This observation is consistent with the findings derived from X-ray diffraction (XRD) and scanning electron microscopy (SEM) investigations. Histogram method (figure 46) revealed a grain size of 130 ± 22 nm and a magnetic domain size of 90 ± 8 nm for $(Bi,Nd)(Fe,Co)O_3$. Figure 45 shows that the grain size of $(Bi,La)(Fe,Co)O_3$ is about 140 ± 20 nm, and the domain size is around 50 ± 5 nm. In contrast, Figure 7 demonstrates that the grain size of $(Bi,Eu)(Fe,Co)O_3$ is approximately 140 ± 10 nm, and the domain size is around 170 ± 12 nm.

Surprisingly, the domain sizes observed in these multiferroic thin films are rather small, falling within the nanometer scale. These films have properties that are in between the magnetic domain size [23, 33] of magnetic thin films and the electric domain size of ferroelectric thin films [34, 35]. This result highlights the appropriateness of using these thin films for magnetic nano device applications, creating opportunities for innovative technologies that utilize the distinct interaction between ferromagnetism and ferroelectricity at the nanoscale.

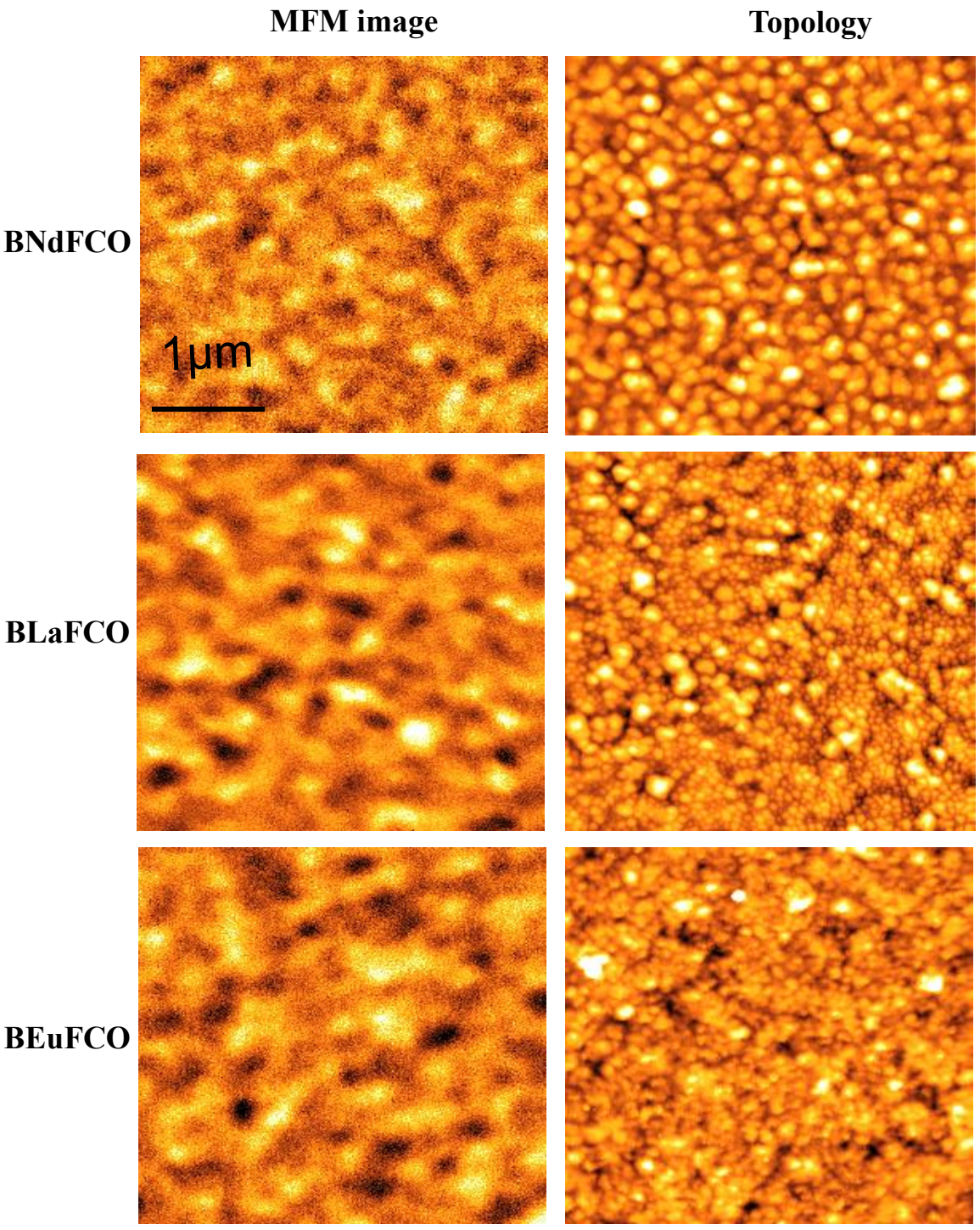

Figure 45. Topographic and MFM images of $(Bi,Nd)(Fe,Co)O_3$, $(Bi,La)(Fe,Co)O_3$ and $(Bi,Eu)(Fe,Co)O_3$ thin films prepared by p-DC reactive sputtering, respectively.

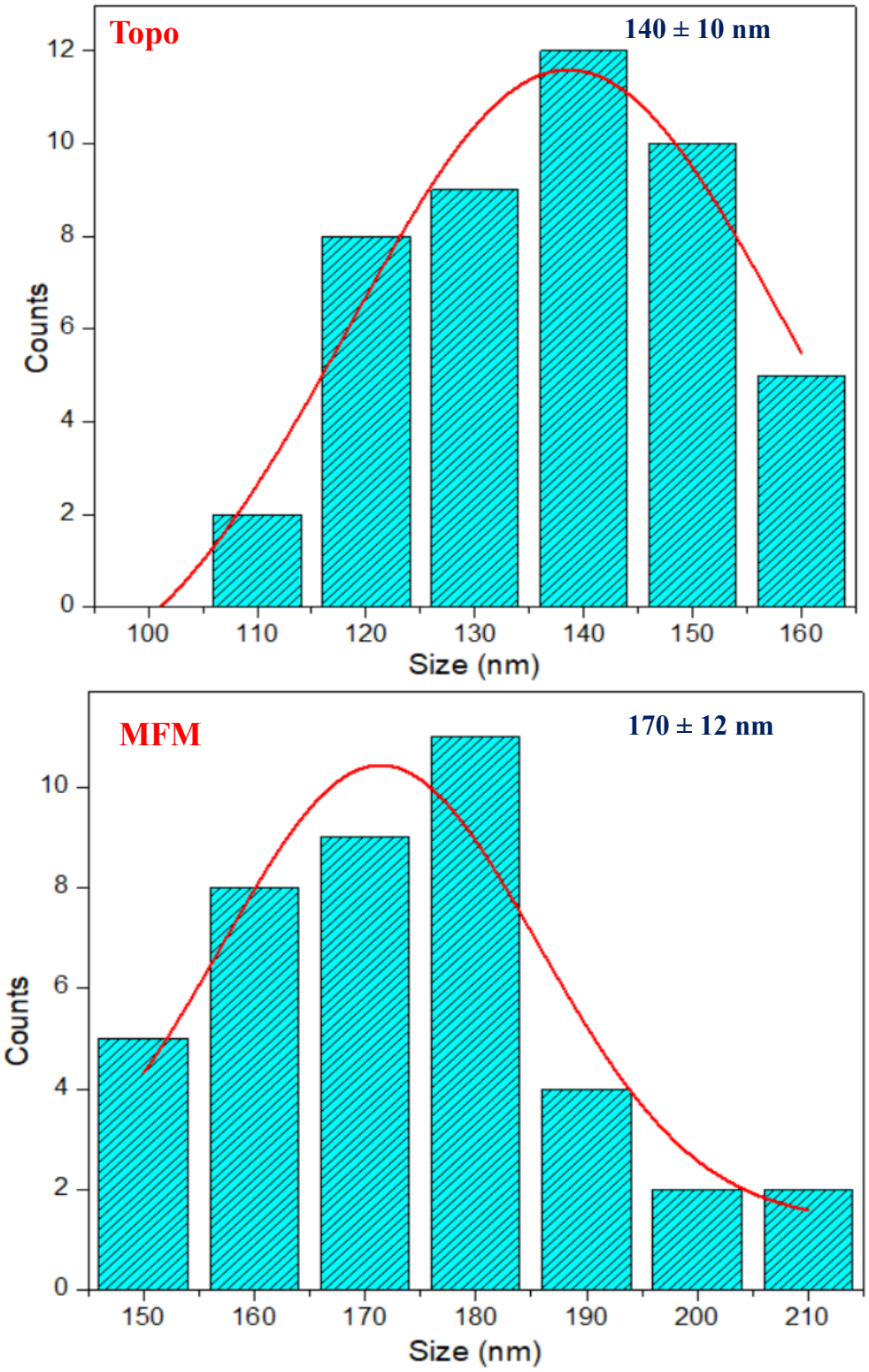

Figure 46. Histogram of grain size and domain size distribution.

4.2. Temperature Dependence Magnetization Study by VSM

Magnetic nanodevices have become crucial components in a wide range of technological applications, including data storage and medical diagnostics. Comprehending the relationship between temperature and magnetism in these devices is essential for maximizing their efficiency and guaranteeing their dependability in various operating settings.

Temperature-dependent magnetization studies are a crucial method for evaluating the thermal durability of magnetic nano electronics. Examining the relationship between magnetization and temperature allows for a better understanding of the material's durability, which is helpful in developing devices that can function effectively in a broad range of temperatures.

The Curie temperature refers to the specific temperature at which a magnetic material experiences a phase transition and ceases to exhibit its magnetic properties. Studying how temperature affects magnetism enables us to identify the Curie temperature, an essential factor in choosing materials appropriate for particular uses.

Materials have large variations in their magnetic properties at different temperatures. Temperature-dependent magnetization studies aid researchers in determining the specific temperature range at which a material has its highest magnetic performance. This knowledge facilitates the development of nano devices that possess improved efficiency.

During operation, magnetic nano devices may experience high temperatures in some applications. Investigating magnetization alterations at elevated temperatures yields crucial insights into the characteristics of the magnetic material in such circumstances, aiding in the identification of materials that retain their magnetic properties at high temperatures.

At higher temperatures, the thermal energy causes the misalignment of magnetic moments in a material. This disturbance undermines the overall magnetic arrangement, resulting in a reduction in magnetization. Under certain circumstances, elevated temperatures can induce a phase transition in a material, leading to changes in its magnetic characteristics or even a complete loss of magnetism.

Temperature-dependent magnetization studies are crucial in customizing magnetic nano electronics for specific applications.

Figure 47 depicts the temperature-dependent characteristics of saturation magnetization (M_s) for thin films of (Bi,Nd)(Fe,Co)O_3 and (Bi,Eu)(Fe,Co)O_3. The figure also includes magnetization curves obtained at three different temperatures (20, 250, and 450 °C). Furthermore, the magnetization curve for the (Bi,La)(Fe,Co)O_3 thin film at room temperature is included as a point of reference, along with the temperature dependence of M_s. At a temperature of 250 °C, a noticeable hysteresis is observed, and examination of the rate of change of magnetization with respect to temperature (dM/dT) suggests a probable Curie temperature (T_c) of approximately 450 °C. The observed high T_c values are of utmost importance for applications in nano devices, indicating strong thermal stability. These discoveries reveal important information on the magnetic characteristics of thin films, which is essential for designing and optimizing nano devices, especially those that need to be resilient and effective at various operational temperatures.

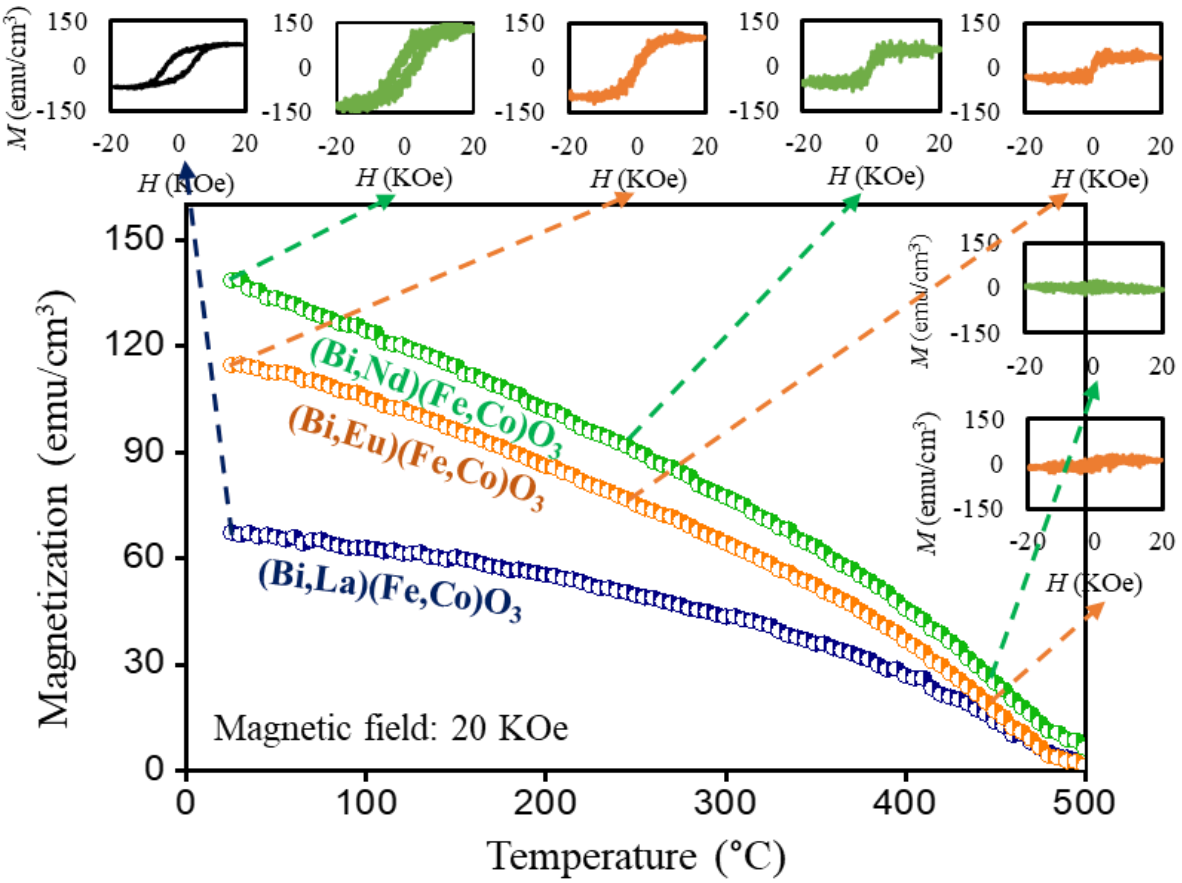

Figure 47. Saturation magnetization for (Bi,Eu)(Fe,Co)O_3, (Bi,Nd)(Fe,Co)O_3, and (Bi,La)(Fe,Co)O_3 thin films prepared by p-DC reactive sputtering as a function of measurement temperature and the magnetization curves at 20 ˚C, 250 ˚C, and 450 ˚C.

4.3. Magnetization Switching Study by EFM

Figure 48 presents the results of an exhaustive investigation that utilized cutting-edge imaging techniques, including atomic force microscopy (AFM), magnetic force microscopy (MFM), and electric force microscopy (EFM), in order to investigate the complex interaction of topographic, magnetic, and electric properties that are present in thin films of (Bi,La)(Fe,Co)O_3. An unexpected alteration takes place as a result of local electric field writing, which is accomplished by a conductive tip at -10 V. This provides insights into the dynamic behavior of these multiferroic materials that have never been seen before.

The process of writing, which is carried out in "contact mode" with a scan speed of 5 μm/s and steps at every 10 nm, methodically catches the subtle changes that occur throughout AFM, MFM, and EFM images. The MFM spatial resolution achieved an astounding 10 nm in the work that came before this one, which was sufficient for distinguishing magnetic domains with widths on the order of several hundred nanometers for the purpose of detection. Before being exposed to a local electric field, the MFM image demonstrates that the subject is in a condition of demagnetization. A striking contrast is provided by the post-writing MFM image, which depicts magnetic domains that are clearly defined and exhibit a definite magnetization direction that goes from down to up.

This particular magnetic pattern is reflected in the appropriate EFM image, which is an extremely important aspect. Nevertheless, a discernible variation in color contrast is brought about as a consequence of the deliberate introduction of a low voltage (-1 V) to the Co-Cr-Pt tip during the EFM measurement process. Due to this purposeful choice, the discrimination between MFM and EFM images is improved, with a particular emphasis placed on the induced magnetization pattern that has a width of 500 nm and originates from the local electric field.

Our comprehension of the dynamic relationship that exists between electric fields and magnetic responses in multiferroic thin films has been significantly advanced as a result of these aforementioned discoveries. With the help of this study, the complicated dynamics of electric field-driven magnetization have been deciphered, which opens up intriguing avenues for designing and modifying magnetic domains in these materials. This lays the groundwork for innovative applications in the arena of multifunctional devices and emerging technologies.

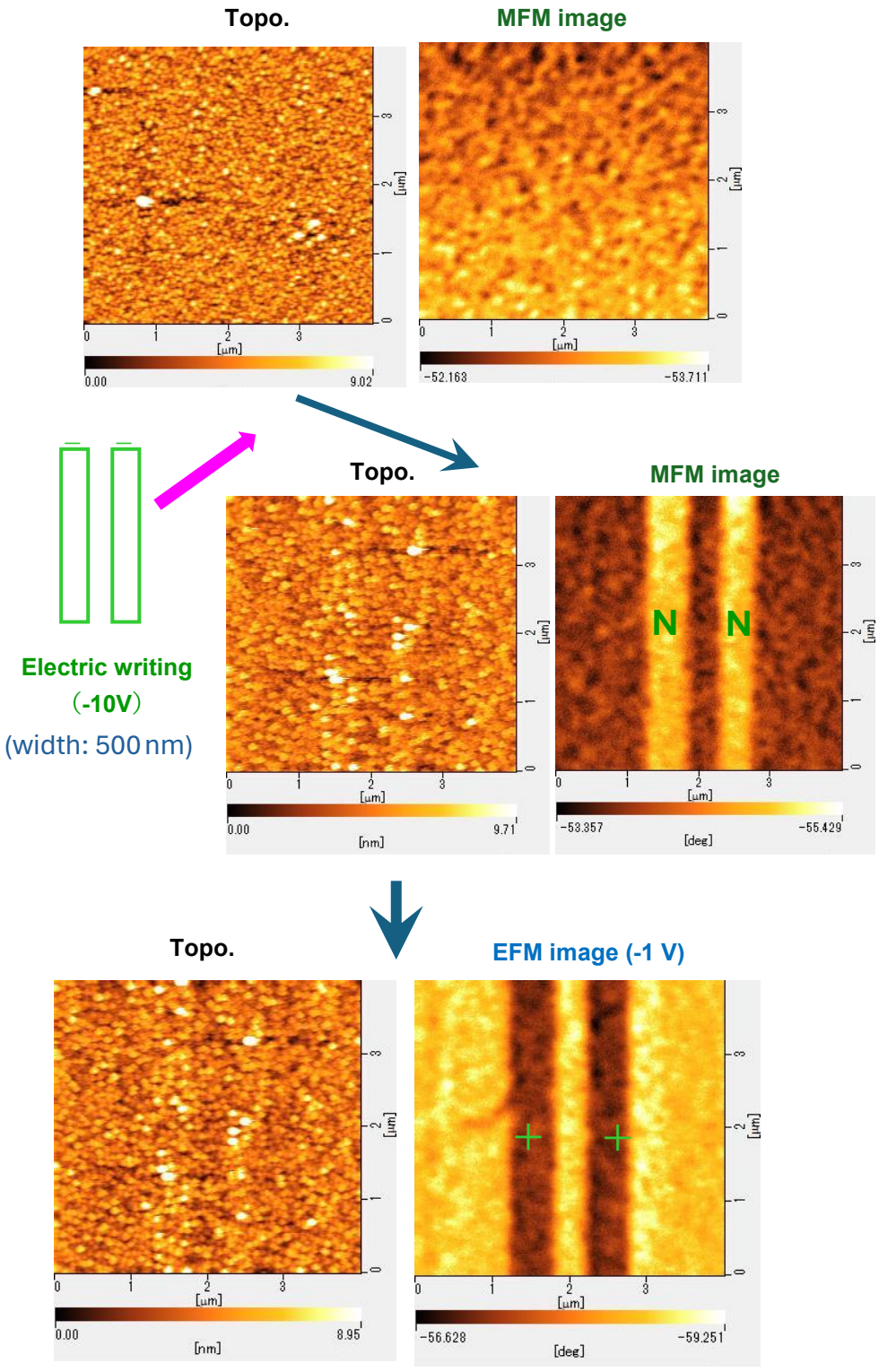

Figure 48. Topographic, MFM (tip end: N), and EFM (tip end: –) images of (Bi,La)(Fe,Co)O_3 thin film of before and after applying DC voltage of − 10 V.

During our study of $(Bi,La)(Fe,Co)O_3$ thin films, we examined the impressive capacity to cause magnetization reversal at a submicron scale by using local electric field writing. We produced Magnetic Force Microscopy (MFM) and Electric Force Microscopy (EFM) images by methodically adjusting the width of the electric field writing from 500 to 100 nm using a conductive tip at -10 V. These images provided insights into the complex behavior of induced domains.

Figure 49 displays the MFM and EFM images obtained by applying a direct current (DC) voltage of -10 V with different widths. Examining the line profiles and Full Width at Half Maximum (FWHM) of induced domains for each width uncovers fascinating observations. For widths up to 300 nm, the full width at half maximum (FWHM) closely corresponds to the expected value of electric field writing. However, when the wavelength is less than 300 nm, the full width at half maximum (FWHM) exceeds the expected width, indicating a subtle impact on the development of domains at these sizes.

A thorough analysis is warranted due to the observed disparity in full width at half maximum (FWHM) values between the magnetic force microscopy (MFM) and electrostatic force microscopy (EFM) pictures. Significantly, the demarcation between domains in the MFM image exhibits reduced clarity in comparison to the EFM image. This phenomenon becomes more noticeable in extremely limited areas, such as those with widths of 100 and 200 nanometers. The MFM line profiles exhibit modest slope and valley features, suggesting a reduced magnetic moment interaction compared to EFM. The presence of this phenomena, which is not frequently observed in ferromagnetic and ferroelectric films, highlights the intermediate characteristics of $(Bi,La)(Fe,Co)O_3$ thin films, where the interactions between magnetic and electric moments have a substantial influence.

These findings signify a significant accomplishment, showcasing the ability to reverse magnetization at a scale smaller than a micron by applying an electric field locally. The discovered interactions between magnetic and electric moments present a new opportunity for the development of sophisticated magnetic devices, which in turn allows for the exploration of fresh applications in magnetoelectric technologies at the submicron scale.

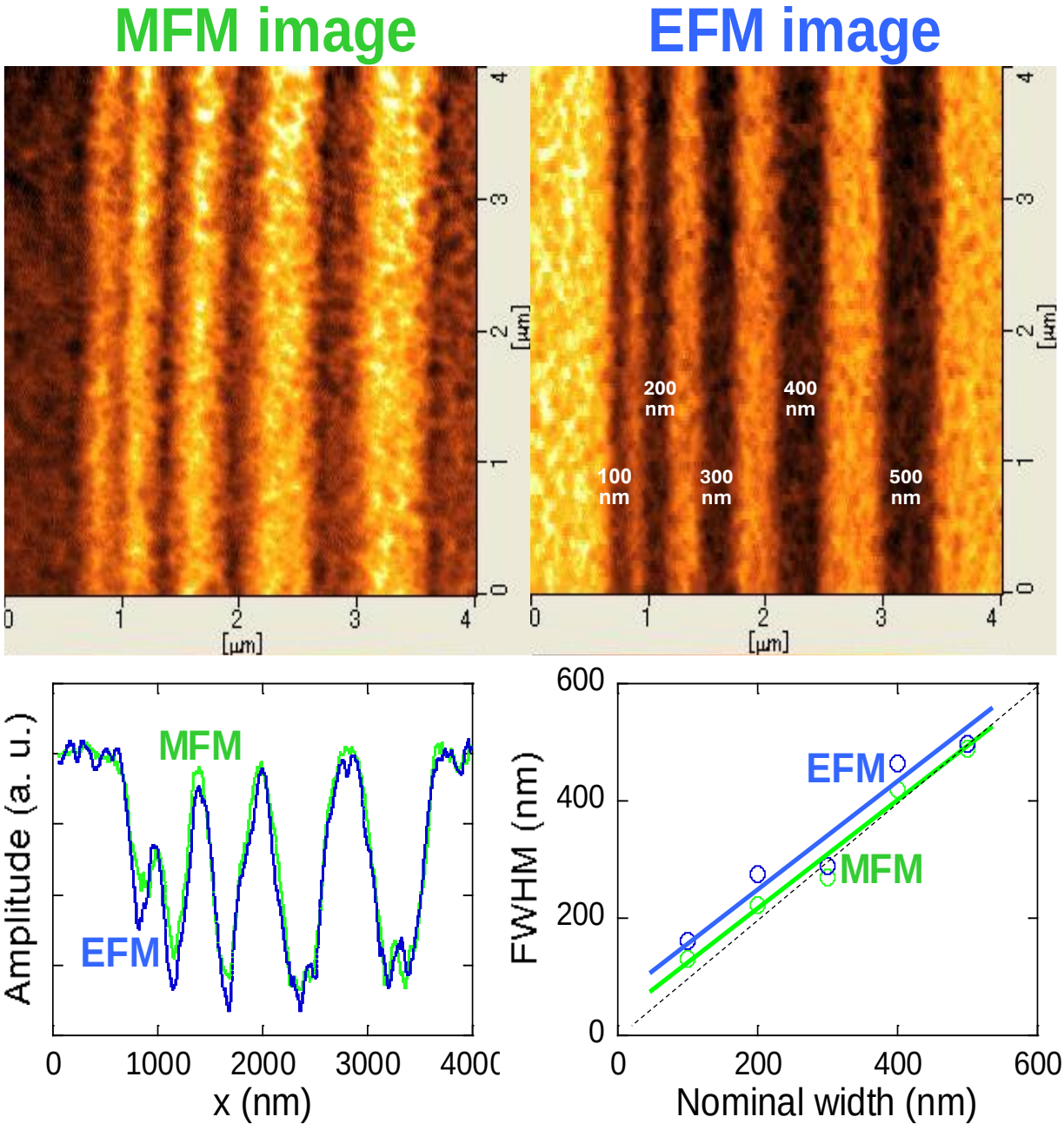

Figure 49. MFM (tip end: N), and EFM (tip end: –) images of (Bi,La)(Fe,Co)O_3 thin film after applying DC voltage of − 10 V with various widths. The line profile of both images and full width at half maximum of each domain.

4.4. Leakage Current and PFM Study

Attaining optimal performance in the field of magnetic nano devices requires careful consideration of the interaction between electrical fields and material reactions. The primary objective is to minimize the leakage current as much as feasible. Ensuring a minimal amount of current leakage is crucial in order to preserve the integrity of magnetic nano devices and avoid any unwanted electrical losses that may potentially undermine their operating effectiveness.

Furthermore, the pursuit of perfection also involves reducing the piezoelectric effect, which occurs when an electric field is applied and can cause strain in addition to magnetization. The simultaneous reaction is a possible obstacle to the durability and consistency of magnetic nano devices. To address this worry, it is necessary to not only reduce the piezoelectric effect but also comprehend and regulate the complex interaction between electric fields and strain in order to maintain the magnetic characteristics.

This study highlights the crucial significance of simultaneously attaining low leakage current and limiting the piezoelectric effect in the context of magnetic nano device applications. By thoroughly investigating materials and designing devices, our goal is to advance the development of magnetic nano devices with improved dependability, less energy wastage, and enhanced overall performance in various technical fields. To study this, we selected $(Bi,Nd)(Fe,Co)O_3$ thin film for leakage current and piezoelectric measurements.

We conducted a detailed study to evaluate the intrinsic properties of multiferroic thin films as part of our efforts to optimize magnetic nano electronics. We utilized a meticulous approach to examine the piezoelectric effect through voltage versus phase (degree) measurements, and to investigate the dynamics of leakage current using voltage versus amplitude (arb. unit) measurements (refer figure 50). The results obtained from this extensive investigation provide strong evidence of significantly reduced piezoelectric effect and negligible leakage current in our carefully fabricated multiferroic thin films.

The voltage-phase measurements conducted in the piezoelectric investigation revealed the material's reaction to electric fields, offering valuable information about the level of strain produced in conjunction with magnetization dynamics. The significant reduction in the piezoelectric effect that we observed highlights the success of our method in minimizing strain that is not desirable when applying an electric field. The decrease in piezoelectric response is

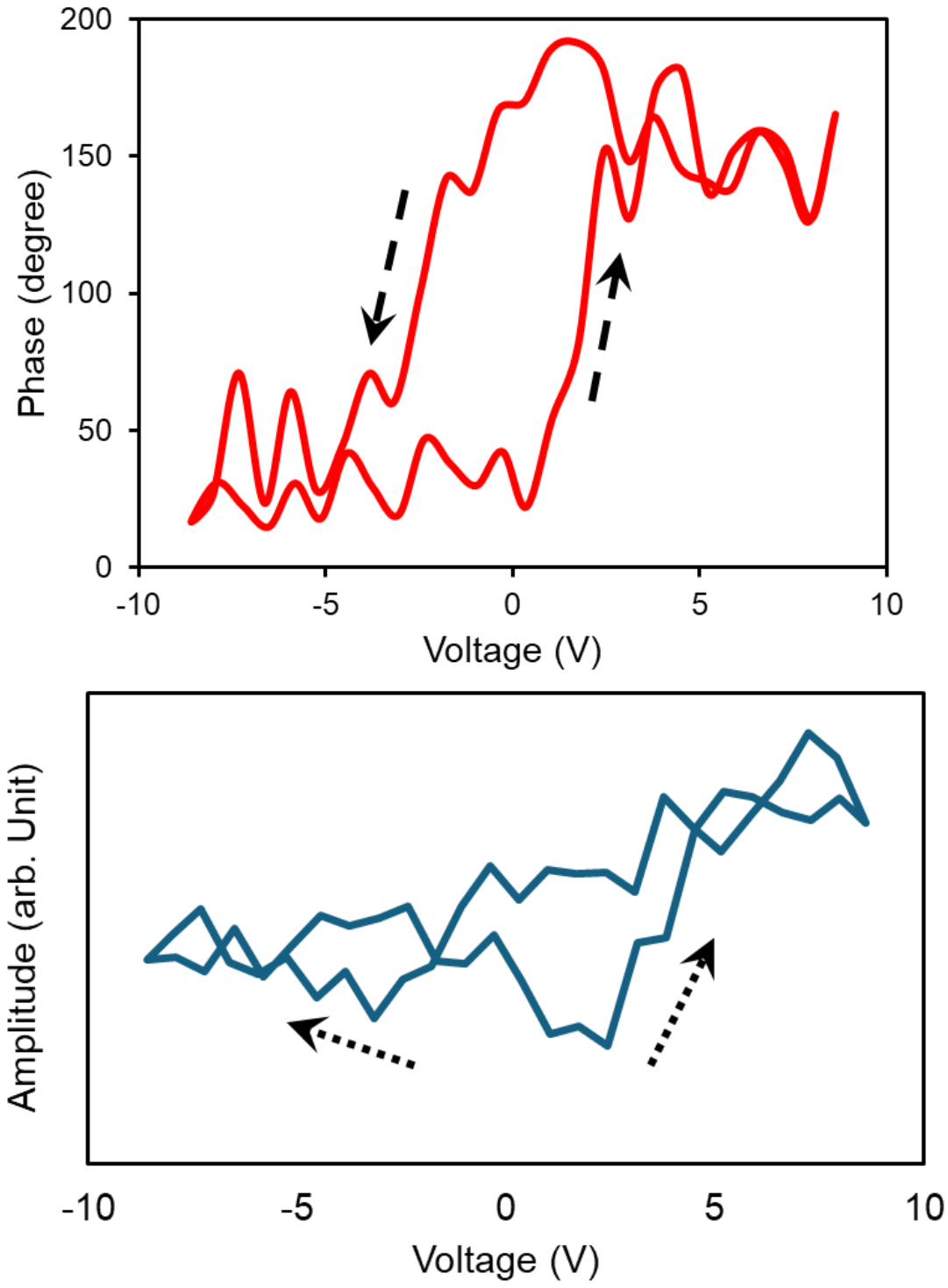

Figure 50. PFM and leakage current study in (Bi,Nd)(Fe,Co)O_3 thin films

crucial for guaranteeing the stability and dependability of magnetic nano devices, where maintaining accurate control over magnetization is of utmost importance.

The voltage versus amplitude measurements conducted during the leakage current study allowed for a thorough investigation of electrical losses occurring within the material. The observed negligible leakage current in our multiferroic thin films has significant implications for magnetic nano devices, as it indicates an enhanced ability to maintain electrical integrity and reduce energy losses during operation.

The successful combination of reduced piezoelectric effect and negligible leakage current in our fabricated multiferroic thin films provides a strong basis for the progress of magnetic nano devices. This study not only enhances our fundamental understanding of material behavior but also establishes our materials as very promising candidates for the advancement of durable and efficient magnetic nano devices in various technological applications.

4.5. Conclusion of Chapter-4

During our thorough examination of potential materials for use in magnetic devices, we conducted a detailed analysis to evaluate the key factors that affect their practical suitability." The thin films, specifically BNdFCO, BLaFCO, and BEuFCO, displayed exceptionally favorable properties. Significantly, their grain size and domain size were determined to be within the nanometer range, which is a desirable characteristic for achieving optimal performance in magnetic devices. In addition, all of the thin films exhibited an exceptionally high Curie temperature, which is a crucial characteristic for assuring stability and usefulness in magnetic applications.

Our work specifically examined the magnetization switching potential of BLaFCO and found that it has successful magnetization switching capabilities. This result highlights the practicality of these materials for creating magnetic devices that are both responsive and efficient. In addition, we conducted research on BNdFCO thin films, and we noticed a minimum amount of leakage current and a significant piezoelectric effect. This is crucial for improving the performance of memory devices. The combination of these features makes the researched thin films highly promising for developing magnetic device technology.

Chapter-5
Investigation on the Etching Resistance

To investigate the resistance of the films against etching (DE & RIE) for microfabrication to apply the films to magnetic nano devices.

The preservation of delicate magnetic properties required for the functionality of magnetic nano devices is of utmost importance in limiting magnetic damage during the etching process in their manufacture. Magnetic nano technologies, such as magnetic sensors, memory elements, and spintronic components, require accurate manipulation and preservation of magnetic states at the nanoscale. The unintentional modification of the magnetic structure during the etching process can greatly impact the performance and dependability of these devices. There are numerous crucial considerations that highlight the significance of minimizing magnetic damage:

1. ***Sustaining Magnetic Order***

The operation of magnetic nano devices frequently relies on the utilization of organized magnetic structures. If the etching process is not meticulously regulated, it might create flaws or modify the magnetic arrangement, resulting in modifications to the magnetic characteristics of the device. Preserving the inherent magnetic order is crucial for attaining the intended magnetic characteristics.

2. ***Preserving Spin States***

The alignment of electron spins is crucial for information storage and processing in spintronic devices. Etching-induced magnetic degradation can disrupt the alignment of spin states, resulting in a decrease in coherence and reliability in spin-based functions. Ensuring the preservation of spin states, which are crucial for spintronic applications, involves minimizing magnetic damage.

3. ***Mitigating the Formation of Domain Walls***

Magnetic nanostructures frequently display discernible magnetic domains. The occurrence of excessive magnetic damage during the etching process can lead to the creation of domain walls. These walls serve as obstacles to energy flow and can have a detrimental effect on the operation of the device. Implementing a regulated etching procedure is crucial in order to prevent inadvertent alterations in domain structures.

4. ***Maintaining Anisotropy***

Magnetic anisotropy, which refers to the directional dependence of magnetic characteristics, plays a crucial role in numerous magnetic nano devices. Unintentional magnetic damage can cause

changes to the anisotropic properties, resulting in a divergence from the desired magnetic behavior. It is essential to minimize damage in order to maintain the necessary anisotropic features.

5. ***Improving Device Efficiency***

Magnetic damage can lead to heightened energy dissipation and diminished signal-to-noise ratios in magnetic devices. By minimizing damage during the etching process, the devices can function more efficiently, resulting in enhanced signal fidelity and decreased energy usage.

6. ***Facilitating Integration***

Magnetic nanodevices frequently serve as constituents inside more extensive integrated systems. Any magnetic harm sustained during the etching procedure could impede the smooth incorporation of these gadgets into intricate circuits and systems. Minimizing damage improves compatibility with other components.

Prior publications have noticeably lacked investigation into appropriate etching gases and exact process parameters for thin films based on Bismuth Ferrite (BFO) in the field of microfabrication for magnetic devices. The ability of these thin films to withstand etching procedures is a crucial factor in microfabrication, necessitating a thorough investigation of the dynamics of dry etching (DE) and reactive ion etching (RIE). Although DE and RIE processes have been thoroughly studied by different researchers in oxide films such SiO_2 and certain metal thin films [36, 37, 38], their effects on BFO-based multiferroic thin films have not been adequately addressed.

The current body of research offers limited understanding of the impact of dielectric engineering (DE) and reactive ion etching (RIE) on the structural stability of thin films based on bismuth ferrite (BFO). These processes have the potential to cause changes in the crystal structure, which may disrupt the ferromagnetic and ferroelectric properties that are characteristic of multiferroic thin films. Our study aims to investigate the potential morphological and magnetic damage caused by RIE in BFO-based thin films, particularly those with the composition $(Bi,Eu)(Fe,Co)O_3$, referred to as BEuFCO. This research is groundbreaking in its exploration of these effects.

In this study, our objective was to determine the most favorable etching setting for both DE and RIE methods, in order to minimize any magnetic damage to the $(Bi,Eu)(Fe,Co)O_3$ thin film. This involves a detailed examination of the complexities associated with microfabrication methods, considering the delicate equilibrium needed to maintain the fragile multiferroic characteristics of the thin film while attaining the desired etching result.

In the end, our research resulted in identifying a specific and clearly defined set of etching parameters that are considered appropriate for creating multiferroic thin films based on BFO. This accomplishment not only enhances the progress of microfabrication methods for magnetic devices, but also offers a basis for future investigations into the complex relationship between etching procedures and the structural stability of multifunctional thin films. The scientific community can utilize these discoveries to improve microfabrication techniques, thereby revealing new opportunities for the creation of durable and precisely designed BFO-based magnetic devices.

5.1. Fabrication of Micro Dots

We utilized a unique approach in our endeavor to create micro dots on Bismuth Ferrite (BFO)-based multiferroic thin films. The method began by applying a positive photoresist layer onto the thin films based on BFO. Following that, the multilayer structure experienced a short duration of heating, lasting for 3 minutes. Subsequently, a controlled amount of light was applied using photolithography to create small dots in the photoresist layer on the surface of BFO.

The main differentiation in this method is based on the following exposure to different etching conditions. By strategically applying the positive photoresist, specific areas of the BFO surface were protected, while leaving other areas uncovered. When exposed to the etching gas, the parts that were covered by the resist were shielded from harm, leading to a clear distinction with the areas that lacked resist. These unprotected areas were directly affected by the etching gas, causing damage to the surface.

The intentional division allowed for a direct comparison of magnetic property alterations between the areas that were damaged (out-of-dot) and the areas that were not harmed (on-dot). Through meticulous manipulation of the etching conditions, we were able to methodically assess the impact of the etching process on the magnetic characteristics of the BFO-based multiferroic thin films.

This methodological approach enables the targeted examination of magnetic damage and serves as a significant tool for comprehending the intricate relationship between etching conditions and the subsequent changes in magnetic properties. The use of micro dots produced using photolithography and resist shielding allows for a focused investigation of magnetic effects caused by etching. This provides important insights for improving the microfabrication methods used in BFO-based multiferroic thin films.

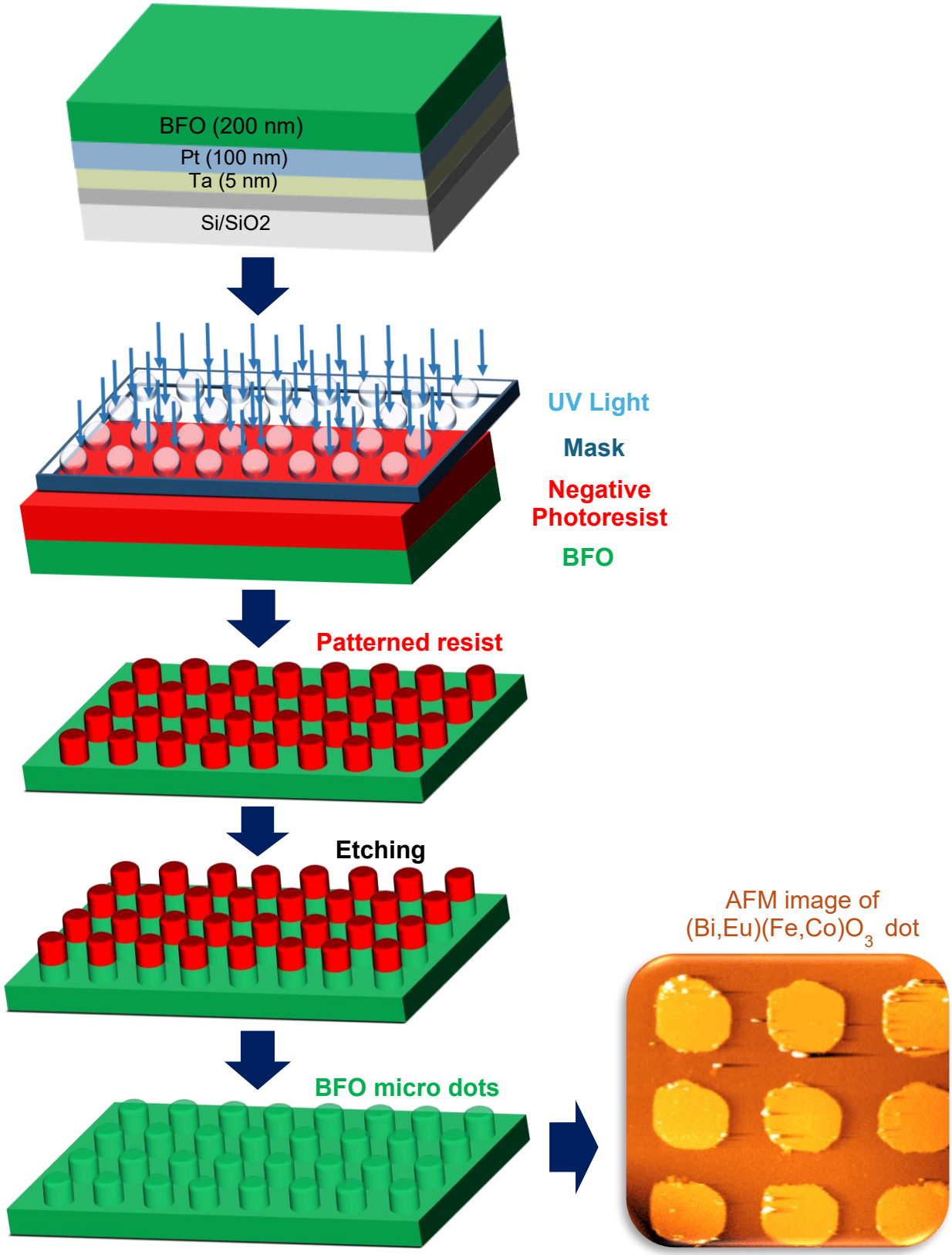

Figure 51. Schematic diagram of fabrication of microdots on (Bi,Eu)(Fe,Co)O_3 thin films

5.2. Reactive Ion Etching (RIE)

One of the important processes in microfabrication is the precise use of etching techniques, which allows for the targeted removal of material from the surface of the substrate [39]. Reactive Ion Etching (RIE) is a commonly used microfabrication technique that has proven to be highly effective. It is known for its exceptional precision in removing materials while causing minimal harm [40].

RIE functions by employing reactive ions to specifically remove compounds off the surface of the substrate. The effectiveness of this technique is based on the production of highly reactive ions in plasma, which is created by exposing a combination of gases to a high-frequency electrical field. This gas mixture commonly consists of a gas that is prone to chemical reactions and a gas that is not reactive [41, 42, 43]. The ionization of the reactive gas in the plasma generates reactive species that can chemically react with the substrate material, causing the development of volatile chemicals that are then eliminated from the surface.

Significantly, the successful control of damage during the etching process depends on two crucial factors: the careful choice of a suitable reactive gas and the fine-tuning of etching parameters. The reactive gas acts as the chemical agent that enables the controlled elimination of material, while the fine-tuning of parameters guarantees that the etching process is customized to the precise properties of the material being patterned.

Although researchers have extensively examined and reported on effective etching gases for thin metal films, there has been relatively little exploration in the field of multiferroic thin films, particularly those based on Bismuth Ferrite (BFO). We conducted an inquiry to address the absence of recorded information regarding the selection of appropriate etching gases and the optimization of etching parameters for multiferroic thin films based on BFO. Our main objective was to obtain precise micro patterning while minimizing damage, especially in terms of magnetic integrity.

This study emphasizes the necessity of a thorough scientific methodology in microfabrication, where every aspect of the process must be meticulously evaluated and enhanced. Our objective was to determine the effects of various reactive gases and optimize etching parameters in order to establish specific conditions that would enable precise microscale patterning while also preserving the complex magnetic properties of BFO-based multiferroic thin films. This study enhances the

overall scientific comprehension of microfabrication procedures for cutting-edge materials, so facilitating the progress of durable and dependable magnetic nano electronics.

Table 4. Etching rates in $(Bi,Eu)(Fe,Co)O_3$ thin films with different etching gases as well as process parameters

RIE Condition No.	Etching gas	Flow Rate (SCCM)	Pressure (Pa)	Power (Watt)	Etching rate (nm/min)
1	SF_6/O_2	50/5	4.0	100	~ 0.0003
2	CHF_3/O_2	50/5	4.0	100	~ 1.0
3	CHF_3	20	1.3	50	~ 0.62
4	CHF_3/O_2	50/5	10	100	~ 0.30
5	CHF_3	20	1.3	100	~ 1.5

In the pursuit of establishing an optimal etching rate for efficient material removal during the etching process, the judicious selection of etching gases and meticulous optimization of process parameters emerge as pivotal considerations, as summarized in Table 4. To assess the etching rates, a systematic approach was employed, wherein the thin film was divided into two halves: one shielded from the etching gas, and the other exposed. Each film underwent a 10-minute exposure to five different conditions, and through Atomic Force Microscopy (AFM), height differences between etched and protected portions were measured.

In our initial attempts, the use of Sulfur hexafluoride (SF_6) as the etching gas in the Reactive Ion Etching (RIE) method yielded a notably low etching rate, rendering it ineffective for rapid material removal. A significant breakthrough was achieved by transitioning to Trifluoromethane (CHF_3) as the etching gas, resulting in markedly increased etching rates that proved conducive to efficient surface removal. Various factors, including the influence of an O_2 environment and several other process parameters, were carefully considered during the optimization process for CHF_3. This method successfully yielded the desired etching rates for effective surface removal under RIE conditions 2 (RIE 2: 1.0 nm/min) and 5 (RIE 5: 1.5 nm/min), as detailed in Table 4.

To discern the most suitable etching condition between RIE 2 and RIE 5, additional investigations were undertaken to evaluate the extent of magnetic damage incurred in (Bi,Eu)(Fe,Co)O_3 thin films subjected to these RIE processes. Dot patterns with dimensions of 3 μm and 10 μm were intricately fabricated using photolithography on the thin films. Throughout the etching process, the dots were shielded by resist, safeguarding them from the etching radicals. This meticulous approach allowed for the attainment of an approximately 10 nm etching depth, facilitating the assessment of magnetic damage by comparing changes in magnetic characteristics between the unetched area (on-dot) and the etched area (out-of-dot). This comparative analysis provided a reliable measure of the magnetic effects induced by the etching process.

In essence, the systematic exploration and optimization of etching conditions, coupled with a thorough evaluation of resulting magnetic damage, exemplify a comprehensive approach toward advancing the microfabrication process for (Bi,Eu)(Fe,Co)O_3 thin films. These findings not only contribute to the development of efficient etching methodologies but also underscore the nuanced balance required to achieve precise material removal while preserving the delicate magnetic properties essential for the functionality of magnetic nano devices.

5.2.1. Local Coercivity Study in Etched Area by micro-MOKE

In Figure 52, the influence of laser position on coercivity, measured through micro-Magneto-Optical Kerr Effect (micro-MOKE) with a laser size of 3 μm, is depicted as the laser traverses from the central region to the outer periphery of a fabricated dot measuring 10 μm. To standardize coercivity values, a normalization technique was applied. This involved calculating the ratio between the coercivity values of each specific component and the average coercivity value (H_c average).

The observed results unveiled a consistent coercivity throughout the central to boundary region (up to 5 μm) of the dot. However, a noteworthy escalation in coercivity manifested in the outer region, particularly evident in the case of RIE 5. In contrast, while RIE 2 exhibited an increment in coercivity, it was comparatively less pronounced. These findings suggest that the introduction of an oxygen environment (CHF_3/O_2) along with Trifluoromethane (CHF_3) gas in the Reactive Ion Etching (RIE) method, as opposed to using CHF_3 alone, can mitigate magnetic damage in multiferroic thin films, thereby preserving their magnetic characteristics during the etching process.

The results of the coercivity variations underscore the dependence of magnetic damage on the etching gas in multiferroic thin films subjected to RIE, especially when the etching environment exclusively utilizes CHF_3 without the presence of O_2. The nuanced interplay between etching gases and environmental factors becomes apparent, demonstrating the critical role of process parameters in influencing the magnetic properties of the thin films during the microfabrication process. This insight contributes to a deeper understanding of the intricacies involved in optimizing etching

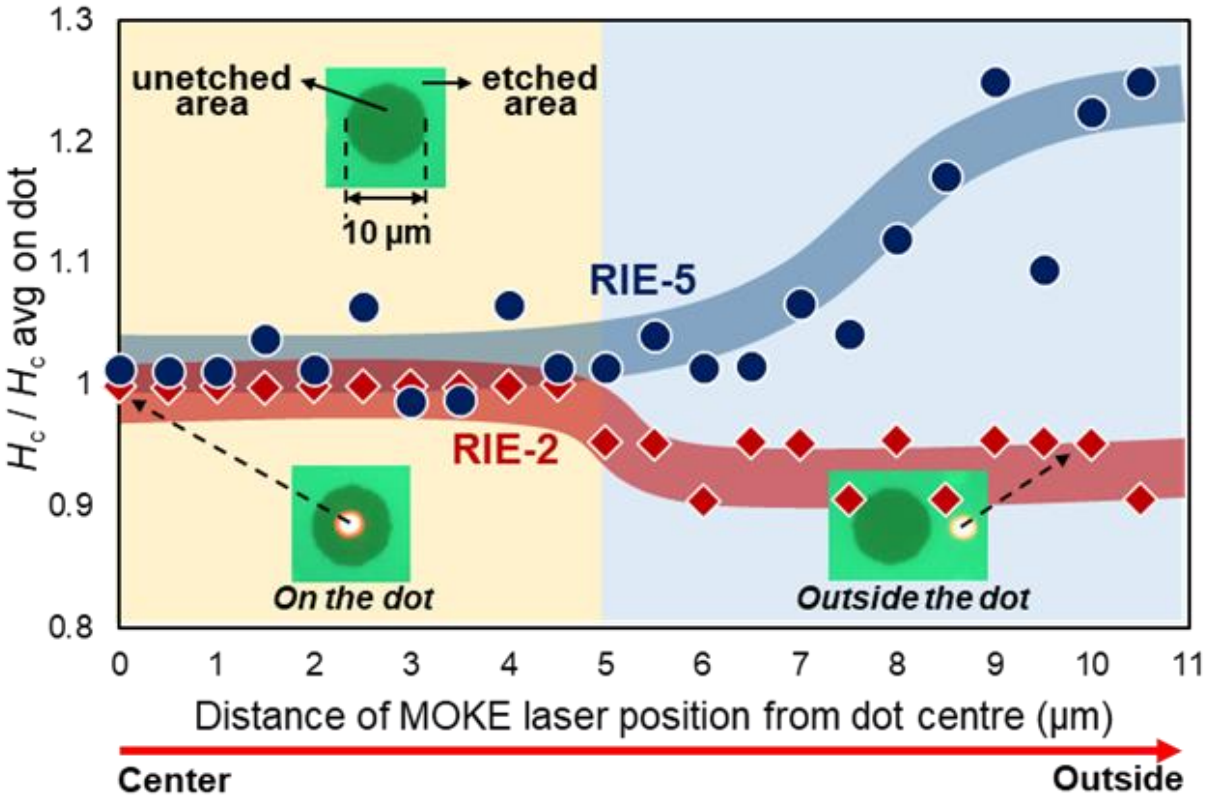

Figure 52. Comparison of coercivity change between etched area (out of dot) and unetched (on dot) area of $(Bi,Eu)(Fe,Co)O_3$ thin films in RIE condition 2 and 5.

conditions for multiferroic thin films, paving the way for more controlled and tailored fabrication methodologies.

5.2.2. Local Microstructure Study in Etched Area by AFM and MFM

Figure 53 provides a comparative analysis of grain size and domain size, assessed through Atomic Force Microscopy (AFM) and Magnetic Force Microscopy (MFM) respectively, subsequent to exposure to Reactive Ion Etching (RIE) in two distinct regions: On-dot (unetched area) and Out-of-dot (etched area). Here also I used histogram method to measure the size.

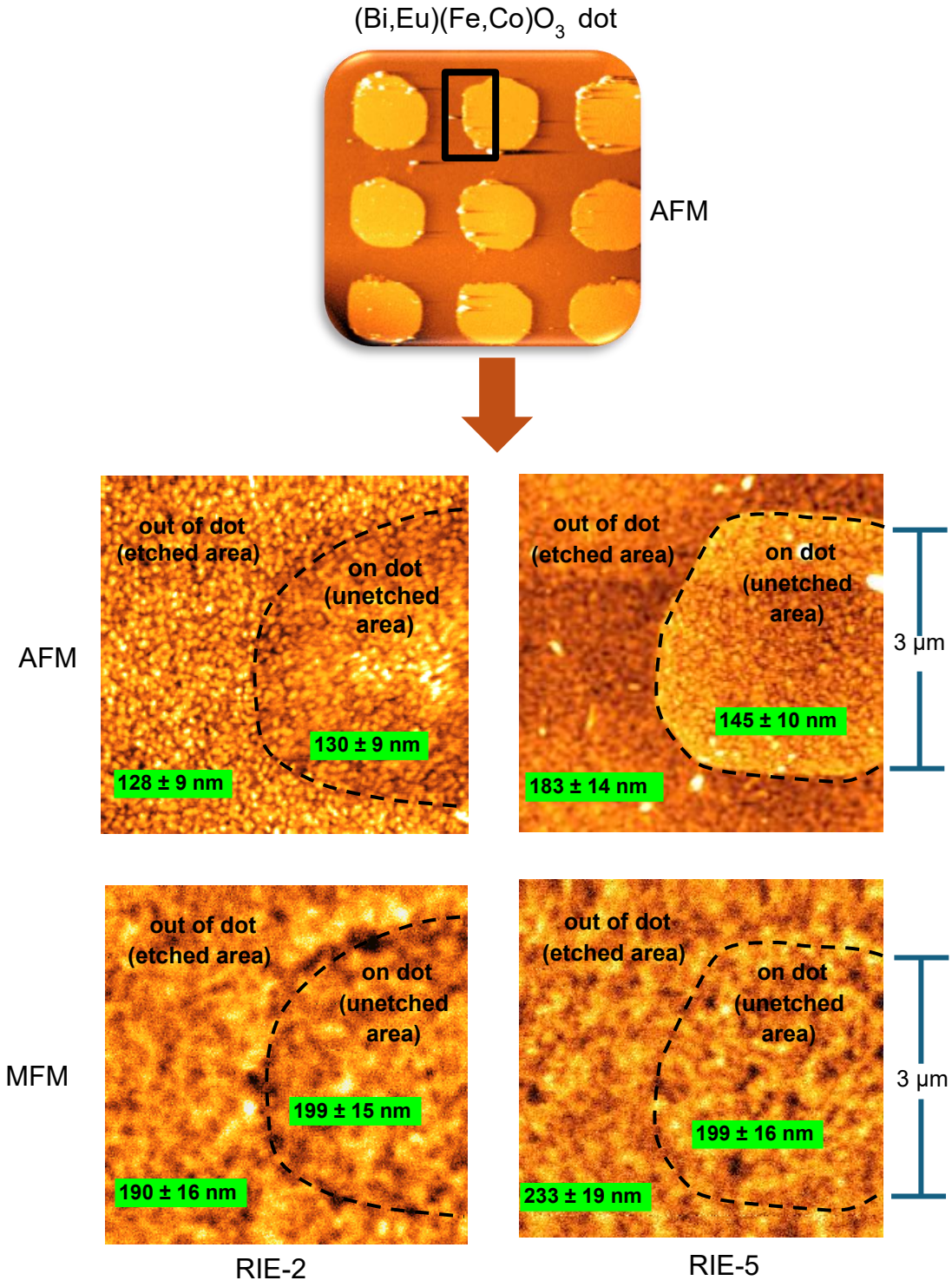

Figure 53. Comparison grain size and domain size between etched area (out of dot) and unetched (on dot) area of $(Bi,Eu)(Fe,Co)O_3$ thin films in RIE condition 2 and 5

Notably, RIE executed with a mixture of Trifluoromethane and Oxygen (CHF_3/O_2, denoted as RIE-2) demonstrated negligible impact on both grain and domain size. In stark contrast, RIE conducted exclusively with Trifluoromethane (CHF_3, denoted as RIE-5) resulted in a conspicuous increase in both grain and domain size, as delineated in Table 5.

The observed augmentation in grain size may be ascribed to the inherent limitations in the resolution of AFM. It is plausible that middle-sized grains merged with smaller ones during measurement, creating an appearance of enlarged grain size. This interpretation gains support from roughness measurements, further detailed in Table 5. Specifically, in RIE-2, a minimal change in roughness was detected, aligning with the absence of alterations in grain size. Conversely, in RIE-5, the etched area exhibited a relatively lower degree of roughness than the unetched area, suggesting a seemingly larger grain size. It is crucial to recognize that this perceived increase in grain size in RIE-5 is likely an artifact of the AFM technique. The challenge lies in discerning small-sized grains with low roughness, leading to the amalgamation of grains during measurement.

Furthermore, the subtle change in roughness and the correlated absence of significant alterations in grain size in RIE-2 align with the consistent domain size observed in MFM measurements. Conversely, the relatively lower roughness in the etched area of RIE-5, suggesting a larger grain size, is not corroborated by corresponding changes in domain size.

Table 5. Grain size, domain size and surface roughness of etched area (out of dot) and unetched (on dot) area of $(Bi,Eu)(Fe,Co)O_3$ thin films in RIE condition 2 and 5.

RIE condition	Grain size (nm)		Domain size (nm)		Surface roughness (nm)	
	Unetched Area	Etched Area	Unetched Area	Etched Area	Unetched Area	Etched Area
RIE-2	140±10	128±9	170±12	175±16	2.56	2.40
RIE-5	145±10	183±14	179±16	233±19	2.08	1.72

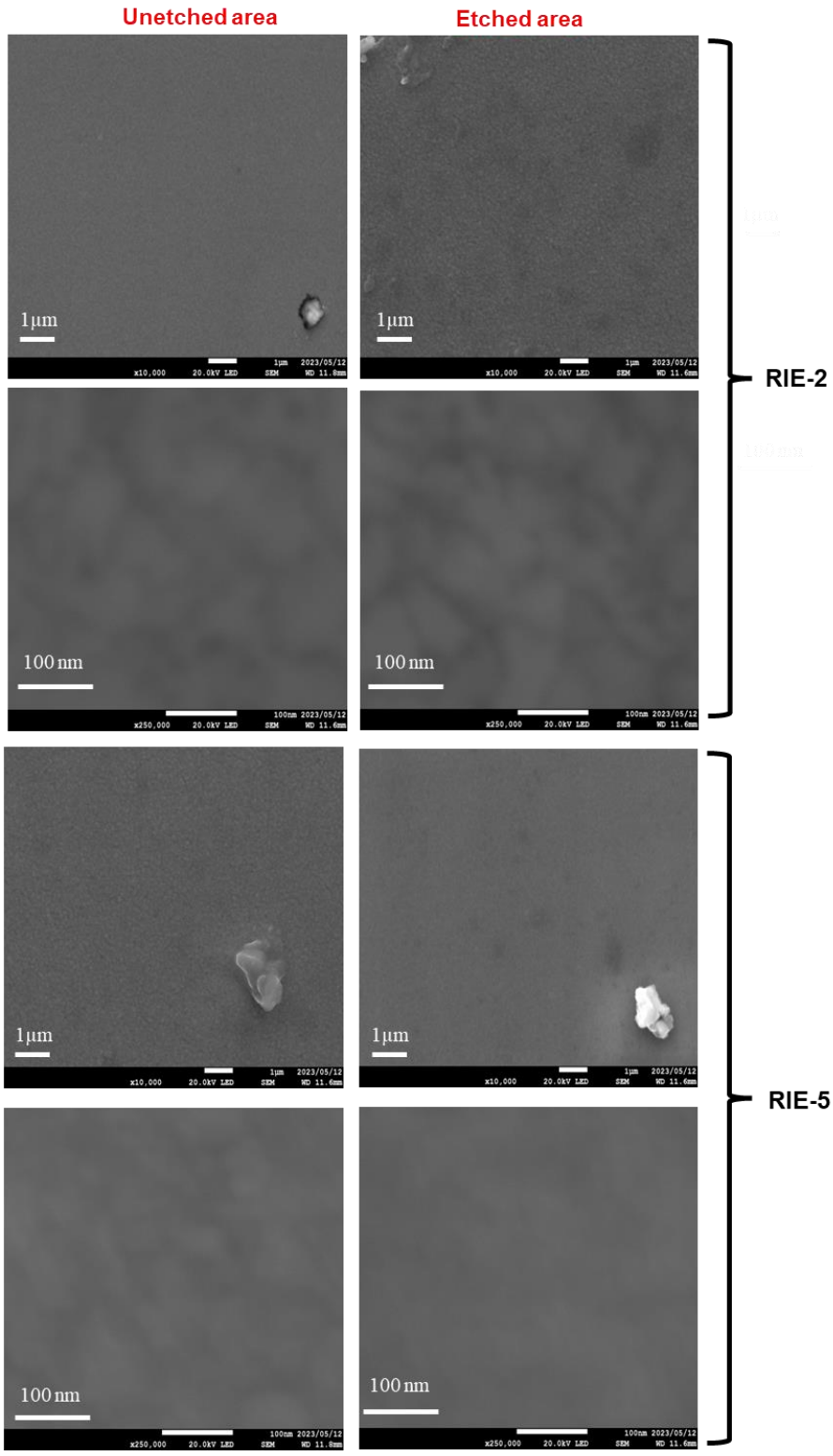

Figure 54. SEM images of etched and unetched surfaces of (Bi,Eu)(Fe,Co)O_3 thin films under RIE-2 and RIE-5

Figure 54 displays scanning electron microscopy (SEM) images that provide information about the structural changes of thin films in etched and unetched regions after being subjected to two different reactive ion etching (RIE) processes: RIE-2 and RIE-5.

Significantly, following the RIE-2 process, the scanning electron microscope (SEM) images demonstrate a consistent and uniform grain structure in both the etched and unetched regions. The distinct difference in appearance between these areas indicates that there are no substantial alterations or harm caused by the RIE-2 etching procedure. The consistent grain morphology indicates that the thin films maintained their structural integrity, supporting the idea that RIE-2 did not produce any obvious changes at the microscale.

In contrast, the RIE-5 instance exhibits clear and significant differences in the characteristics of the grains and grain boundaries between the portions that have been etched and those that have not. The striking contrast suggests that the RIE-5 procedure has caused major changes in the morphology. The observed differences in grain shape align with the previously documented increase in grain dimensions, providing further evidence that RIE-5 has a more significant influence on the microstructure of the thin films compared to RIE-2.

To summarize, the scanning electron microscope (SEM) photos visually depict the contrasting impacts of RIE-2 and RIE-5 on the grain morphology of the thin film. The regularity observed in RIE-2 indicates minimal morphological changes or damage, whereas the striking contrasts in RIE-5 emphasize the more significant alterations caused by this etching procedure. These discoveries are consistent with the extensive knowledge acquired from multiple methods of characterizing, which together contribute to a detailed analysis of how varied RIE settings affect the microstructure of the thin films.

5.2.3. Oxygen Vacancies Study by Using XPS

The X-ray Photoelectron Spectroscopy (XPS) technique was used to examine the chemical environment of oxygen (O) in (Bi,Eu)(Fe,Co)O_3 thin films. The objective was to evaluate the extent of oxygen deficiency under various etching circumstances. Figure 55 displays the XPS spectra of the O 1s peaks for the unetched (Bi,Eu)(Fe,Co)O_3 thin film, as well as the etched (Bi,Eu)(Fe,Co)O_3 thin films that underwent RIE-2 and RIE-5 operations.

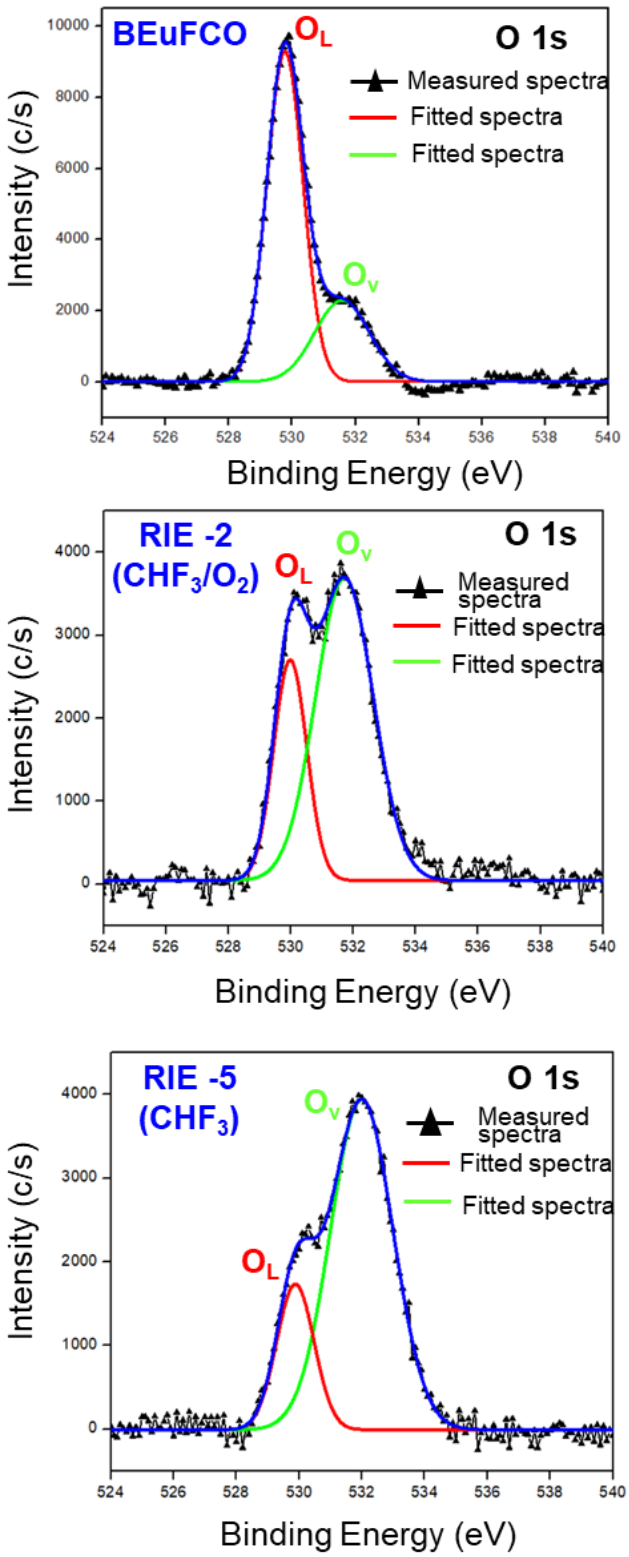

Figure 55. XPS spectra of O 1s in unetched (Bi,Eu)(Fe,Co)O_3 thin film (a) and etched (Bi,Eu)(Fe,Co)O_3 thin film (b), (c) under different etching conditions; RIE-2 and RIE-5

The spectra reveal two clearly distinguishable oxygen states: vacancy oxygen (O_V) and lattice oxygen (O_L). The deconvolution of each O 1s level spectrum comprises two Gaussian components, each having a corresponding binding energy of 532 and 530 eV, respectively. The peak at approximately 530 eV corresponds to negatively charged O^{2-} ions in the BFO lattice (O_L), while the peak at around 532 eV is associated with O^{2-} ions in regions of oxygen deficiency within the BFO lattice (O_V). The regions beneath these curves were computed to approximate the proportion of oxygen vacancies following the application of the Pseudo-Voigt function, which is a combination of Gaussian and Lorentzian functions.

The projected proportions of oxygen vacancies in unetched thin films and etched (Bi,Eu)(Fe,Co)O_3 thin films for RIE-2 and RIE-5 are 27%, 60%, and 79%, respectively. Significantly, conducting the etching procedure in the absence of an oxygen environment (RIE-5) led to a rise in the number of oxygen vacancies. In contrast, the etching process carried out in the presence of an oxygen environment (RIE-2) resulted in a decrease in oxygen vacancies, suggesting that oxygen was replenished in the vacancies formed during the etching process.

This observation is consistent with the results presented in Figure 52, 53, 54 and 55, which indicate that RIE-2 showed less magnetic damage than RIE-5. The decreased presence of oxygen vacancies in RIE-2 resulted in a more advantageous magnetic result, notwithstanding the etching procedure. On the other hand, RIE-5, which is distinguished by a rise in oxygen vacancies, displayed a higher coercivity (H_c), greater grain and magnetic domain size, and a more noticeable scanning electron microscope (SEM) contrast between the portions that were etched and those that were not.

5.2.4. Discussions

Successful preservation of magnetic characteristics in etched Bismuth Ferrite (BFO) thin films was accomplished by employing a CHF_3/O_2 mixture as the etching gas. The implementation of an oxygen-rich atmosphere, along with a decrease in the level of unstable molecules, supported by oxygen plasma, had a crucial impact in preventing the buildup of reactive substances during the etching process. The decrease in the likelihood of magnetic damage was ascribed to the effectiveness of oxygen plasma in hindering the accumulation of reactive species. Moreover, the oxygen plasma performed a vital role in restoring oxygen vacancies that are commonly created at grain boundaries during the etching process.

The provided data demonstrates that the utilization of CHF_3/O_2 led to negligible alterations in coercivity, grain size, and domain size. This event was linked to the extraction and subsequent restoration of oxygen in the CHF_3/O_2 environment. The controlled oxidative environment successfully reduced any potential negative impact on the magnetic characteristics of the BFO thin films.

On the other hand, when CHF_3 was used as the only etching gas, there was a noticeable tendency for the build-up of reactive intermediates. Consequently, there was a surge in the generation of free radicals, leading to magnetic impairment. CHF_3 is frequently used to etch different materials due to its notable selectivity and fast etch rates. Furthermore, fluorine, which is a constituent of CHF_3, is an extremely powerful oxidizing agent. When it comes to BFO-based thin films, the utilization of CHF_3 enabled effective elimination of materials, especially oxygen, from grain boundaries through chemical etching. Fluorine atoms engaged with the surface and boundaries of the film, producing volatile chemicals that were subsequently eliminated from the surface.

The SEM pictures clearly demonstrated the removal of material from grain borders by the use of CHF_3, as seen by the significant contrast observed between the grains and grain boundaries. This discrepancy led to an overestimation of grain size, which can be related to the perceived fusion of medium-sized and small-sized grains, as found in AFM. The removal process also caused changes in the crystal structure or chemical composition within domain walls, which impacted the layout of magnetic domains and increased the size of the domains, as detected by Magnetic Force Microscopy (MFM).

5.2.5. Conclusion of RIE

During the reactive ion etching (RIE) procedure, a comparative evaluation of etching gases was conducted to determine the most favorable conditions for etching multiferroic thin films. The assessment found that CHF_3/O_2 is the most appropriate choice, as it minimizes magnetic damage compared to CHF_3 and SF_6. The lack of oxygen in the etching environment was found to be associated with an escalation in magnetic harm, emphasizing the crucial function of oxygen in maintaining the magnetic integrity of the thin films. This discovery highlights the significance of carefully choosing etching conditions in microfabrication procedures. Specifically, the inclusion of oxygen in the etching gas is a critical element in reducing unwanted magnetic effects. The found compatibility of CHF_3/O_2 provides useful direction for improving the accuracy and dependability

of microfabrication techniques that involve multiferroic thin films. This discovery also creates opportunities for the advancement of magnetic nano electronics.

5.3. Dry Etching (DE)

Within the field of microfabrication, dry etching has emerged as a crucial method for effectively removing metals and thin layers. This is mostly owing to the accelerated etching speeds achieved through the use of powerful Ar ions. Nevertheless, the utilization of this technique in multiferroic thin films, specifically those derived from Bismuth Ferrite (BFO), has not been extensively investigated. This study aims to address this significant deficiency by conducting a methodical examination of BFO thin films through the utilization of a particular dry etching technique. The aim is to evaluate the efficacy of dry etching in contrast to reactive ion etching (RIE), a technique previously examined in this context. The objective is to determine if dry etching provides better capabilities for microfabrication in multiferroic materials and, if so, to optimize the process parameters to minimize magnetic damage in thin films based on BFO.

The experimental methodology entails the utilization of meticulously chosen BFO thin films as exemplar multiferroic materials. The selected dry etching technique, employing highly energetic Ar ions, will be subjected to regular adjustments in parameters such as gas composition, pressure, and power in order to optimize the etching conditions. Afterwards, a thorough comparative study using RIE will be performed to clarify the relative benefits and drawbacks of each technique. If dry etching demonstrates superior efficacy compared to RIE, the investigation will focus on optimizing the dry etching parameters to achieve a delicate equilibrium between etching efficiency and the preservation of essential magnetic properties in BFO-based thin films. The objective of this research is to provide significant insights that will help improve microfabrication methods for multiferroic materials. This, in turn, would facilitate breakthroughs in device fabrication and technology.

Our work centered on analyzing identical BEuFCO thin films, utilizing precise process settings of 400 V, a current of 90 mA, and an argon (Ar) gas flow rate of 6 SCCM. In these circumstances, we noted a remarkable rate of etching of 6 nm per minute, providing insight into the effectiveness of the utilized approach in accurately altering the thin films.

5.3.1. Local Coercivity Study in Etched Area by micro-MOKE

We conducted a thorough research of coercivity variations in BEuFCO thin films using the micro MOKE measurement equipment. More precisely, we employed this approach to produce local hysteresis curves, providing an accurate method for determining coercivity in both the etched (out-of-dot) and unetched (on-dot) regions. The methodology used to test coercivity followed the same strategy as discussed earlier for RIE. After identifying changes in coercivity in the etched area, a comparative study was conducted, comparing the results with the optimal conditions found for RIE as shown in figure 56.

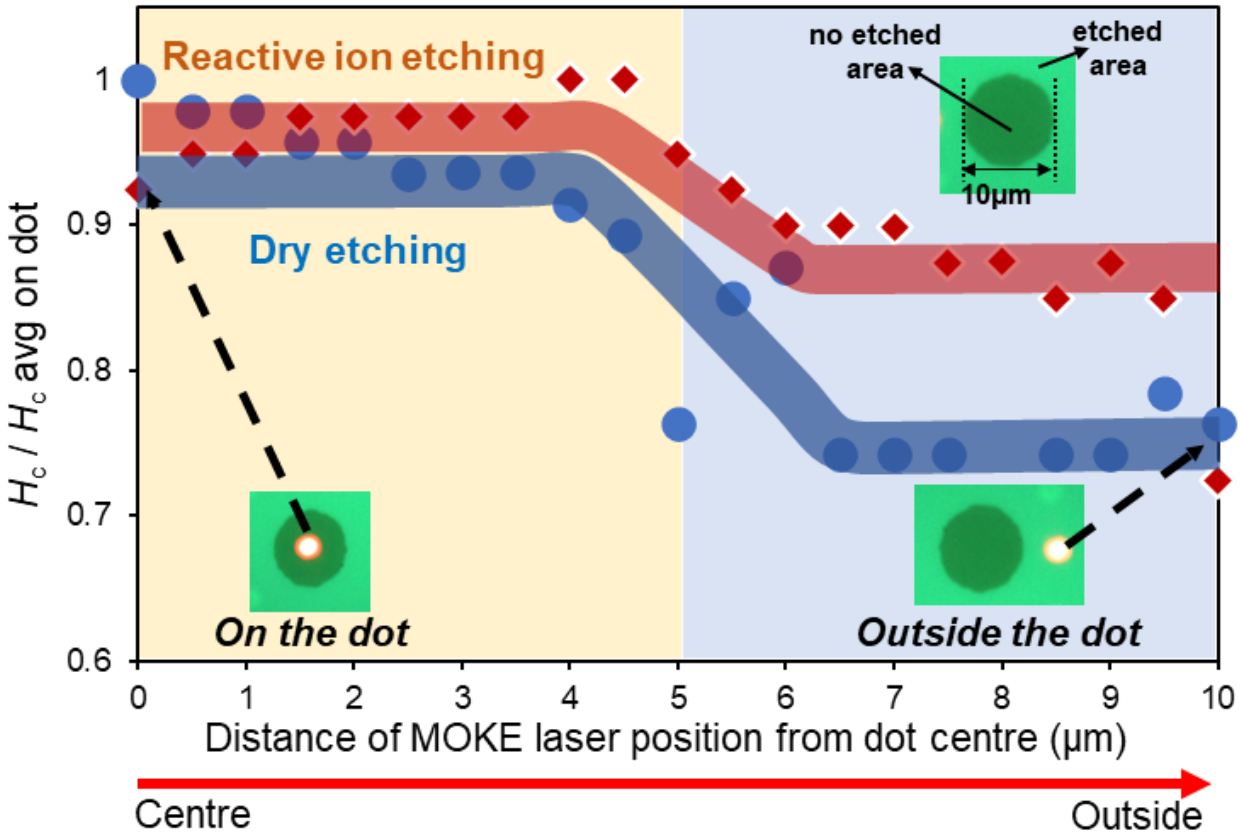

Figure 56. Comparison of coercivity change in DE and RIE

Surprisingly, the coercivity in the unetched portions remained constant, showing no noticeable alteration. Nevertheless, a notable and discernible reduction in coercivity was noted in the etched regions, especially after dry etching in comparison to RIE. The variation in changes in coercivity can be ascribed to the different physical characteristics linked to each etching process. The

significant decrease in coercivity during dry etching suggests a greater degree of magnetic damage in comparison to the comparatively well-preserved coercivity under the conditions optimal for reactive ion etching (RIE). This detailed analysis clarifies the complex relationship between etching techniques and their effects on the magnetic characteristics of BEuFCO thin films, providing crucial knowledge to improve the precision of microfabrication methods in multiferroic materials.

5.3.2. Local Microstructure Study in Etched Area by AFM and MFM

Figure 57 showcases a thorough analysis of the dimensions of grains and domains in BEuFCO thin films using Atomic Force Microscopy (AFM) and Magnetic Force Microscopy (MFM), respectively. The examination covers two separate areas: the On-dot region (unetched area) and the Out-of-dot region (etched area), allowing for a comparative analysis with the optimal circumstances of Reactive Ion Etching (RIE). The measurement of particle size and domain size was performed using the histogram method, a reliable methodology for analyzing the structural characteristics of nanomaterials.

After applying dry etching (DE) to the samples, a little change in grain size was detected. The grain size in both the etched and unetched sections exhibited a high degree of uniformity, suggesting that the crystal structure was minimally affected by dry etching. There was a significant difference in the size of the domain between the etched area and the unetched region, with the etched area showing a noticeable rise. The considerable difference in domain size indicates a major alteration in the magnetic characteristics, highlighting the susceptibility of magnetic nanostructures to the etching processes used.

The differences in grain and domain size between dry etching and RIE-optimized circumstances confirm that the etching methods have an impact on the physical characteristics of BEuFCO thin films. These findings provide useful insights for developing and optimizing manufacturing processes in magnetic nano devices, highlighting the importance of carefully considering etching procedures to reduce potential magnetic damage.

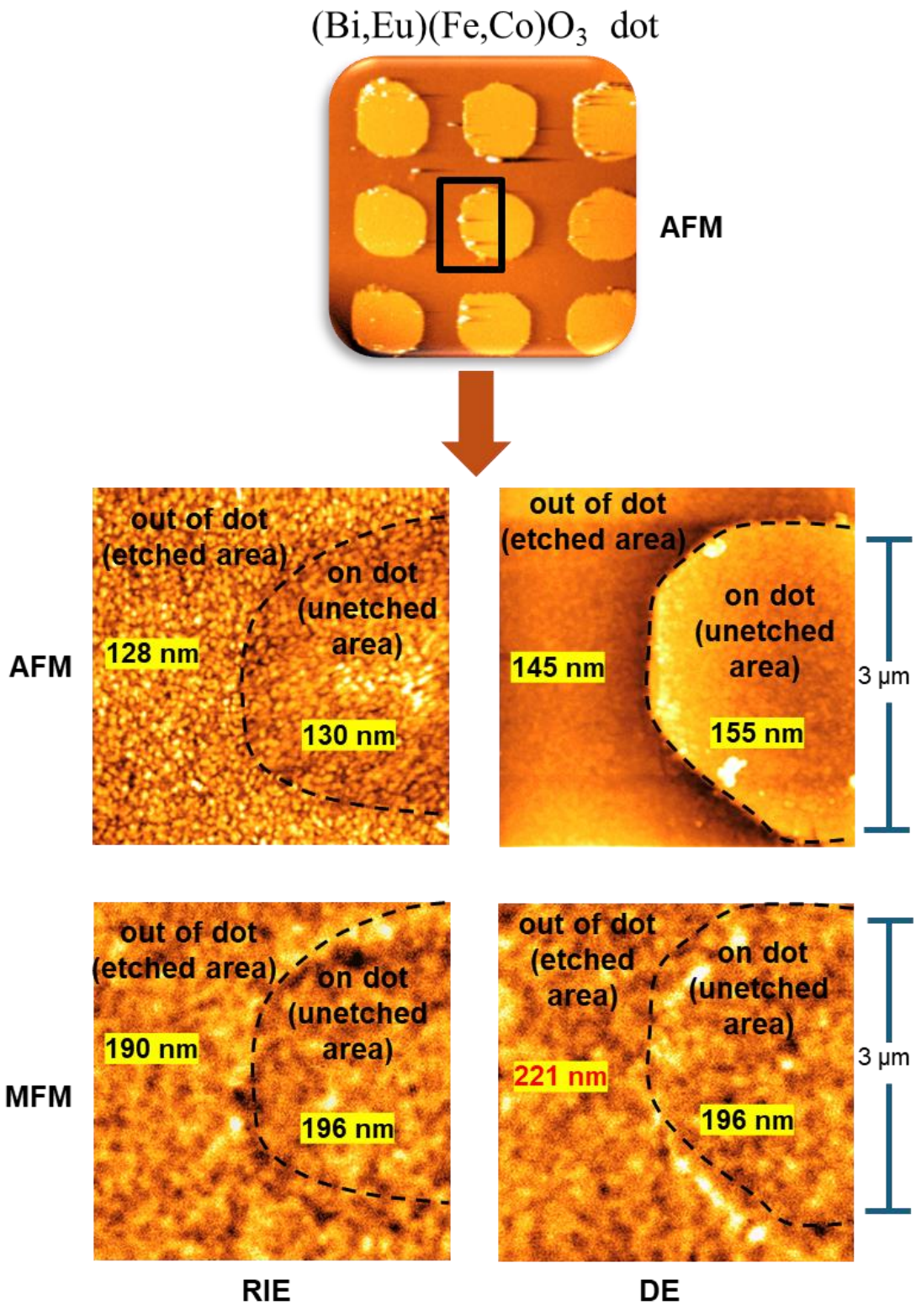

Figure 57. Comparison of microstructural changes (grain size and domain size) between DE and RIE.

5.3.3. Discussion

The work highlights the significant influence of dry etching on multiferroic thin films, namely architectures based on BFO. The incorporation of highly energetic Ar ions during the dry etching process leads to noticeable physical harm, resulting in a considerable enlargement of magnetic domains without affecting the size of the grains. The increase in magnetic domain size is accompanied by a significant decrease in coercivity, indicating that the material is more susceptible to changes in its inherent magnetic characteristics. These findings provide insight into the complex interactions that occur during microfabrication processes. They highlight the importance of optimizing etching techniques to minimize negative effects and maintain the quality of multiferroic thin films. This is essential for the development of magnetic nano electronics.

5.3.4. Conclusion of Chapter 5

Chapter 5 provided a comprehensive account of our initial efforts to reduce magnetic harm when microfabricating multiferroic thin films. Our investigations have shown that Reactive Ion Etching (RIE) has emerged as a superior etching process, especially for materials such as Bismuth Ferrite (BFO). More precisely, the use of CHF_3 in a controlled oxygen atmosphere was crucial in reducing magnetic harm. The inclusion of supplementary oxygen in the reactive ion etching (RIE) procedure played a vital function in offsetting the oxygen deficiencies produced during the etching process, thereby safeguarding the magnetic consistency of the material. On the contrary, Dry Etching (DE) was discovered to cause significant physical harm, leading to an intensified magnetic damage profile throughout the process of microfabrication. The significance of carefully choosing etching conditions, especially the utilization of RIE with precise gas compositions and environmental factors, in the production of magnetic nano devices cannot be overstated.

CHAPTER – 6
Summary and Future Challenges

6.1. Summary

In the domain of magnetic devices, such as racetrack memory and spatial optical modulators, the issues of energy consumption and weak output signals in hard disk drives have been longstanding concerns. The emergence of spin current has offered a viable approach to tackle these problems. There is an increasing interest in investigating alternative materials that may switch their magnetization when an electric field is applied, in order to overcome the limits of existing materials. Out of the many different materials, multiferroic substances have become especially fascinating due to their ability to exhibit magnetoelectric coupling, which is a highly desired attribute. Bismuth ferrite ($BiFeO_3$) has been carefully selected for its ability to provide efficient solutions that work at room temperature. By implementing a range of improvements in the methods used to create films, making precise tweaks to the composition, and strategically replacing different parts, we have effectively created three unique materials designed for specific uses in devices.

The thin film material $(Bi,Nd)(Fe,Co)O_3$ has demonstrated outstanding effectiveness in the important duty of writing data in racetrack memory. Similarly, the material $(Bi,La)(Fe,Co)O_3$ has proven to be the most effective writing element for spatial optical modulators. Moreover, the designed material $(Bi,Eu)(Fe,Co)O_3$ has demonstrated exceptional efficiency in the crucial function of reading heads in hard disk drives.

6.1.1. $(Bi,Nd)(Fe,Co)O_3$ thin film

By strategically replacing Nd and Co elements at optimal compositions of 50 at% and 25 at%, respectively, in both the A-site and B-site of Bismuth ferrite (BFO), we have effectively improved its magnetic characteristics. The customized strategy has led to a significant enhancement, especially attaining an M_s of 140 emu/cm^3. The ratio of perpendicular-to-parallel coercivity ($H_{c\perp}/H_{c//}$) and the ratio of perpendicular-to-parallel squareness ($S_\perp/S_{//}$) have been increased greatly to 2.6 and 1.0, respectively. The progress made in this field establishes the thin film as a highly promising option for use in the writing component of racetrack memory, which is a relevant issue extensively explored in Chapter 1.

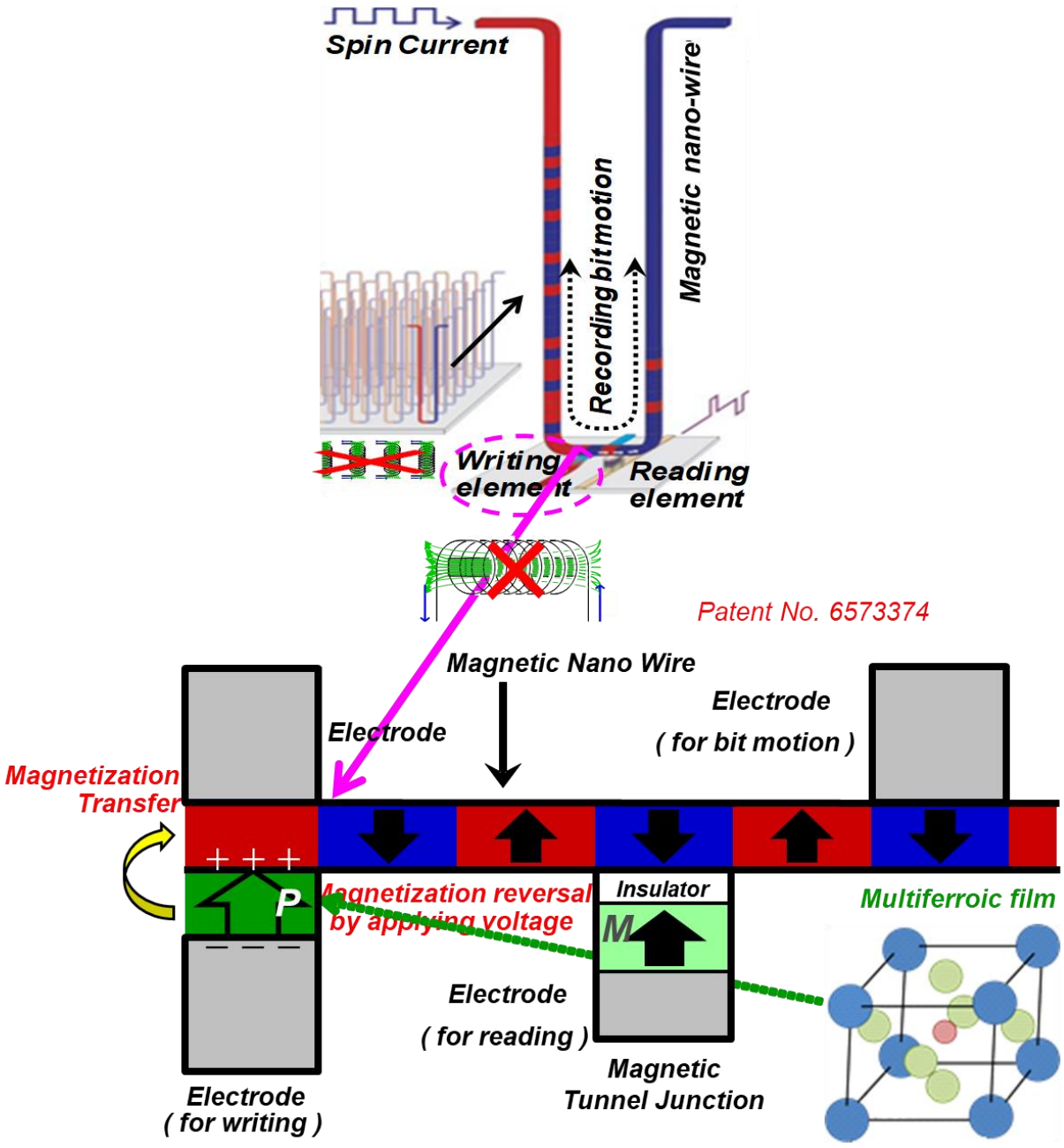

Figure 58. Application of BFO based thin films in writing element of Racetrack memory instead of coils.

An novel solution for racetrack memory involves using this $(Bi,Nd)(Fe,Co)O_3$, instead of traditional writing elements and energy-intensive coil configurations. By utilizing the inherent magnetoelectric coupling capabilities of BFO, we can take advantage of its sensitivity to electric polarization caused by applied voltage variations. The polarization of the BFO thin sheet induces magnetization. Surprisingly, this induced magnetism acts as a catalyst, expanding its impact to the nano wires in the racetrack memory. By inducing voltage differences in opposite directions, we may effortlessly alter the direction of magnetization. This innovative procedure not only removes the requirement for massive coil systems but also substantially decreases energy usage, as demonstrated in Figure 58. The incorporation of BNdFCO thin films is a crucial development that provides a more effective and environmentally friendly alternative for data writing in racetrack memory devices.

6.1.2. $(Bi,La)(Fe,Co)O_3$ thin film

By strategically replacing La and Co elements at carefully selected concentrations of 50 at% and 25 at%, respectively, in both the A-site and B-site of Bismuth ferrite (BFO), we have effectively improved its magnetic characteristics. The optimized method has resulted in a significant enhancement, particularly attaining a magnetization saturation (M_s) of 80 emu/cm^3. The ratio of perpendicular-to-parallel coercivity ($H_{c\perp}/H_{c//}$), the ratio of perpendicular-to-parallel squareness ($S_\perp/S_{//}$) have shown substantial increases, with values of 1.6 and 1.3, and an improved Kerr angle of 0.67˚ respectively. The progress made in thin film technology makes it a very promising option for incorporating into the writing part of spatial optical modulators. This specific topic is thoroughly discussed in Chapter 1.

The introduction of $(Bi,La)(Fe,Co)O_3$ thin film, presents a compelling alternative to conventional writing elements in spatial optical modulators. This innovative approach eliminates the necessity for extensive data storage arrays, effectively mitigating the associated increase in energy consumption. Leveraging the magnetoelectric properties of these thin films, the direction of magnetization can be seamlessly switched by simply altering the direction of the applied electric field, as visually represented in Figure 59.

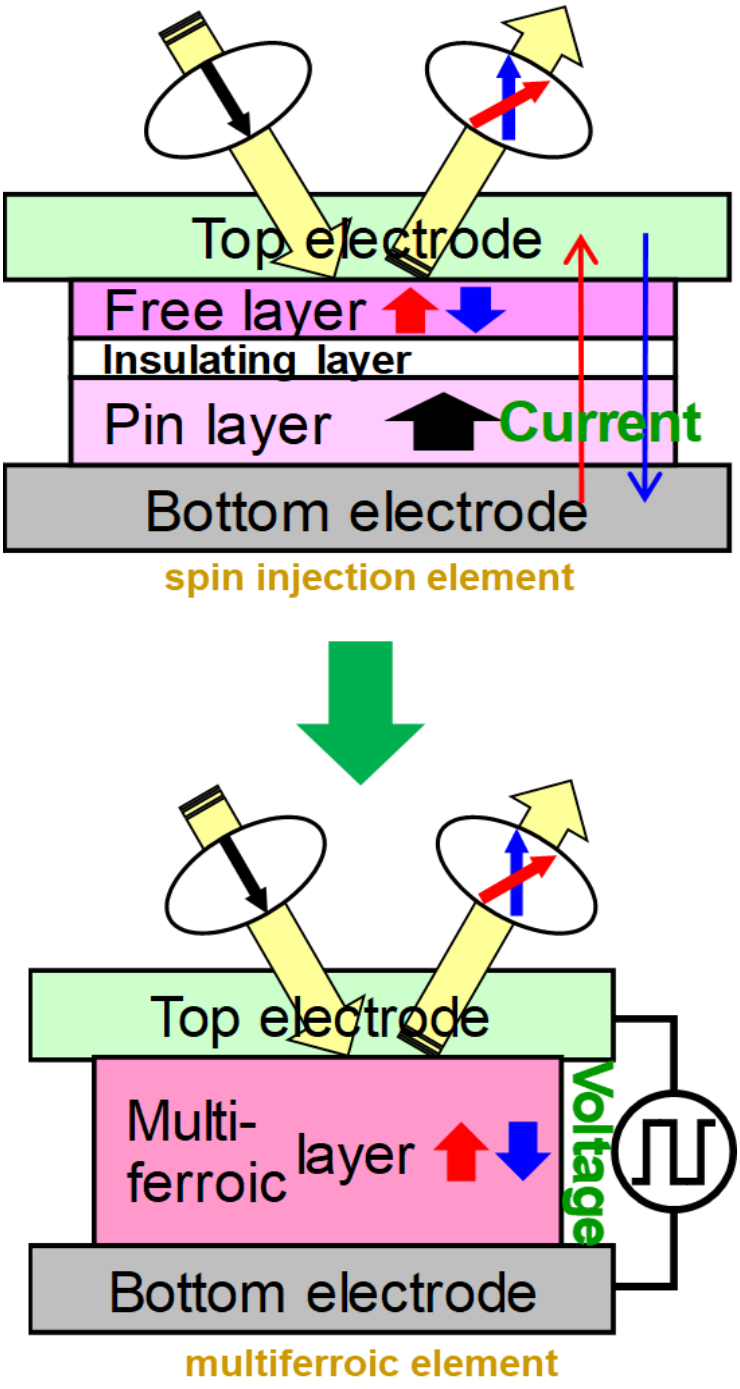

Figure 59. Application of multiferroic element instead of spin current in writing element of spatial optical modulator

6.1.3. (Bi,Eu)(Fe,Co)O_3 thin film

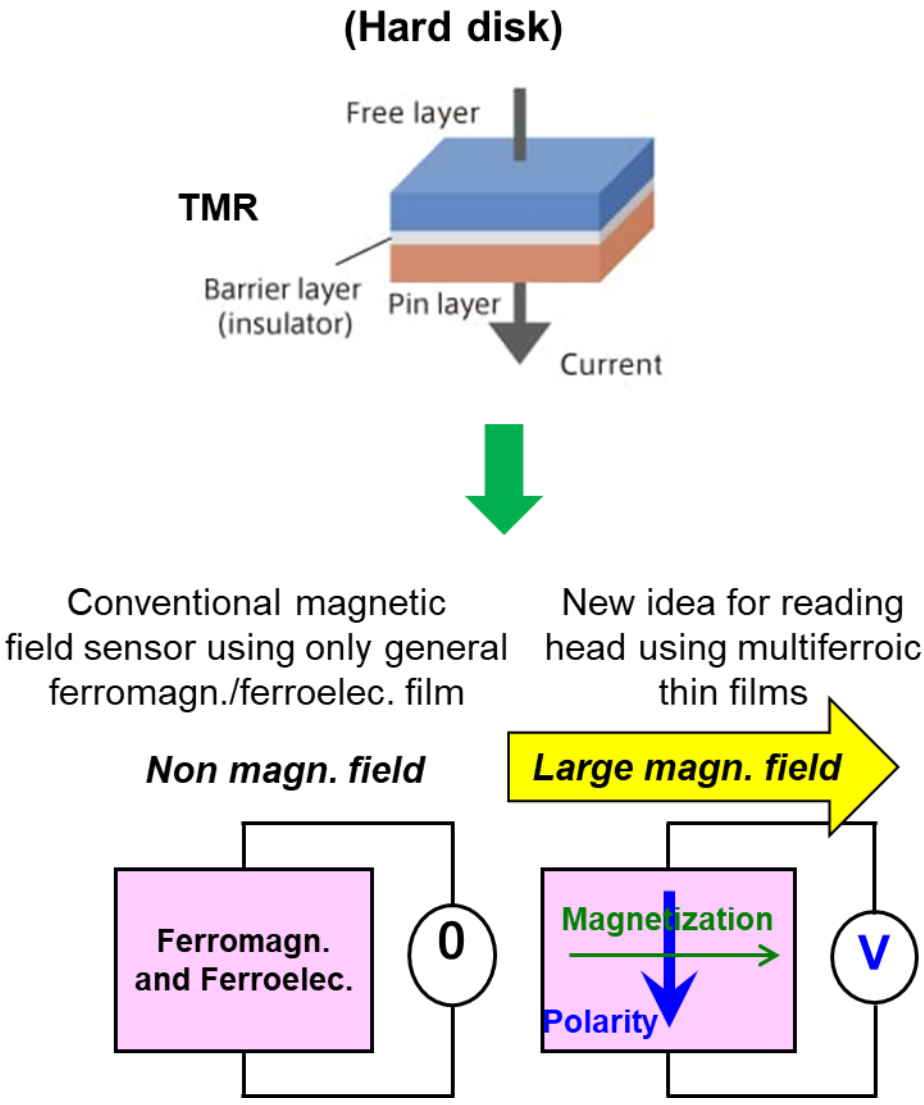

Figure 60. Application of multiferroic thin films in reading head of HDD

Through meticulous substitution of Eu and Co elements at precisely determined concentrations of 50 at% and 25 at%, respectively, within both the A-site and B-site of Bismuth ferrite (BFO), we have successfully enhanced its magnetic properties. This optimized approach has yielded a substantial improvement, notably achieving a magnetization saturation (M_s) of 110 emu/cm3. Notably, a remarkable low coercivity of 0.5 kOe has been observed, underscoring the efficiency of the tailored composition. The advancements in thin film technology position it as an exceedingly promising candidate for integration into the reading head of hard disk drives, particularly due to

its heightened sensitivity to external magnetic fields. This specific subject matter is comprehensively explored in Chapter 1.

The conventional approach to reading data in hard disk drives relies on Tunneling Magnetoresistance (TMR), which, while highly sensitive to external magnetic fields, presents challenges due to relatively low output signals. This limitation can impede accurate data reading. The incorporation of (Bi,Eu)(Fe,Co)O_3 thin films offers a promising solution to this issue. The exceptionally low coercivity (H_C) of BFO thin films renders them highly responsive to external magnetic fields. As an external magnetic field interacts with the BFO, it induces magnetization within the thin film, subsequently generating polarization. This induced polarization proves advantageous for facilitating the accurate detection of information, as illustrated in Figure 60. The utilization of BFO thin films thus represents a significant advancement in addressing the sensitivity-output trade-off commonly encountered in traditional TMR-based approaches for data reading in hard disk drives.

6.1.4. Ferroelectricity of BFO based Thin Films

Though all fabricated thin films showed ferroelectric properties, those doped with Er, Dr, and Gd exhibited poor ferroelectric curves. To understand the reason, we analyzed it by using XPS in the Er doped film (BErFCO) (poor ferroelectric property) and Eu doped thin film (BEuFCO) (good ferroelectric property) as discussed in chapter 3. A high intensity of oxygen vacancy (Ov) in BErFCO was observed compared to BEuFCO, which arises from Er's higher tendency to undergo oxidation compared to Eu. The high oxidation tendency of Erbium (Er) leads to the creation of Er-O phases, which disturb the perovskite structure by extracting oxygen from the face center. The presence of these oxygen vacancies serves as holes, increasing the amount of current leakage and negatively affecting the ferroelectric characteristics when substituting materials with significant oxidation tendencies, such as Er, Dr and Gd.

6.1.5. Investigation on Potential in Device Applications

To ascertain the practical viability of the aforementioned thin films, a comprehensive investigation into their microstructures, encompassing parameters such as grain size of 140 nm and domain size of 170 nm, was conducted, revealing observations within the nano range. Remarkably, a notably high T_C of 450 ˚C was recorded, substantiating the stability of the material at elevated temperatures. Furthermore, our exploration included a demonstration of the thin films' capability for

magnetization switching. To bolster these findings, the study reported minimal leakage current and a diminished piezoelectric effect. Collectively, these factors provide robust confirmation of the applicability of these thin films in the envisaged devices, marking a significant stride towards their effective integration into practical applications.

6.1.6. Investigation on Suitable Etching Conditions

Upon confirming the material suitability for our multiferroic thin films, our attention turned to the critical aspect of microfabrication, particularly in the realm of oxide materials—a domain with limited precedent. A dedicated investigation into suitable etching conditions, focusing on both Dry Etching (DE) and Reactive Ion Etching (RIE), unfolded. Notably, DE was found to induce excessive physical damage, raising concerns about its appropriateness for multiferroic thin films. In contrast, RIE emerged as a more fitting candidate, and through meticulous study, we identified RIE with CHF3 as particularly effective, yielding a remarkable etching rate.

Further refinement was achieved by introducing oxygen during the etching process, a technique detailed in Chapter-5. This strategic inclusion of oxygen proved highly effective in mitigating magnetic damage during microfabrication processes involving oxide materials.

6.2. Future Challenges

Bismuth ferrite (BFO) thin films are an advanced type of material that has great potential in various applications. However, their practical use has not been thoroughly studied. This work focuses on improving the magnetic characteristics of BFO, taking into account the current issues that require additional exploration. The future challenges are

1. ***Improvement of Magnetic Characteristics:***

The main objective is to enhance the magnetic characteristics of Bismuth ferrite (BFO) thin films, specifically by increasing Perpendicular Magnetic Anisotropy (PMA).

2. ***Minimization of electrical current leakage and enhancement of ferroelectric characteristics:***

Seeking to reduce the flow of electric current while simultaneously improving the properties of ferroelectricity in thin films of BFO.

3. ***Grain and domain size reduction:***

Exploring techniques to decrease the diameters of both individual grains and structural domains in order to enhance the microstructure of BFO thin films.

4. ***Attainment of Magnetic Switching in Nano-Scale Width:***

Seeking methods to facilitate magnetic switching at the nano-scale level, a crucial development for diverse applications.

5. ***Analyzing the Mechanisms of Magnetization in Doped BFO Thin Films:***

Conducting a systematic investigation into the mechanisms that control magnetization in BFO thin films that have been doped with additional elements, with the goal of achieving a thorough comprehension.

6. ***An inquiry into optimal etching conditions with notable etching rates:***

Thorough investigation of the most effective conditions for etching, with a specific emphasis on Reactive Ion Etching (RIE) and its many parameters, in order to obtain exceptional etching rates in BFO thin films.

References

[1] Z. G. Li, Y. Yang, A. Z. Liu, Z. D. Jia, D. X. Huang, L. Liu, N. Yan, Y. H. Ding, J. J. Sun, Z. H. Zhang and S. K. Ren, "Energy Storage in Magnetic Devices air gap and Application Analysis," *Energy Reports,* vol. 8, pp. 152-161, 2022.

[2] O. Gutfleisch, M. A. Willard, E. Bruck, C. H. Chen, S. G. Sankar and P. Liu, "Magnetic Materials and devices for the 21st Century: Stromger, Lighter, and More Energy Efficient," *Advanced Materials,* vol. 23, no. 7, pp. 821-842, 2011.

[3] J. Puebla, J. Kim, K. Kondou and Y. Otani, "Spintronics devices for energy efficient data storage and energy harvesting," *communication materials,* vol. 1, 2020.

[4] K. Hono, Y. K. Takahashi, G. Ju, J. U. Thiele, A. Ajan, X. Yang, R. Ruiz and L. Wan, "Heat assisted magnetic recording media materials," *MRS Bulletin,* vol. 43, pp. 93-99, 2018.

[5] S. N. Piramanayagam, "Perpendicular recording media for hard disk drives," *Journal of applied physics,* vol. 102, 2007.

[6] S. Parkin and S. H. Yang, "Memory on the racetrack," *Nature nanotechnology,* vol. 10, pp. 195-198, 2015.

[7] K. Gu, Y. Guan, B. K. Hazra, H. Deniz, A. Migliorini, W. Zhang and S. Parkin, "Three dimensional racetrack memory devices designed from freestanding magentic heterostructures," *Nature nanotechnology ,* vol. 17, pp. 1065-1071, 2022.

[8] A. L. Lentine, J. N. Lee, S. H. Lee and U. Efron, "Optica," *Introduction to the feature on spatial light modulators and their applications,* vol. 33, no. 14, p. 2767, 1994.

[9] S. K. Yun, "Spatial optical modulator (SOM): Samsung's light modulator for next generation laser displays," *Society for information display,* 2012.

[10] C. Safranski , J. Z. Sun and A. D. Kent, "A perspective on electrical generation of spin current for magnetic random access memories," *Applied physics letter,* vol. 120, 2022.

[11] B. Y. Jiang, K. Zhang, T. Machita, W. Chen and M. Dovek, "Tunneling magnetoresistive devices as read heads in hard disk drives," *Journal of magnetism and magnetic materials,* vol. 571, 2023.

[12] N. A. Spaldin and R. Ramesh, "Advances in magnetoelectric multiferroics," *Nature materials,* vol. 18, pp. 203-212, 2019.

[13] A. Roy, R. Gupta and A. Garg, "Multiferroic memories," *Advances in condensed matter physics,* 2012.

[14] A. Loidl, H. V. Loehneysen and G. M. Kalvius, "Multiferroics," *Journal of Physics; Condensed matter ,* vol. 20, 2008.

[15] M. Fiebig, T. Lottermoser, D. Meier and M. Trassin, "The evolution of multiferroics," *Nature Reviews Materials,* vol. 1, p. 16046, 2016.

[16] J. Wang, J. B. Neaton, H. Zheng, V. Nagarajan, S. B. Ogale, B. Liu, D. Viehland, V. Vaithyanathan, D. G. Schlom, U. V. Waghmare, N. A. Spaldin, K. M. Rabe, M. Wuttig and R. Ramesh, "Epitaxial $BiFeO_3$ Multiferroic Thin Film Heterostructures," *Science,* vol. 299, p. 1719, 2003.

[17] D. H. Wang, W. C. Goh, M. Ning and C. K. Ong, "Effect of Ba doping on magnetic, ferroelectric, and magnetoelectric properties in mutiferroic $BiFeO_3$ at room temperature," *Applied Physics Letters,* vol. 88, p. 212907, 2006.

[18] N. W. Price, R. D. Johnson, W. Saenrang, A. Bombardi, F. P. Chmiel, C. B. Eom and P. G. Radaelli, "Electrical switching of magnetic polarity in a multiferroic $BiFeO_3$ device at room temperature," *Physical review applied ,* vol. 8, no. 1, p. 014033, 2017.

[19] M. M. Vopson, "Fundamentals of multiferroic materials and their posible applications," *Critical reviews in solid state and materials sciences ,* vol. 40, no. 4, pp. 223-250, 2015.

[20] M. A. Zurbuchen, T. Wu, S. Saha and J. Mitchell, "Multiferroic composite ferroelctric-ferromagnetic films," *Applied physics letters,* vol. 87, no. 23, p. 232908, 2005.

[21] J. M. Hu, T. Nan, N. X. Sun and L. Q. Chen, "Multiferroic magnetoelectric nanostructures for novel device applications," *MRS Bulletin ,* vol. 40, no. 9, pp. 728-735, 2015.

[22] J. Ryu, A. V. Carazo, K. Uchino and H. E. Kim, "Magnetoelectric Properties in Piezoelectric and Magnetostrictive Laminate Composites," *The Japan Society of Applied Physics,* vol. 40, p. 4948, 2001.

[23] T. Maruyama, Y. Shiota, T. Nozaki, K. Ohta, N. Toda, M. Mizuguchi, A. A. Tulapurkar, T. Shinjo, M. Shiraishi, S. Mizukami, Y. Ando and Y. suzuki, "Large voltage-induced magnetic anisotropy," *Nature Nanotechnology,* vol. 4, p. 158, 2009.

[24] S. Yoshimura and M. Kuppan, "Fabrication of high-qualified $(Bi_{1-x}Ba_x)FeO_3$ multiferroic thin films by using a pulsed DC reactive sputtering method and demonstration of magnetization reversal by electric field," *Japanese Journal of Applied,* vol. 57, p. 9, 2018.

[25] M. Kuppan, D. Yamamoto, G. Egawa, S. Kalainathan and S. Yoshimura, "Magnetic properties of $(Bi_{1-x}La_x)(Fe,Co)O_3$ flms fabricated by a pulsed DC reactive sputtering and demonstration of magnetization reversal by electric feld," *Scientifc Reports,* vol. 11, p. 11118, 2021.

[26] S. Rossnagel, "Sputtering and sputterinf deposition," in *Hand book of thin film deposition processes and techniques (second edition)*, 2001, pp. 319-348.

[27] K. Wasa, I. Kanno and H. Kotera, Handbook of sputtering deposition technology, william andrew, 2012.

[28] S. Swann, "Magnetron sputtering," *Physics in technology,* vol. 19, 1988.

[29] S. Yoshimura, H. Kobayashi, G. Egawa, H. Saito and S. Ishida, "Acceleration of ordering transformation of a new $Fe_2(Mn,Cr)Si$ Heusler-alloy film by VHF plasma irradiation process during RF sputter deposition," *Journal of Applied Physics,* vol. 109, p. 7, 2011.

[30] Y. Waseda, E. Matsubara and K. Shinoda, X-Ray Difraction Crystallography, Springer, 2011.

[31] T. Ozeki, D. Yamamoto, G. Egawa and S. Yoshimura, "Development of $BiFeO_3$ based multiferroic thin films with large saturation magnetization and perpendicular magnetic anisotropy," *Journal of the Magnetic Society of Japan,* vol. 46, p. 64, 2022.

[32] G. Adachi and M. Imanaka, "The binary rare earth oxides," *Chemical Reviews,* vol. 98, p. 1479, 1998.

[33] Y. Maeda, T. Ohkubo, K. Takei, D. J. Rogers and K. L. Babcock, "Studied on the effect of compositional separation on the magnetic domain configuration in sputtered Co-Cr thin films using magnetic force microscopy," *J. Mag. Soc. Japan,* vol. 19, p. 706, 1995.

[34] A. S. Everhardt, S. Matzen, N. Domingo and G. Catalan, "Ferroelectric Domain Structurres in Low-Strain $BaTiO_3$," *Advanced electronic materials,* vol. 2, p. 1, 2015.

[35] Y. Cho, K. Fujimoto, Y. Hiranaga and Y. Wagatsuma, "Tbit/inch^2 ferroelectric data storage based on scanning nonliner dielectric microscopy," *Applied Physics Letters,* vol. 81, p. 23, 2002.

[36] S. Watanabe, W. A. Dino, H. Nakanishi, H. Kasai and H. Akinaga, "Reactive Ion Etching of NiFe Thin Films from First-Principles Study: A Case Study," *Japanese Journal of Applied Physics,* vol. 44 (2), p. 30, 2005.

[37] M. Mizuhata, T. Miyake, Y. Nomoto and S. deki, "Deep reactive ion etching (Deep-RIE) process for fabrication of ordered structural metal oxide thin films by the liquid phase infiltration method," *Microelectronic Engineering,* vol. 85, pp. 355-364, 2008.

[38] S. D. Kim, J. J. Lee, S. H. Lim and H. J. Kim, "Reactive Ion Etching Characteristics of Permalloy Thin Films," *Japanese Magnetic Society,* vol. 23, pp. 252-254, 1999.

[39] J. W. Coburn, "Role of ions in reactive ion etching," *Journal of Vacuum Science & Technology A,* vol. 12, pp. 1417-1424, 1994.

[40] M. Ganjian, K. Modaresifar, H. Zhang, P. L. Hagedoorn, L. E. F. Apachitei and A. A. Zadpoor, "Reactive ion etching for fabrication of biofunctional titanium nanostructures," *Scientific Reports,* vol. 9, p. 18815, 2019.

[41] F. Karouta, "A practical approach to reactive ion etching," *Journal of Physics D: Applied Physics,* vol. 47, p. 233501, 2014.

[42] T. Kim and J. Lee, "Optimization of deep reactive ion etching for microscale silicon hole arrays with high aspect ratio," *Micro and Nano Systems Letters,* vol. 10, p. 12, 2022.

[43] H. Jansen, H. Gardeniers, M. Boer, M. Elwenspoek and J. Fluitman, "A Survey on the reactive ion etching of silicon in microtechnology," *Journal of Micromechanics and Microengineering,* vol. 6, p. 14, 1996.